A CLOSED-LOOP, FORCED-CONVECTION DRYING PROCESS FOR WATER RECOVERY AND MICROBIAL STABILIZATION OF ASTRONAUT CABIN WASTE

A Dissertation

Presented to the Faculty of the Graduate School

of Cornell University

In Partial Fulfillment of the Requirements for the Degree of

Doctor of Philosophy

by

JMR Apollo Arquiza

August 2012

A CLOSED-LOOP, FORCED-CONVECTION DRYING PROCESS FOR WATER RECOVERY AND MICROBIAL STABILIZATION OF ASTRONAUT CABIN WASTE

JMR Apollo Arquiza, Ph.D.

Cornell University 2012

During long-term space missions, astronauts generate wet trash, including food residues, moist hygiene wipes and wet paper towels. This waste produces two problems: first, the loss of water; second, the generation of odors and potential health hazards by microbial growth. These problems are solved by a closed-loop, forced-convection, heat-pump drying system which stops microbial activity by both pasteurization and desiccation, and recovers moisture in a gravity-independent porous media condensing heat exchanger (PMCHX). Detailed transport models were developed for the two major processes involved: drying of the fixed bed of trash and condensation of water vapor in the PMCHX. The conservation equations for mass, energy, and fluid flow were applied to these systems to give a set of differential equations that was solved numerically by the finite element method using the commercial software COMSOL. Simulation values were compared with experimental data to validate the model for various operating conditions at sea-level pressure and unit gravity. The model predicts the system performance, energy use per unit of recovered water, and effectiveness of enthalpy recovery options. This can be used to optimize the performance of the drying system for various space habitat conditions.

The energy invested in removing a unit mass of water from the trash increases as the evaporation rate falls toward the end of drying. Knowledge of the lowest water activity at which microorganisms will grow on the waste can be used to specify a minimum drying endpoint. This should ensure the production of microbiologically stable trash for storage without extra energy consumption due to further drying below this moisture content. A real-

time PCR-based biomass assay for measuring fungal growth rates on solid media was developed for this purpose. The procedure was used to monitor the biomass of *Penicillium chrysogenum*, a species commonly involved in food spoilage, during growth on a model food at different water activities (a_w = 0.973, 0.936, and 0.843). The specific growth rate of *P. chrysogenum* was also measured. The results show that growth decreases as water activity is lowered and at a_w = 0.843, the *P. chrysogenum* spores remained dormant. The specificity of the rt-PCR assay was demonstrated by measuring the biomass of *P. chrysogenum* while growing together with *Aspergillus niger* on solid media.

BIOGRAPHICAL SKETCH

Jose Maria Reynaldo Apollo Corpus Arquiza (a.k.a. JMR Apollo Arquiza) was born in Manila, Philippines to his loving parents, Antonio Generoso Arquiza and Shirley Corpus Arquiza during the time when the United States Apollo Project was sending men to the moon. This great achievement has a special significance for him because his parents named him Apollo in honor of the Moon missions. His name has made him feel intimately linked to this historic event and as a child, he often dreamed of becoming involved in the exploration of outer space (as in Star Trek). Yet the reality was that he was in the Philippines and the probability of his being involved in space was almost none.

But surprise, surprise! Here he is now at Cornell University doing research on Advanced Life Support for the U.S. Space Program. He may not be an astronaut but he is working on how to keep them alive and comfortable in the harsh conditions of outer space. He will be forever grateful to his Ph.D. adviser, Jean B. Hunter, and the Department of Biological and Environmental Engineering for giving him this wonderful opportunity.

He completed his secondary education at the Philippine Science High School in Quezon City. He then took up Chemical Engineering at the University of the Philippines Los Baños and stayed there after graduating *Magna cum laude* to teach in the Institute of Chemistry and Department of Chemical Engineering. During this time he obtained his Master's degree in Chemical Engineering from the University of the Philippines Diliman. He also passed and placed first in the nationwide Philippine Chemical Engineering Licensure Exam.

He is happily married to the former Amihan Mercado Lubag. He came to the United States to be with her while she was studying for her Ph.D. in Horticulture at Cornell. Before he started his own Ph.D., he worked as research staff in the Dept. of Horticulture and Dept. of Food Science at Cornell. His major field is Biological & Environmental Engineering with minors in Chemical Engineering and Computational Science & Engineering.

He has a sister, Veronica and a niece, Mary Pauline.

He enjoys living in Ithaca. Yes, even when it's January and he's cold and walking through the heavy snow and thinking of the hot and sunny Philippines. He knows that in spite of the long winter, Ithaca is actually a very warm place. The natural beauty, the University and town community, the cultural diversity and most of all, the friendly atmosphere have a way of making him feel right at home.

He is looking forward to contributing towards making humankind a spacefaring race and is hoping to see us walking on Mars in his lifetime.

ACKNOWLEDGEMENTS

The pursuit of my Ph.D. has been a great adventure and God has blessed me with wonderful people who helped me along the way. It is with great pleasure that I express my heartfelt gratitude to them here:

Jean Hunter, my adviser and mentor, for her unfailing and generous support through the years. You have helped immensely in my development as a scientist and a person. Your right mix of guidance and freedom gave me both direction and satisfaction in my research. I know your enthusiasm for learning and teaching will inspire me the rest of my life.

Ashim Datta, my committee member, for always being there for my consultations and teaching me mathematical modeling. Thank you also for taking me as a Teaching Assistant, I know that the experience will make me a better teacher in the future.

Larry Walker, my committee member, for the invaluable comments and suggestions, especially on the molecular biology part of my research. Thank you also for allowing me to work in the Biofuels Research Laboratory.

The late Kenneth Torrance, my former committee member, for a wonderful class.

NASA, for funding my research.

Orbital Technologies Corporation especially Robert Morrow, Ross Remiker, and William Butrymowicz, for building the DRYER prototype and assistance during testing.

Dan Luo and Ed Rice, for the use of the gel imager in their lab.

Tammo Steenhuis, Todd Walter and Brian Richards for letting me use equipment in the Soil & Water lab.

Roger Spanswich, for the use of the fluorescence spectrophotometer.

Lars Angenent, for the use of the UV-vis spectrophotometer.

Ed Evans and Stephane Corgie for their assistance in my work at the Biofuels Research Lab

Michael Walter, Dan Aneshansley and Beth Ahner for awarding me Teaching Assistantships when they were Department Chairs.

Jean-Yves Parlange, for always having time for my questions. Your courses gave me a deeper appreciation of mathematics and thermodynamics. Your generous compliments are greatly appreciated.

Beth Ahner for taking me as a Teaching Assistant and encouraging me to work hard to finish my studies.

The BEE faculty, especially those whom I've had the pleasure of being their student: John March and Peter Hess.

The wonderful BEE staff, Alley, Brenda, Debbie, Nancy, Peggy, Sue, Tami and Val, for all their help and support.

My fellow BEE graduate students, especially my roommates in 164: Srabani Das, Timothy Shelford and Mike Walsh, for sharing the ups and downs of being a Ph.D. student

My Filipino friends, whose companionship and support I can always count on, especially Dito and Tess Savella, Cynthia Santos, Mimi Melegrito, Joy and Florio Arguillas, Emily Graw, Jose Beduya, Jessica del Mundo, Angel Caoile, and Natalia Cushman.

My family back home in the Philippines for their love and support. Thank you Mama, Ate Corrie, Maple and my late Papa.

My beloved wife, Amy. You always inspire me to do my best. Thank you for always being with me through it all!

Finally, I give all glory to Almighty God:

Unless the Lord builds the house,

Its builders labor in vain.

Psalm 127:1

Yours sincerely,

Apollo

TABLE OF CONTENTS

LIST OF FIGURES

LIST OF TABLES

CHAPTER 1

GENERAL INTRODUCTION AND BACKGROUND

Like people on earth, astronauts living in space also produce garbage. This "space trash" is mostly made up of discarded food and drink containers (with unconsumed portions), used moist hygiene wipes and paper towels (no showers in microgravity), plastic packaging, and paper (Hunter et al., 2006). The current method of treating space trash is storage and then disposal. Since the Space shuttle missions are of short duration, small amounts of trash are produced and keeping them in bags until the return to earth is manageable (Fig. 1.1). In the International Space Station (ISS), trash are also stored in bags until removed by the Space Shuttle or the Russian spaceship Progress which is an unmanned vessel used to bring supplies to the ISS. For long duration manned missions to distant destinations, such as the planned rendezvous with an asteroid or future Mars landing, resource recovery and stabilization of trash will be critical for success. It has been estimated that a four-person crew would discard an average of 1 kg day $^{-1}$ of water in their trash (Fisher et al., 2009) and recovery of this water would be highly desirable in order to reduce payload mass and associated lift costs. Another problem with wet trash is its susceptibility to microbial growth due to the presence of food and hygiene wipes. As the experience of Mir and ISS amply demonstrates, spoilage may lead to the generation of odors, allergens, and potential health hazards (Makimura et al., 2001; Vesper et al., 2008).

Drying of the wet trash by forced convection with hot air is a viable and simple way of stopping microbial activity by combined pasteurization and desiccation. The water vapor produced can then be recovered by a condenser. Our research group, together with Orbital Technologies Corp. (ORBITEC), has been studying a closed air-loop, dryer and condenser

system (DRYER) for astronaut cabin waste. The DRYER consists of a blower, air heater, wet material container, a gravity-independent Porous Membrane Condensing Heat Exchanger (PMCHX), thermoelectric heat pump, and waste heat recovery module. The schematic for the DRYER is shown in Figure 1.2. The prototype that was fabricated by ORBITEC and given to us for testing is shown in Figure 1.3. The system may be adapted for use in the drying of crew laundry, water recovery from water-reprocessing brines, and ultimately, food and biomass drying in a biogenerative life support system.

Figure 1.1 Trash from the Space Shuttle (Fisher et al., 2009)

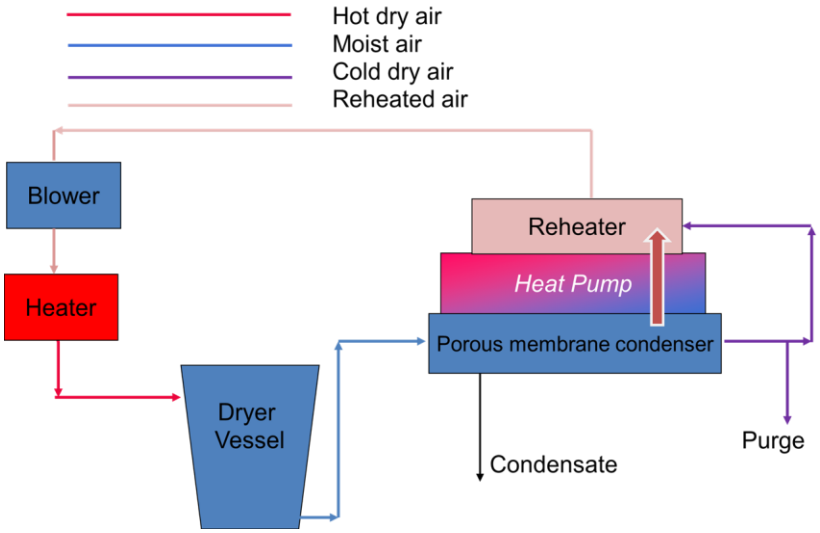

Figure 1.2 DRYER system schematic

Figure 1.3 DRYER system prototype

In connection with our research on the DRYER system, I have completed three papers for my Ph.D. Dissertation. A brief description and discussion of relevant studies for each will be presented in this section.

1. Modeling and Simulation of the Drying of Cabin Solid Waste in Long-Term Space Missions (Chapter 2)

Drying is extensively used in agricultural post-processing and in the food, pharmaceutical and chemical industries. Its importance is shown by the overwhelming number of publications on drying principles, models, and sample-specific data that is in the literature. Several books have been written on the topic (see Brooker et al., 1992; Kowalski, 2007; Tsotsas and Mujumdar, 2007; Turner and Mujumdar. 1997) and there is a journal dedicated to it (Drying Technology, Taylor & Francis, Philadelphia, PA). However, the drying of astronaut cabin waste (space trash)

or any type of trash has not yet been studied. This is probably because drying is an energy-intensive process and is usually done because the final product is of high value. In long-term space missions, the water in the wet trash becomes valuable enough to justify its recovery by drying but the process still has to be energy efficient to get the maximum benefit. A computational model of the drying of space trash would be needed to determine the optimal conditions for the operation of a drying system such as the closed-loop, forced convection process being investigated by our research group. In the paper, the trash was considered as porous media with large pores (Hoang et al., 2003; Datta, 2007). It was also assumed that a pseudo-homogeneous continuum model can be used for the system (Castillo-Araiza et al., 2007). The development of a model was complicated by the heterogeneous nature of the trash, its variable composition and the presence of dry and wet components. The model required knowledge of the heat and mass transfer coefficients for the system and these were determined by experimentally from the drying of single layers of trash with varying proportions of wet and dry material. Determination of the rate of evaporation from the solids also required the water vapor concentration of the gas at the surface and this was calculated from the obtained drying curves. A system of partial differential equations for the drying process was derived from the conservation equations for energy and moisture applied to the air and solid phases. Two pieces of information required for the proper design of the DRYER system are the maximum rate of evaporation and the drying time needed to ensure that the wet materials in the trash have moisture contents below the minimum value for microbial growth. These were predicted by the validated model for different air flow rates and varying proportions of wet and dry solids in the trash.

2. Modeling of a Closed-loop, Forced-convection, Heat-pump Drying System for Space Operations (Chapter 3)

In this study, a computational model of the DRYER system was developed and validated with experimental data. The main components of the model are: (1) a bypass factor to specify the drying efficiency, (2) a system of partial differential equations based on the conservation of mass, energy, and fluid flow applied to the porous media condensing heat exchanger, and (3) performance expressions for the thermoelectric cooler used by the condenser. Simulations of the DRYER were done to predict the system performance, energy use per unit of recovered water, and effectiveness of enthalpy recovery options.

As a supplement to the paper, a discussion on the porous-membrane condenser is given next.

2.1 The Porous Membrane Condensing Heat Exchanger (PMCHX)

Condensers have been used in manned space missions to control astronaut living conditions (temperature, humidity) and to recover water in wastewater treatment systems involving evaporation or distillation. In addition to providing adequate heat transfer rates to meet condensation requirements, condensers in space need to incorporate a mechanism to separate the condensate from the gas stream in the absence of gravity (Faghri and Chow, 1988). In most designs, the heat exchanger and gas-liquid separator are two different pieces of equipment. The condensers currently installed in the International Space Station (ISS) and the Space Shuttle use rotary motion to remove the condensate from the gas-liquid mixture by centrifugal force (Eckart, 1996). However, the use of moving parts in this process adds to the power load and increases the risks of mechanical failure.

An alternative to the use of centrifugal force for separating condensate and gas is the use of capillary force which becomes dominant in the absence of gravity. Condensers based on this involve a hydrophilic porous media that is filled with water by capillary action. The saturated porous media allows condensate collection while preventing gas from passing through. The surface of the porous solid in contact with the vapor is kept cool to promote condensation while a pressure difference between the humid air/vapor and collection sides of the media removes the condensate. This porous media condensing heat exchanger (PMCHX) therefore combines condensation and gas-liquid separation in one piece of equipment without the use of moving parts. When properly designed, the PMCHX produces no free liquid since the condensate is confined inside the porous media by capillary forces. Other advantages of the PMCHX include enhanced heat transfer due to the thinning of the condensate film covering the cold surface (Balasubramaniam, R. et al., 2006; Faghri and Chow, 1988; Frankel and Bankoff, 1965) and the option of keeping entrained pathogens out of the water product by the use of media with pore diameters (< 0.45 mm) less than the average size of bacteria (Scovazzo et al., 1998).

At present, porous media condensers have only been successfully tested for temperature and humidity control of enclosed chambers for plant growth experiments in outer space (Iverson et al., 2003). In these systems, the condenser operates at temperatures near 25°C and condensation rates involved are moderate (Iverson et al., 2003). This is in contrast with condensers designed for space wastewater treatment processes or drying of wet solids, where higher temperatures and larger water vapor loads are expected. There is therefore a need to study the performance of the PMCHX at these more severe conditions. In this connection, a PMCHX has been fabricated as part of a closed air-loop drying system for astronaut cabin waste (Hunter et al., 2006). The PMCHX was designed to condense water vapor from the hot, moist air

leaving the drying chamber while recovering some of the latent enthalpy to heat the air leaving the condenser before it returns to the drying chamber. The porous media in contact with the humid air is saturated by water cooled by a thermoelectric (TE) heat pump.

2.2 Microgravity condensers used by the United States space program

The humidity and temperature of the air in the space habitat of the shuttle and International Space Station (ISS) are controlled by the Common Cabin Air Assembly (CCAA) shown in Figure 1.4 (Eckart, 1996). The air is cooled and water vapor is condensed by a multipass plate fin exchanger in which air and cooling water flow perpendicular to each other. The condensate formed is then forced by the air into holes at the outlet. Both air and condensate enter these holes into "slurper bars" which bring the two-phase mixture into a rotary separator. The heat exchanger and gas-liquid separator are therefore two different pieces of equipment in this case.

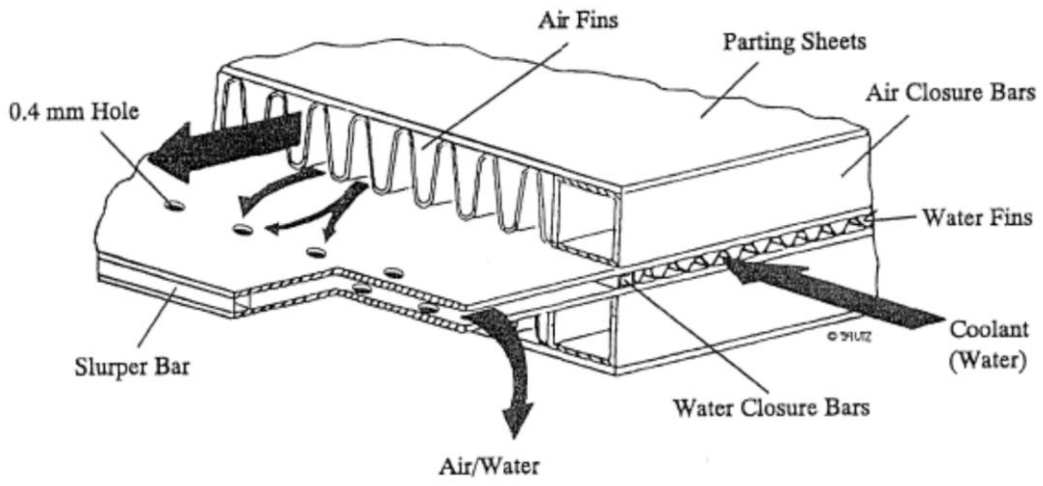

Figure1.4 The Common Cabin Air Assembly condensing heat exchanger for humidity and temperature control in the shuttle and ISS (Eckart, 1996)

In the ISS, water is recovered from wastewater (mostly urine and flush water) using the Vapor Compression Distillation (VCD) process (Figure 1.5). The feed water enters an evaporator to produce water vapor which goes to a compressor and then to a condenser. The pressure differential between the evaporator and condenser produces a saturation temperature driving force that allows the latent heat of condensation to be reused for evaporation. The process is complicated by the need to rotate the entire set-up (evaporator, compressor, condenser, and condensate collector) in order to separate the condensate from the vapor in microgravity (Eckart, 1996).

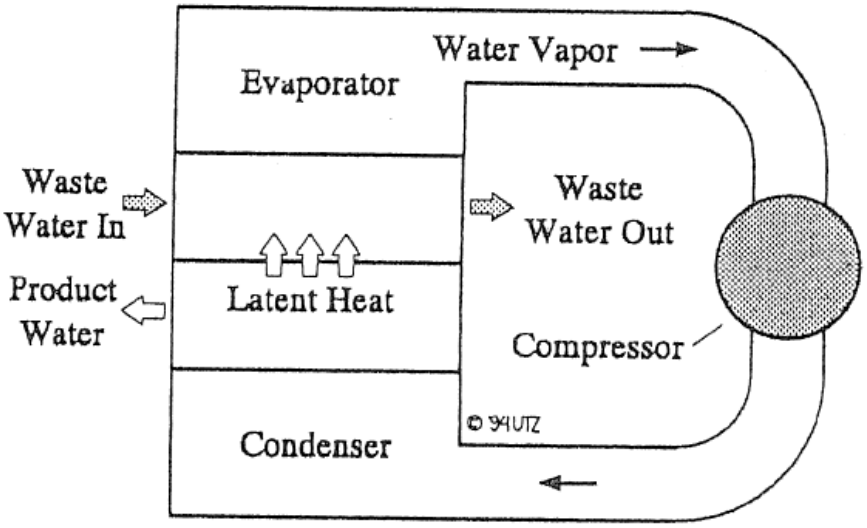

Figure 1.5 Schematic of the Vapor Compression Distillation process for water recovery from space water in microgravity.

The main disadvantage of these condensers is the use of centrifugal force to separate the condensate from the gas phase. This necessitates the use of rotating equipment which adds to the power consumption. The use of moving parts also increases the risk of mechanical failure and the inventory of replacement parts adds to the launch cost.

2.3 Physical basis of porous media condensers

Porous media condensers depend on the capillary force to produce a water seal that separates the condensate from the gas phase. A brief review of the concepts of surface tension and capillarity is presented in this section.

Surface tension and Laplace's theorem

A molecule beneath the liquid surface experiences molecular attractive forces from all directions due to the surrounding molecules. Some of these attractions have to be broken in order for an internal molecule to go to the surface. The macroscopic result of bringing molecules within a liquid to the surface is a change in surface area. Since this involves breaking molecular attractions, energy has to be added to the system to accomplish this. The work that will increase the surface area of a liquid by a unit amount is known as the surface tension, γ, with dimensions of energy area^{-1} or force length^{-1}(de Gennes et al., 2004).

When a curved interface exists between two fluid phases, the hydrostatic pressure difference across the boundary is related by Laplace's theorem

$$\Delta p = \gamma C = \gamma \left(\frac{1}{R} + \frac{1}{R\prime}\right) \qquad (1)$$

where γ is the surface tension and C is the curvature of the surface (expressed in terms of its radii, R and R'). Consider as an example an air bubble immersed in water. If the bubble is a sphere, then R and R' are both equal to the radius of the sphere, R_S, and the curvature of the surface is given by $C = \left(\frac{1}{R} + \frac{1}{R'}\right) = \frac{2}{R_S}$. The change in pressure across the bubble boundary is therefore $\Delta p = p_{air} - p_{water} = \frac{2\gamma}{R_S}$ and $p_{air} = p_{water} + \frac{2\gamma}{R_S}$. This shows that the pressure inside the bubble is greater than the water directly surrounding it.

Capillary rise and Jurin's Law

The rise of liquids against gravity in small tubes can be explained by Laplace's theorem. The meniscus forms a curved surface between the gas phase and the liquid and in this case Laplace's theorem dictates that the pressure in the liquid just beneath the surface is less than that in the gas phase (see bubble example above). Since pressure on the flat surface of the liquid outside the tube is still equal to the gas phase, the liquid inside the tube rises to compensate for the underpressure there. The height of this capillary rise is determined by the balance between the pressure at the base of the liquid column and the outside pressure. For a cylindrical tube that has a radius very much less than the height of the raised liquid, the maximum capillary rise (H) can be derived as

$$H = \frac{2\gamma(cos\theta)}{\rho g r} \qquad (2)$$

Where θ is the contact angle of the liquid meniscus with the walls, ρ is the density of the liquid, g is the acceleration due to gravity and r is the radius of the tube. This equation (Jurin's law) tells us that in microgravity, where g is near zero, capillary rise will be very high even for larger tubes (~mm) since the denominator becomes very small in this case (Wang et al., 2009).

The analysis of capillary rise in porous media is complicated by the fact that its pores are not vertical tubes with uniform diameters. However, a macroscopic analysis of the balance between capillary forces and gravity shows that the level to which the liquid rises within the porous media is still approximated by Jurin's law using average properties (Gennes et al., 2004). This implies that in microgravity, a hydrophilic porous-media condenser will maintain complete saturation and prevent gas bleed-off as long as the pressure at the tank reservoir for the condensate is between the gas pressure above the porous media and the pressure just under the gas-liquid interface (given by Laplace's law).

2.4 Porous media condensers

Several designs for porous media condensers have been proposed and tested. These include the use of pipes with porous walls (Frankel and Bankoff, 1965; Faghri and Chow, 1988; Scovazzo et al., 1998), shell-and-tube configurations (Scovazzo et al. 1998, Newbold, 1993) and porous flat plates (Yang, 1970; Scovazzo et al. 1998; Hasan et al., 2005; Balasubramanian et al., 2006).

Pipes with porous walls

Early research on condensation on a porous pipe wall was in the context of enhancing heat transfer by decreasing the thickness of the condensate on the wall surface. Since this liquid layer adds another resistance to heat transfer, minimizing it by suction through the porous wall would avoid its detrimental effect on heat transfer. However, it was also realized that this set-up would allow the separation of the condensate from the bulk gas in the absence of gravity. Frankel and Bankoff (1965) solved the simplified momentum and energy transport equations for a system where pure vapor is condensing on the outside of a horizontal pipe with a porous wall. Cold water flowing inside the pipe both served as the cooling medium and collection reservoir for the condensate. A constant velocity of condensate passing through the wall was assumed. Faghri and Chow (1988) performed almost the same analysis for an annular system with the pure vapor condensing on the interior walls of the inner pipe. Both studies showed that the condensate layer was considerably decreased by suction and this gave significantly higher heat transfer rates compared to similar systems with solid pipe walls. However, in both cases the results of their analysis were not compared with experimental data.

Scovazzo and co-workers (1998) evaluated the performance of a porous-pipe condenser for the dehumidification of moist air. In contrast with studies involving pure vapor where heat transfer is controlling, the presence of a large amount of air in dehumidification makes the effect of mass transfer of water vapor through the gas phase) more significant (Newbold, 1993; Scovazzo et al.,1998). The temperature of the liquid water saturating the porous material is set to a low value such that the partial pressure of water vapor at its surface is less than that in the humid air. This concentration difference results in the diffusion of water vapor from the bulk phase to the surface of the porous membrane where condensation occurs. Since the surface is cold, the air also gets cooled but importantly, not enough to lower its bulk temperature to below its dewpoint. This is critical in microgravity since condensation only at the solid surface would ensure that liquid droplets within the gas phase will not be formed.

The set-up used by Scovazzo et al. (1998) involved single porous pipes made of either metal (316 Stainless steel, 0.5 um pore size) or ceramic (Al_2O_3, 0.2 um), both with inner diameters of 0.635 cm. Humid air flowed inside the pipe with cooling water on the outside. The obtained mass transfer coefficients were found to increase with gas Reynolds number with the metal giving higher values. Since they considered the heat transfer to be just incidental due to the necessity of using cold water to produce a low water vapor concentration at the surface, the heat transfer performance of the porous pipes was not even reported. The process of initially saturating the porous pipe wall with water (priming) was also described.

Shell-and-tube Configurations

Studies under this category used hollow-fibers for the tube bundles. Newbold (1993) analyzed the use of a membrane-based condensate recovery heat exchanger (CRX) with hollow-fiber tube bundles that have porous walls. The CRX is a shell-and-tube heat exchanger where hot

humid air comes in contact with the outside of the tubes in cross-flow with cold water flowing inside. Water vapor from the air condenses on the external surface of the tubes and the higher pressure on the outside forces the liquid water through the walls. Using correlation equations for heat and mass transfer coefficients, Newbold (1993) made calculations to show the capability of the CRX for temperature control and condensate recovery under possible operating conditions in space (NASA baseline and spacecraft cabin).

Scovazzo et al. (1998) performed condensing experiments on humid air using a hollow fiber module consisting of 40 mixed cellulose ester tubes with 0.06 cm internal diameter and 0.1 um pore size. This gave higher overall mass transfer coefficients compared to metal and ceramic pipes with porous walls. However, the hollow fibers were observed to fail after operating for several hours, allowing gas to bleed into the cooling water flowing outside the bundle. This led them to conclude that the use of mixed cellulose ester as porous material is not feasible.

Porous Flat plate

The condensation of a pure vapor on a vertical, flat, porous plate with uniform suction was solved analytically by Yang in 1970. The system studied was the liquid film on the surface and the goal was to determine how suction decreases its thickness. An analysis of the condensation of water from humid air flowing over a horizontal, flat, cooled porous plate was done by Balasubramanian et al. (2006). They analytically solved a simplified, one-dimensional problem involving momentum, energy, and water vapor transport equations in the gas phase, condensate layer on the surface, and within the porous media. A constant liquid velocity through the porous plate was also assumed. Flow of condensate through the porous wall was assumed to follow Darcy's law. As in the case of a porous pipe wall, both of these studies showed that the

thinning of the condensate layer significantly increases the rate of heat transfer. However, no comparison with actual data was given in the papers.

Scovazzo and co-workers (2000) experimentally studied condensation of water vapor from humid air using saturated porous plates. They specifically wanted to investigate the effect of porous material (stainless steel and hydrophilic polymers) on the performance of a porous media condenser. They fed humid air into a small rectangular duct (height = 2.5 mm, width = 25 mm, length = 75 mm) in which one of the larger wall was a porous plate saturated with cold water (5 or 10°C) and then measured the condensation rate. The temperature of the water was controlled using thermoelectric coolers. There was no significant difference in the obtained mass transfer coefficients for the different materials used.

They also tested their "surface-sticking coefficient hypothesis" which states that water vapor will much more readily condense if it hits the air-water interface at the surface pores ("sticks") compared to hitting dry metal surface of the porous plate (Scovazzo et al., 1998). This model predicts that the rate of condensation should be a function of the porosity of the porous media. This theory would follow only if the solid surfaces of the porous media are not covered by a thin layer of water. However, since water readily spreads out over most hydrophilic materials like metals (Gennes et al., 2004), the sticking theory may not be applicable to hydrophilic porous media. This seems to be the case since when they used stainless steel plates with different porosities (0.26 and 0.068), the results showed negligible difference between their mass transfer coefficients. The steel surface probably had a thin layer of liquid water covering them so that water vapor hitting the plate always comes in contact with liquid water. From the perspective of the water vapor molecule, there is no difference whether it hits the solid or pore part of the porous media surface and condensation is not dependent on the porosity. This is an

important result for modeling since this implies that the heat and mass transfer area for condensation on a saturated porous plate is not only the open pores but the entire surface area exposed to the moist air.

A condenser consisting of two types of porous media for use in space missions involving variable gravity was described by Hasan et al. in 2005. The humid air comes in contact with the outer porous substrate and water vapor condenses on the surface because its temperature is kept below the dewpoint by cold water circulating through embedded copper tubes. The hydrophilic property of the porous media causes the imbibition of the condensate into its pores, preventing the accumulation of liquid on the surface. The condensate collected in the porous media is removed by suction from porous tubes installed in it. In order to drain the outer porous media while keeping the porous tubes saturated, the underpressure due to the water surface tension in the pores of the internal tubes should be greater than that in the outer substrate. This is achieved by using internal tubes with pores smaller than that in the outer media since according to Laplace's law, the underpressure is inversely related to the pore diameter. The effect of the percent saturation of the outer substrate on the condensate flow rate under different suction pressures was also measured in this paper. They noted that the liquid flow from the unsaturated outer media as a function of saturation and pressure gradient would be difficult to predict because of its complex nature. The condensation rates for this type of condenser was experimentally studied by the same group using a porous graphite block with 30 μm pore size and 48% porosity (Khan et al., 2006). The effect of shaping the outer substrate (graphite) into fins was theoretically analyzed by Althausen et al. in 2006. However, no experimental results on the extended area design were reported.

3. Development of a Quantitative Real-time PCR Method for Measuring the Biomass of Fungi in the Food Components of Space Trash (Chapter 4)

The experiments on the DRYER have shown that the energy invested per unit mass of water removed increases as the drying rate falls toward the end of drying. For a deep bed drying of a batch of ersatz trash with initial moisture content of 2.75 g water per g^{-1} of bone-dry initially-wet solids using air at 60°C with superficial velocity of 2.2 cm s^{-1} , removal of the last 20% of water takes as much time as that for the initial 80% (see Chapter 2). It would therefore be advantageous to know what minimum moisture content (water activity) must be reached to prevent microbial proliferation in the waste. Stable trash for storage can then be produced without extra energy consumption by drying beyond this point. This paper reports the development of a DNA-based method that determines the amount of microorganisms in solid samples. It uses the species-specific real-time polymerase chain reaction (rt-PCR) to quantify the DNA of a target species and then relate this to its biomass. Since fungi are most suited to grow on wet solids, the procedure was tested using *Penicillium chrysogenum*, a species commonly involved in food spoilage. The advantage of this method is that fungal growth can be measured even with extensive substrate infiltration and that the growth rates of individual species in the presence of other fungi can be also be obtained. The kinetic parameters of the growth of *P.chrysogenum* on a model food (cooked wheat flour) were measured at different water activities. The specificity of this method was demonstrated by measuring the biomass of *P. chrysogenum* while growing together with *Aspergillus niger* on solid media.

The following discussion on real-time polymerase reaction is given here to provide the appropriate background for the paper.

3.1 Conventional PCR

The invention of the polymerase chain reaction (PCR) has made possible the fast, accurate, and reliable replication of specific sequences from a DNA sample. The basic PCR method involves the following components: DNA template, two primers, a heat-stable DNA polymerase, and deoxynucleoside triphosphates (dNTPs) of the four DNA bases. The primers (forward and reverse) are synthetic oligonucleotides that are complementary to sequences bordering the DNA section of interest. They determine what sequences the PCR will copy and are carefully designed according to certain guidelines (Nitsche, 2006). The polymerase (usually Taq) starts replicating the DNA sequence from the primer ends using dNTPs as building material. The cyclical heating and cooling of the mixture brings about the necessary reactions. The temperature is first raised to 95°C to separate the strands of the double helical DNA (known as melting the DNA) and then decreased to a value that allows the attachment of the primers to the single-stranded DNA (annealing). This temperature may be estimated from the primers' sequences but experimental testing is usually done to ensure that the primers anneal only to the sequences bordering the desired DNA fragment, preventing the formation of other PCR products (non-specific amplification). Elongation of the primers to duplicate the template is achieved by raising the temperature to 72°C which is the optimum temperature for polymerase activity. Each cycle should theoretically double the amount of target DNA present but this happens only for a short period near the beginning of the run. This is known as the exponential stage, when PCR efficiency is almost 100%. As the PCR proceeds, the rate of replication of the template slows down until it reaches a point where additional cycles no longer increase the amount of DNA. The decrease in PCR efficiency has been attributed to the exhaustion of the primers or dNTPs, accumulation of PCR-inhibiting byproducts, and loss of polymerase activity (Arya et al., 2005).

Shipley (2006) also notes that the high concentration of PCR products favors association over dissociation, possibly preventing the complete separation of double-stranded DNA during the denaturation step. This limits amplification because the partially separated DNA rapidly rejoins together before the primer attaches during the annealing step and replication cannot proceed. The endpoint of a conventional PCR analysis is usually at this stage, where the number of DNA copies remains constant. The final concentration of DNA is therefore no longer correlated to the initial amount of target sequence present. This makes conventional PCR a qualitative technique; it can be used to determine the presence of a particular DNA sequence in the sample but quantifying it is beyond its capability.

3.2 Quantifying DNA with real-time PCR

In the PCR reaction, the number of DNA copies can be related to the starting amount during the exponential stage by the following equation:

$$N_t = N_t^0 * 2^X \qquad (3)$$

where N_t is the number of template molecules after X amplification cycles and N_t^0 is the starting amount of double-stranded DNA template. This shows that the initial quantity of target DNA in a sample can be determined if data on the amount of PCR products in the exponential stage of the reaction is available. The procedure which uses this principle in the quantification of DNA is known as real-time PCR (rt-PCR). This method involves the "reliable detection and measurement of products generated during each cycle of the PCR process" (Arya et al., 2005). The PCR is monitored using fluorescent dyes that emit a signal upon binding to the PCR products (Kubista et al., 2006).

At present, two different dye chemistries have gained widespread use in reporting the amount of target produced in rt-PCR: Hybridization probes and SYBR Green I. Hybridization probes, of which Taqman is the most popular, belong to the class of fluorogenic oligonucleotide probes that are designed to hybridize within the target DNA sequence. The mode of action is described by Arya et al. (2005) as follows and shown in Figure 1:

> "The probe has a reporter dye attached to its 5' end and a quencher dye at its 3' terminus. If the target sequence is present, the probe anneals downstream from one of the primer sites and is cleaved by the 5' nuclease activity of the Taq polymerase during the extension phase of the PCR. While the probe is intact, the close proximity of the quencher significantly decreases the fluorescence emitted by the reporter dye since the quencher absorbs the reporter dye emission according to the principles of fluorescence resonance energy transfer (FRET). Once the reporter is separated from the quencher by cleavage of the probe, the fluorescence of the reporter dye becomes easily detectable. This set-up allows the measurement of target DNA amplification through the intensity of the reporter signal. Cleavage also removes the probe from the target strand, allowing extension to continue to the end, thereby not interfering with the PCR. The Taqman name is derived from an analogy with the popular Pacman video game."

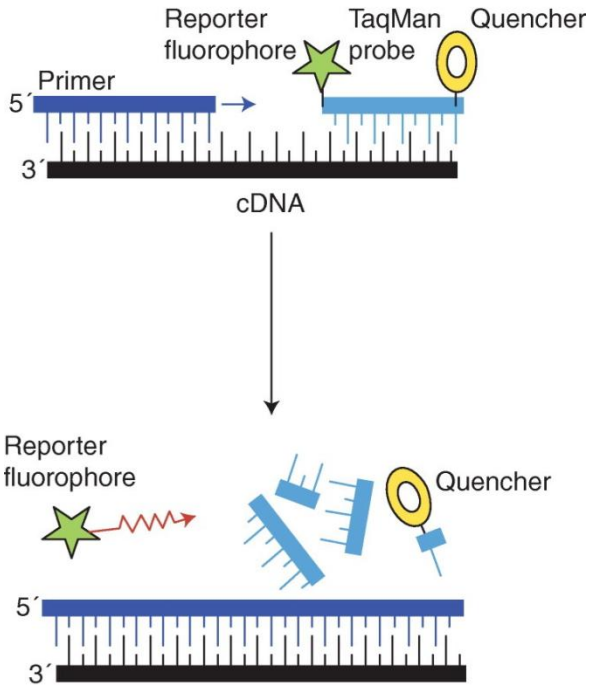

Figure 1.6 Mode of action of hybridization probe reporters (taken from Arya et al., 2005)

SYBR Green I is a member of the group of DNA-intercalating reporters that bind only to double-stranded DNA (ds DNA) and then emit a signal which is proportional to the amount present (Figure 2). Since after each PCR cycle the products are ds DNA, the signal from the SYBR Green I-DNA complex would allow measurement of amplicon concentration (Arya et al., 2005). When compared to Taqman, SYBR Green I is simpler and less expensive since the use of target-specific hybridization probes are not required. However, SYBR Green I is more prone to false positives and overestimation of initial target content because it binds to any ds DNAs produced by the PCR and will consequently report non-specific PCR products and primer-dimers. The careful design of primers and optimization of rt-PCR assays to avoid non-target ds DNA is therefore critical when using SYBR Green I (Arya et al., 2005). The use of melting curve analysis after the rt-PCR is also necessary to check whether the only ds DNA present is the desired sequence (Ponchel, 2006).

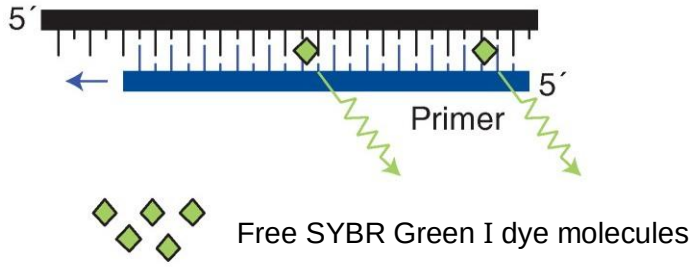

Figure 1.7 Mode of action of DNA-intercalating reporters (taken from Arya et al., 2005)

Instruments for rt-PCR analysis are normally designed to analyze samples in 96-well plates but signal variations due to the different locations of the wells are usually observed. To compensate for this, a passive reference dye, 6-carboxy-X-rhodamine (ROX), is included in the reaction mixture. The fluorescent signal from the reporter is then normalized by dividing its intensity by that of the reference dye in the same well during the rt-PCR, giving its Rn+ value.

The normalized reporter signal is also measured for the complete reaction mixture prior to initiation of PCR and this is designated as Rn. The final signal that is reported as the rt-PCR data is the Δ Rn which is the difference between Rn+ and Rn. (Adams, 2006)

$$\Delta R_n = (R_n +) - (R_n) \qquad (4)$$

When a PCR run is observed using real-time PCR, the characteristic graph of fluorescent signal against time shown in Figure 1.8 is obtained. This plot is divided into the following four stages (Shipley, 2006):

1. *Baseline*. During the early stages of the run, amplification is occurring but the low amount of DNA copies present makes their fluorescent signal indistinguishable from background noise. By default, the baseline setting is chosen by the instrument software, usually within cycles 3 to 15 but this can be changed manually if needed (Arya et al., 2005)
2. *Exponential*. This starts when there are enough PCR products to give a signal above the baseline. At this stage PCR efficiency is maximum (~ 100%) and amplification is at an exponential rate.
3. *Linear*. The PCR efficiency begins to decrease due to reasons discussed earlier
4. *Plateau*. There is no more amplification per cycle so the fluorescent signal of the reporter dye remains constant.

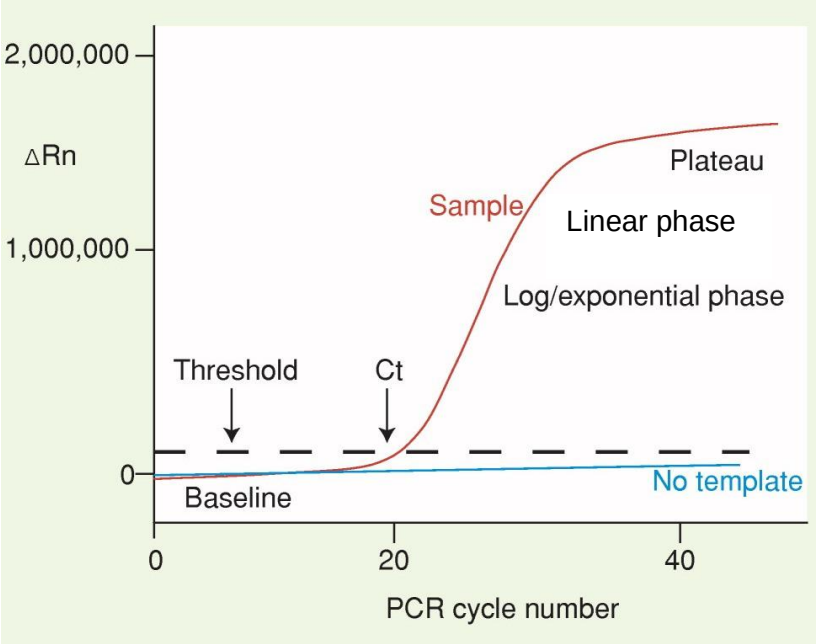

Figure 1.8 Characteristic plot for a real-time PCR run (taken from Arya et al., 2005)

3.3 How real-time PCR is used to quantify target DNA from a sample

Most of the discussion in this section is taken from Mackay et al. (2007). In an ideal PCR run, each cycle doubles the amount of template in the reaction vessel as given by Equation (1). For this to be strictly followed, four assumptions would have to be valid:

1. *The initial template is double stranded.* If it is single stranded, the equation becomes $N = N_0 * 2^{X-1}$ since the first cycle simply forms the complement of the initial DNA.
2. *The PCR efficiency is 100% and full length copies of each strand of template are produced after each cycle.*

   This assumption is never totally valid since experience has shown that PCR efficiency is always less than 100%. The possible causes of inefficiency in an rt-PCR run are:

   a. PCR inhibitors from the sample was co-purified with the DNA

b. Primer hybridization is inefficient, so not all of the template is replicated per cycle.

c. The template forms secondary structures (folding, supercoiling) that hinder polymerization

However, Equation (1) can be modified to account for the actual PCR efficiency, E_{ts}:

$$N_t = N_t^0(1 + E_{ts})^X \quad (3)$$

The E_{ts} has a value between 0 and 1. It has two subscripts to indicate that it is dependent on both the template (t) and the sample (s).

3. *PCR efficiency is constant throughout the amplification process.*

4. *The reporter fluorescence is proportional to the amount of template.* It should be noted that the fluorescence is affected by several factors

    a. Dye or probe used

    b. Amplified sequence

    c. Length of the PCR product (longer amplicons bind more dye)

    d. Optical properties of the instrument

    e. Data acquisition temperature

    f. Instrument settings (gain, etc.)

In rt-PCR, the initial amount of target DNA in a sample is inversely related to its threshold cycle, CT. The CT is the cycle number in the PCR run that crosses the value of the reporter signal that has been chosen as the threshold. This threshold fluorescence is set by the computer software using different algorithms (e.g. 10x the standard deviation of the signals below the baseline) but may be also be adjusted manually. Studies have shown that the threshold

setting does not significantly affect the difference between CT values of samples with different target contents as long as it is within the exponential stage (Adams, 2006; Kubista et al., 2006).

The numerical relationship between CT and amount of target can be derived by first considering two samples, A and B, with initial target contents of N_{tA}^0 and N_{tB}^0, respectively. When the samples are at their own threshold cycles (CT_{tA} and CT_{tB}), the following equations apply (from Eq. 2)

$$N_{tA} = N_{tA}^0(1 + E_{tA})^{CT_{tA}} \quad (5)$$

$$N_{tB} = N_{tB}^0(1 + E_{tB})^{CT_{tB}} \quad (6)$$

Since at the threshold the reporter signals from A and B have the same intensity, it follows that $N_{tA} = N_{tB}$ and

$$N_{tA}^0(1 + E_{tA})^{CT_{tA}} = N_{tB}^0(1 + E_{tB})^{CT_{tB}} \quad (7)$$

Assuming that the PCR efficiencies for A and B are the same and using $\bar{E}_t$ to represent it, manipulation of Eq. 3 gives the following relationship between the ratio of target to their CT's

$$\frac{N_{tA}^0}{N_{tB}^0} = \frac{(1+E_{tB})^{CT_{tB}}}{(1+E_{tA})^{CT_{tA}}} \cong (1 + \bar{E}_t)^{(CT_{tB} - CT_{tA})} \quad (8)$$

This equation also highlights how the PCR efficiency affects the reported relative amounts of target present between samples in rt-PCR. Assays that have different $\bar{E}_t$ values would mean different target ratios among samples even if the observed CT's are the same (Kubista et al., 2006).

If A is any sample and B one with only a single copy of the target, $N_{tA}^0 = N_t^0$, $N_{tB}^0 = 1$, CT_{tB} = CT(sc), and CT_{tA} = CT

$$N_t^0 = (1 + \bar{E}_t)^{(CT(sc)-CT)} \quad (9)$$

Getting the log of both sides and rearranging

$$logN_t^0 = (CT(sc) - CT)log(1 + \bar{E}_t) \quad (10)$$

$$CT = \left[\frac{-1}{log(1+\bar{E}_t)}\right] logN_t^0 + CT(sc) \quad (11)$$

Equation (10) shows that if the plot of CT against $logN_t^0$ is linear, then its slope is $-1/log(1 + \bar{E}_t)$ and the y-intercept is the CT for a single copy of the target. In most cases, rt-PCR experiments produce a linear CT vs. $logN_t^0$ plot for a wide range of target DNA concentrations (at least eight units of $logN_t^0$ values). A Standard curve for a specific target is constructed by performing rt-PCR on several prepared samples with known DNA content (usually tenfold serial dilutions from 10 to 10^7 copies) and plotting CT vs. $logN_t^0$ (Figure 1.9). The slope of the resulting line gives the PCR efficiency by using the equation

$$\bar{E}_t = 10^{-1/slope} - 1 \quad (12)$$

For an rt-PCR run that is 100% efficient, with $\bar{E}_t$ = 1, the above equation gives a standard curve with a slope of -3.32. Adams (2006) also states that based on the signal intensity of the most common hybridization probe dye 6-carboxy-fluorescein (FAM), a 100% efficient PCR would detect a single copy of template between 33 and 37 cycles. This may not apply to DNA-intercalating dyes like SYBR Green I since the fluorescent intensity of a single copy of the target would depend on its length.

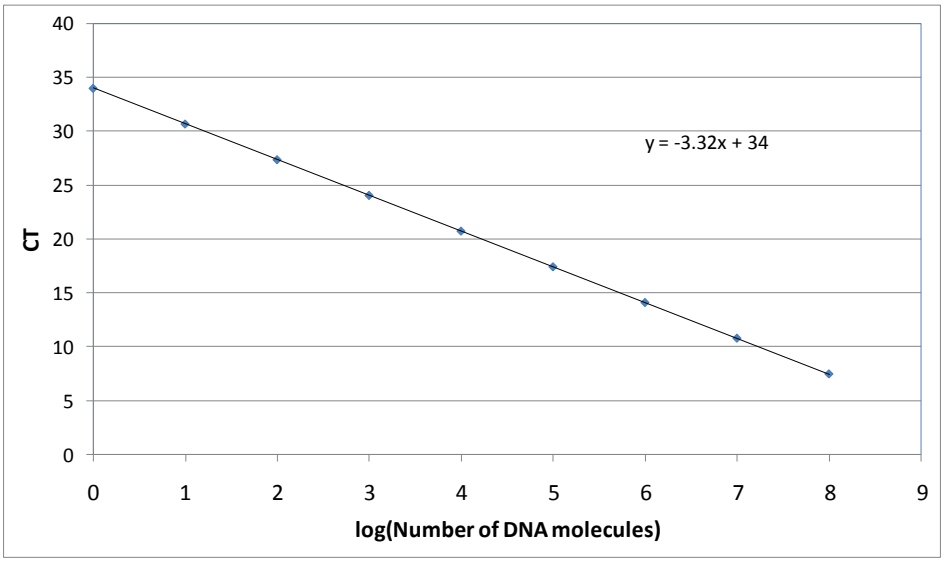

Figure 1.9 Ideal standard curve for rt-PCR.

Quantification of the target in unknown samples is achieved by interpolation of their CT's within the standard curve. It should be noted that the use of a standard curve would give accurate results only if the PCR efficiencies for the standards and unknowns are identical. Significant error is possible if there are PCR inhibitors in the sample that are absent in the standards since the CT for the sample would be higher and the target content will be underestimated. This will be discussed further in the section "PCR inhibition and its effect on real-time PCR assays."

The previous discussion has shown that real-time PCR can accurately determine the number of copies of a particular DNA sequence in a sample. However, knowing the amount of DNA by itself is not particularly useful since it is usually the quantity of a specific microorganism that is needed. The DNA sequence chosen should therefore be able to distinguish the target group or species from other microorganisms. The rt-PCR results should also be converted to more relatable measures of microbial load such as biomass or cell concentrations. A

survey of the literature on the use of rt-PCR for microbial quantification gives a wide array of information: what microorganisms were studied, what primers or probes were used, what were the rt-PCR conditions, what was the PCR efficiency, etc. These details are important in the actual performance of the rt-PCR assay but in order to get an overview of the topic, this review will focus on the following general questions that are important for accurate quantification:

(1) What DNA sequences can be used for microbial identification?

(2) How are the rt-PCR results related to the amount of microorganisms present?

(3) How is PCR inhibition identified? What can be done to minimize its effect on the accuracy of rt-PCR assays?

3.4 What DNA sequences can be used for microbial identification?

To use rt-PCR to quantify the amount of microorganisms present, a DNA sequence unique to the desired taxonomic level (genus or species) for the target should be available. The development of PCR, mRNA reverse transcription, and DNA sequencing technology has enabled researchers to determine the nucleotide sequences of genes and even whole genomes. Comparative analysis of the genetic code for certain genes of microorganisms showed that their similarities and differences can be used to study how closely or distantly species are related (Kennedy and Clipson, 2003). Among the genes that can be used, the most widely utilized for analyzing phylogenetic relationships is the one that codes for the ribosomal RNA, designated as rDNA (White et al., 1990). Hibbett (1992) gives the following reasons why rDNA has been popular for molecular systematics:

1. *Ribosomal RNA can be easily isolated and sequenced.* This has led to the availability of a large database of microbial rDNA sequences.

2. *There are multiple copies of rDNA in microbial genomes*. This greatly increases the probability of successful amplification by PCR even if the number of cells in the sample is low.

3. *The rDNA gene has many strongly conserved and variable regions.* This makes possible consistent comparisons at many taxonomic levels among microorganisms.

For most eukaryotes (including fungi), the ribosome consists of two components which are known as the large (60S) and small (40S) subunits. Each subunit has rRNA as a structural molecule together with several associated proteins. The large subunit is made up of the 28S, 5.8S and 5S rRNA molecules while the small subunit contains the 18S rRNA molecule. The genes coding for these rRNA molecules are separated by the internally transcribed spacer regions (ITS) as shown in Figure 5 (Kennedy and Clipson, 2003). The DNA sequence for the 18S rRNA in the small subunit evolves relatively slowly and has been found to be suitable for investigating distantly related organisms. The ITS sequence, on the other hand, has evolved the fastest and is observed to vary among species within a genus. These differences have made the rDNA region an invaluable tool for identifying microbial groups by molecular biology methods. The primers are initially chosen based on the known DNA sequences but actual testing using a panel of non-target challenge microorganisms is needed to ensure that only the template from the fungi of interest is amplified by PCR (Haugland et al., 2004; Weber et al., 2009; White et al., 1990; Wu et al., 2002).

Figure 1.10 The ribosomal RNA gene structure in fungi

Real-time PCR assays that target the rDNA region have been used to quantify fungi that contaminate agricultural crops with mycotoxins. Luo et al. (2009) developed an assay based on the ITS region that measured the conidial density of aflatoxin-producing *Aspergillus flavus* and *A. parasiticus*. The protocol was tested on soil samples from almond and pistachio orchards in California with good results. *A. flavus* was also measured by Mideros et al. (2009) on maize kernels with an assay using the ITS1 region. Another assay for *A. flavus* was developed by Cruz et al. (2008) based on the ITS2 region and a small portion of the 28S rDNA. Fungi that produce the harmful substance ochratoxin A have also been quantified by rt-PCR. An assay for *Aspergillus ochraceus* and *A. westerdijkiae* based on the ITS1-5.8S-ITS2 region was developed for use on coffee beans and grape berries (Gil-Serna et al., 2009). Another ochratoxin A producer , *A. carbonarius* , was quantified by an ITS2-dependent method that was also tested on grapes (Gonzales-Salgado et al., 2009).

A comprehensive study on the use of the ITS region for rt-PCR assays of the most common fungi in indoor environments that produce allergens and mycotoxins (total of 65 species) was undertaken by Haugland and coworkers (2004). Primers that can distinguish between *Aspergillus*, *Penicillium*, and *Paecilomyces* species within this group were identified and tested. These are now posted at http://www.epa.gov/nerlcwww/moldtech.htm#primers. Vesper et al. (2008) used the primers from this collection to quantify molds in dirt inside vacuum bags from the International Space Station. Among the 39 molds that were tested for, the most noteworthy were *Aspergillus flavus, A. niger, Penicillium chrysogenum,* and *P. brevicompactum*. A study that measured the amount of allergy-causing fungi in homes was conducted by Bellanger et al. (2009) using the primers designed by Haugland for *Cladosporium sphaerospermum,*

Penicillium chrysogenum, *Aspergillus versicolor*, *Alternaria alternata* and *Stachybotrys chartarum*.

Other fungi that have been quantified by rt-PCR using the ITS regions include the biocontrol agent *Trichoderma harzianum* (Lopez-Mondejara et al., 2010), the ectomycorrhizal fungi *Piloderma Croceum* (Raidl, S.R. et al., 2005), and the wood decomposer (white-rot fungi) *Trametes versicolor* (Eikenes, M. et al., 2005). Fungi involved in the spoilage of orange juice were investigated by Wan et al. (2006) using rt-PCR based on the 18S rDNA of *Byssochlamys fulva, Penicillium digitatum* and *Penicillium* sp. KW01 isolate.

A few studies using rt-PCR based on sequences other than that from the rDNA region have also been reported. Savazzini et al. (2008) successfully measured the amount of a *Trichoderma atrovide* mutant used as a biocontrol agent with an assay involving the endochitinase 42 gene. Eleven species of the phytopathogenic *Fusarium* genus were quantified on cereals using an rt-PCR assay based on the elongation factor 1 α gene (Nicolaisen et al., 2009). Eikenes et al. (2005) monitored the DNA concentration of the dioxin-degrading white rot fungi *Pleurotus pulmonarius* in soil with rt-PCR designed from the manganese peroxidase gene.

3.5 How are the rt-PCR results related to the amount of fungi present?

Since microbial load is more useful if expressed in terms of biomass or conidial density, the number of DNA molecules that is reported by a real-time PCR assay is usually related to these. Experimentally, it is much easier to quantify spores than biomass so most of the papers on rt-PCR quantification of fungi use a standard curve based on solutions of known conidial concentrations with the linear range spanning up to seven tenfold dilutions (10 to 10^7 spores). This has been reported for aflatoxin-producing fungi (Cruz and Buttner, 2008; Luo et al., 2009)

and common fungal allergens in buildings (Haugland et al., 2004; Bellanger et al., 2009). The assay results from test samples can only be reported as equivalent spore counts since target DNA could also have come from mycelia.

The study by Yamaguchi et al. (2009) related the amount of DNA to actual biomass by first growing the *Pleurotus pulmonarius* in liquid media for two weeks in the dark and then harvesting them by filtration. The collected solids were subsequently freeze-dried and DNA extracted from a known mass of the dried fungi. This allowed correlation of the rt-PCR results to fungal biomass. However, this method may not apply to cases where the system of interest involves fungi growing on solid substrate since there is the possibility that the DNA-biomass ratio here is not the same as the one derived using liquid culture. The growth rate and physiology of the fungi in the two kinds of media would most probably also be different.

A study that attempted to relate rt-PCR data with biomass from fungi growing on solid media are those involving Raidl's research group (Raidl et al., 2005; Lopez-Mondejara et al., 2010). Their methodology involves growing the fungi on thin layers of agar covering a glass slide, taking digital pictures of the mycelia and then using image analysis to measure the total hyphal length. The hyphae were assumed to be perfect cylinders and their volume calculated by using an average diameter. The resulting hyphal volume was then converted into dry weight by using the density of 0.22 g cm^{-3} given by Fogel and Hunt (1978) for dried fungal biomass. The mycelia on the slide were then subjected to DNA extraction and rt-PCR performed afterwards. This methodology was used in the quantification of the ectomycorrhizal fungi *Piloderma Croceum* (Raidl, S.R. et al., 2005) and biocontrol agent *Trichoderma harzianum* (Lopez-Mondejara et al., 2010). The results gave high standard deviations (16%) for the ratio of number of DNA molecules to biomass even though the fungi were grown under identical conditions and

observed after equal incubation periods. The linear correlation between amount of DNA and hyphal length only gave a regression coefficient (R^2) of 0.749. Since it is expected that the number of copies of DNA is directly proportional to the microbial load, most of the error were attributed to the difficulty in accounting for all the individual hyphae in the pictures due to insufficient contrast, especially in areas of thick growth. The process of measuring the hyphal lengths also proved to be the most time-consuming step.

The problem of measuring fungal biomass from solid cultures have been explored in studies investigating how mycelial weight can be determined indirectly by correlating it with colony diameter or chemical assays of fungi-specific components like chitin, glucosamine or ergosterol. One method is by growing the fungi on agar, melting the agar, and then weighing the recovered mycelia after drying (Taniwaki et al., 2006). This procedure is more easily done using gelling agents that lower the melting point of the solid media (Reeslev and Kjoller, 1995). Another method is to culture the fungi on agar covered with autoclaved porous cellophane and then collecting the mycelia for weighing. Studies have shown that growth by most fungi is not affected by the cellophane, indicating that diffusion of substances through the membrane is fast enough (Marin et al, 2005; Ramos et al., 1999; Reeslev et al., 2003).

3.6 PCR inhibition and its effect on real-time PCR assay

The accepted mechanism for PCR amplification predicts that the number of target DNA should double every cycle. In practice, PCR runs do not reach this theoretical replication rate and so have PCR efficiencies less than 100%. Studies have shown that certain substances, designated as PCR inhibitors, contribute to this decrease in amplification efficiency. For conventional PCR, inhibition becomes a problem only if it is to the extent that no PCR takes place even when the target is present (false negative result). This is not the case for real-time PCR since the Ct

method used for quantifying initial DNA content requires that the PCR efficiency for both the reference solutions used in the construction of the standard curve and the unknown test samples be the same to give reliable results. Inhibitors present in the sample but not in the standards reduces the amplification rate of the target DNA in the unknown, resulting in more cycles needed to reach the threshold fluorescence. This higher Ct would lead to an underestimation of the amount of DNA in the sample when the standard curve is used. Note that inhibition by itself is not the problem for rt-PCR; accurate results can still be possible even with reduced PCR efficiency as long as it is the same for both the reference and test samples.

The inhibitors are usually present in the samples themselves and are co-purified together with the DNA. They have been identified in body fluids (e.g., hemoglobin, urea, and heparin), food constituents (e.g., organic and phenolic compounds, glycogen, and fats), and environmental compounds (e.g., phenolic compounds, humic acids, and heavy metals). Other inhibitors may be due to contamination and include constituents of bacterial cells, non-target DNA, pollen, glove powder, laboratory plasticware, and cellulose (Wilson, 1997).

Inhibitors have been shown to decrease PCR efficiency through the following mechanisms (Wilson, 1997; Opel et al., 2010):

1. They bind, modify, or even degrade the DNA template or primer so that less will be available for amplification,
2. They decrease the activity of the DNA polymerase, and
3. They interfere with other PCR reagents (e.g. chelating substances can decrease the effective Mg^{2+} concentration in the reaction mixture).

Protocols for DNA extraction from samples that are known to have PCR inhibitors usually include the addition of a substance that has a strong affinity for the inhibitors to minimize their negative effect on PCR efficiency. Dilution of samples, as with enrichment culture in the presence of potential growth inhibitors such as spices and disinfectants, provides a simple method that can facilitate amplification, albeit with reduced sensitivity. The sensitivity of PCR can be exploited to amplify target DNA that is still present when inhibitors have been diluted out

The use of positive controls to determine the degree of PCR inhibition may not always be accurate since Huggett et al. (2008) has shown that the PCR efficiencies of different amplicon and primer sets are not affected to the same extent by co-purified inhibitors. The reason for the different responses was not clear since no correlation was found between the degree of inhibition and primer/amplicon characteristics such as size, T_m, GC content, and tendency to form secondary structures.

It is recommended that the efficiency of the rt-PCR be calculated from the slope of data from rt-PCR runs using serial dilution of the sample and then use only those with efficiencies comparable to that of the standard curve (Bustin et al., 2009).

REFERENCES

Adams, P. S. "Data Analysis and Reporting." *Real Time PCR*. Ed. T. M. Dorak. 1st ed. New York, U.S.A.: Taylor & Francis, 2006. 39-62.

Arya, M., et al. "Basic Principles of Real-Time Quantitative PCR." *Expert review of molecular diagnostics* 5.2 (2005): 209-19.

Balasubramaniam, R., et al. "Analysis of Heat and Mass Transfer during Condensation Over a Porous Substrate." *Annals of the New York Academy of Science* 1077. September (2006): 459-70.

Bellanger, A-P, et al. "Indoor Fungal Contamination of Moisture-Damaged and Allergic Patient Housing Analysed using Real-Time PCR." *Letters in applied microbiology* 49.2 (2009): 260-6.

Brooker, Donald B., Fred W. Bakker-Arkema, and Carl W. Hall. *Drying and Storage of Grains and Oilseeds*. 1st ed. NY, New York USA: Van Nostrand Reinhold, 1992.

Bustin, S. A., et al. "The MIQE Guidelines: Minimum Information for Publication of Quantitative Real-Time PCR Experiments." *Clinical chemistry* 55.4 (2009): 611-22.

Castillo-Araiza, C. O., H. Jimenez-Islas, and F. Lopez-Isunza. "Heat-Transfer Studies in Packed-Bed Catalytic Reactors of Low tube/particle Diameter Ratio." *Industrial & Engineering Chemistry Research* 46.23 (2007): 7426-35.

Cruz, P., and M. P. Buttner. "Development and Evaluation of a Real-Time Quantitative PCR Assay for *Aspergillus Flavus* ." *Mycologia* 100.5 (2008): 683-90.

Datta, A. K. "Porous Media Approaches to Studying Simultaneous Heat and Mass Transfer in Food Processes. I: Problem Formulations." *Journal of food engineering* 80.1 (2007): 80-95.

Eckart, Peter. *Spaceflight Life Support and Biospherics*. Torrance, Calif.; Dordrecht; Boston: Microcosm Press ; Kluwer Academic, 1996.

Eikenes, M., et al. "Comparison of Quantitative Real-Time PCR, Chitin and Ergosterol Assays for Monitoring Colonization of *Trametes Versicolor* in Birch Wood." *Holzforschung* 59.5 (2005): 568-73.

Faghri, A., and L. C. Chow. "Forced Condensation in a Tube with Suction at the Wall for Microgravitational Applications." *Journal of heat transfer-Transactions of the ASME* 110.4A (1988): 982-5.

Fisher, J. W., Hogan, J.A., Delzeit, L., Wignarajah, K., Alba, R., Pace, G. Fox, T.A. "Water Recovery from Wastes in Space Habitats - a Comparative Evaluation of SBIR Prototypes." 39th International Conference on Environmental Systems. Savannah, GA, July 2009.

Fogel, R., and G. Hunt. "Fungal and Arboreal Biomass in a Western Oregon Douglas-Fir Ecosystem - Distribution Patterns and Turnover." *Canadian journal of forest research revue canadienne de recherche forestiere* 9.2 (1979): 245-56.

Frankel, N. A., and S. G. Bankoff. "Laminar Film Condensation on a Porous Horizontal Tube with Uniform Suction Velocity." *Journal of heat transfer-Transactions of the ASME* 87.1 (1965): 95-102.

Gennes, Pierre-Gilles de. *Capillarity and Wetting Phenomena* : Drops, Bubbles, Pearls, Waves. Ed. Francoise Quéré Brochard-Wyart David. New York: Springer, 2004.

Gil-Serna, J., et al. "ITS-Based Detection and Quantification of *Aspergillus Ochraceus* and *Aspergillus Westerdijkiae* in Grapes and Green Coffee Beans by Real-Time Quantitative PCR." *International journal of food microbiology* 131.2-3 (2009): 162-7.

Gonzalez-Salgado, A., et al. "Specific Detection of *Aspergillus Carbonarius* by SYBR Green and Taqman Quantitative PCR Assays Based on the Multicopy ITS2 Region of the rRNA Gene." *FEMS microbiology letters* 295.1 (2009): 57-66.

Hasan, M. M., et al. "Conceptual Design of a Condensing Heat Exchanger for Space Systems using Porous Media." 35th International Conference on Environmental Systems (ICES). Rome, Italy, July 2005.

Haugland, R. A., et al. "Quantitative PCR Analysis of Selected *Aspergillus, Penicillium* and *Paecilomyces* Species." *Systematic and applied microbiology* 27.2 (2004): 198-210.

Hibbett, D. S. "Ribosomal RNA and Fungal Systematics." *Transactions of the mycological society of Japan* 33.4 (1996): 533-56.

Hoang, M. L., et al. "A Continuum Model for Airflow, Heat and Mass Transfer in Bulk of Chicory Roots." *Transactions of the ASAE* 46.6 (2003): 1603-11.

Hunter, J. B., et al. "Energy-Efficient Closed Loop Heat Pump Dryer for Solid Waste Stabilization on Long Duration Space Missions." 36th International Conference on Environmental Systems. Norfolk, VA, July 2006.

Huggett, J. F., et al. "Differential Susceptibility of PCR Reactions to Inhibitors: An Important and Unrecognised Phenomenon." *BMC research notes* 1.70 (2008).

Kennedy, N., and N. Clipson. "Fingerprinting the Fungal Community." *Mycologist* 17.part 4 (2003): 158-64.

Khan, I., and M. M. Hasan. "Porous Media Based Phase Separation in Condensing Heat Exchanger for Space Systems." 36th International Conference on Environmental Systems. Norfolk, VA, USA, July 2006.

Kowalski, S. J., ed. *Drying of Porous Materials*. London: Springer, 2007.

Kubista, M., et al. "The Real-Time Polymerase Chain Reaction." *Molecular aspects of medicine* 27.2-3 (2006): 95-125.

López-Mondéjara, R., et al. "Quantification of the Biocontrol Agent *Trichoderma harzianum* with Real-Time TaqMan PCR and its Potential Extrapolation to the Hyphal Biomass." *Bioresource Technology* 101.8 (2010): 2888-91.

Luo, Y., et al. "Quantification of Conidial Density of *Aspergillus flavus* and *A. Parasiticus* in Soil from Almond Orchards using Real-Time PCR." *Journal of applied microbiology* 106.5 (2009): 1649-60.

Mackay, I. M., et al. "Quantification of Microorganisms - Not Human, Not Simple, Not Quick." Real-Time PCR in Microbiology. from *Diagnosis to Characterization*. Ed. I. M. Mackay. 1st ed. Norwich , United Kingdom: Caister Academic Press., 2007. 133-182.

Makimura, K., et al. "Fungal Flora on Board the Mir-Space Station, Identification by Morphological Features and Ribosomal DNA Sequences." *Microbiology and immunology* 45.5 (2001): 357-63.

Marin, S., et al. "Fitting of Colony Diameter and Ergosterol as Indicators of Food Borne Mould Growth to Known Growth Models in Solid Medium." *International journal of food microbiology* 121.2 (2008): 139-49.

Marin, S., A. J. Ramos, and V. Sanchis. "Comparison of Methods for the Assessment of Growth of Food Spoilage Molds in Solid Substrates." *International journal of food microbiology* 99.3 (2005): 329-41.

Mideros, S. X., et al. "*Aspergillus flavus* biomass in Maize Estimated by Quantitative Real-Time Polymerase Chain Reaction is Strongly Correlated with Aflatoxin Concentration." *Plant disease* 93.11 (2009): 1163-70

Newbold, D. D. (1993). Analysis of a membrane-based condensate recovery heat exchanger (CRX). SAE PAPER 932089.

Nicolaisen, M., et al. "Real-Time PCR for Quantification of Eleven Individual *Fusarium* Species in Cereals." *Journal of microbiological methods* 76.3 (2009): 234-40.

Nitsche, A. "Oligonuleotide Design for in-House Real-Time PCR Applications in Microbiology." *Real-Time PCR in Microbiology*. Ed. I. M. Mackay. 1st ed. Norfolk, UK: Caister Academic Press, 2007. 41-69.

Opel, K., D. Chung, and B. R. McCord. "A Study of PCR Inhibition Mechanisms using Real Time PCR." *Journal of forensic sciences* 55.1 (2010): 25-33.

Ponchel, F. "Real-Time PCR using SYBR Green." *Real-Time PCR*. Ed. T. M. Dorak. 1st ed. New York, U.S.A.: Taylor & Francis, 2006. 139-154.

Raidl, S., R. Bonfigli, and R. Agerer. "Calibration of Quantitative Real-Time Taqman PCR by Correlation with Hyphal Biomass and its Copies in Mycelia of *Piloderma croceum*." *Plant biology* 7.6 (2005): 713-7.

Ramos, A. J., N. Magan, and V. Sanchis. "Osmotic and Matric Potential Effects on Growth, Sclerotia and Partitioning of Polyols and Sugars in Colonies and Spores of *Aspergillus Ochraceus*." *Mycological research* 103 (1999): 141-7.

Reeslev, M., and A. Kjoller. "Comparison of Biomass Dry Weights and Radial Growth-Rates of Fungal Colonies on Media Solidified with Different Gelling Compounds." *Applied and environmental microbiology* 61.12 (1995): 4236-9.

Savazzini, F., et al. "Real-Time PCR for Detection and Quantification of the Biocontrol Agent *Trichoderma atroviride* Strain SC1 in Soil." *Journal of microbiological methods* 73.2 (2008): 185-94.

Scovazzo, P., et al. "Hydrophilic Membrane-Based Humidity Control." *Journal of membrane science* 149.1 (1998): 69-81.

Scovazzo, P., A. Hoehn, and P. Todd. "Membrane Porosity and Hydrophilic Membrane-Based Dehumidification Performance." *Journal of membrane science* 167.2 (2000): 217-25.

Shipley, G. L. "An Introduction to Real-Time PCR." *Real-Time PCR*. Ed. T. M. Dorak. 1st ed. New York, U.S.A.: Taylor & Francis, 2006. 1-37.

Taniwaki, M. H., et al. "Comparison of Hyphal Length, Ergosterol, Mycelium Dry Weight, and Colony Diameter for Quantifying Growth of Fungi from Foods." *Advances in food mycology* 571 (2006): 49-67.

Tsotsas, E. and A.S. Mujumdar, eds. *Modern Drying Technology*. Weinheim: Wiley-VCH, 2007.

Turner, Ian and A.S. Mujumdar, eds. *Mathematical Modeling and Numerical Techniques in Drying Technology*. New York: Marcel Dekker, 1997.

Vesper, S. J., et al. "Mold Species in Dust from the International Space Station Identified and Quantified by Mold-Specific Quantitative PCR." *Research in microbiology* 159.6 (2008): 432-5.

Wang, C. X., et al. "Influence of Contact Angle and Tube Size on Capillary-Driven Flow Under Microgravity." *AIAA Journal* 47.11 (2009): 2642-8.

Wan, K., et al. "Rapid, Specific, and Sensitive Detection of Spoilage Molds in Orange Juice using a Real-Time Taqman PCR Assay." *Journal of food protection* 69.2 (2006): 385-90.

Weber, S. D., et al. "The Diversity of Fungi in Aerobic Sewage Granules Assessed by 18s rRNA Gene and its Sequence Analyses." *FEMS microbiology ecology* 68.2 (2009): 246-54.

White, T. J., et al. "Amplification and Direct Sequencing of Fungal Ribosomal RNA Genes for Phylogenetics." *PCR Protocols: A Guide to Methods and Applications*. Ed. M. A. Innis, et al. 1st ed. San Diego, CA, USA: Academic Press, Inc., 1990. 315-322.

Wilson, I. G. "Inhibition and Facilitation of Nucleic Acid Amplification." Applied and Environmental Microbiology 63.10 (1997): 3741-51.

Wu, Z., X. R. Wang, and G. Blomquist. "Evaluation of PCR Primers and PCR Conditions for Specific Detection of Common Airborne Fungi." *Journal of environmental monitoring* 4.3 (2002): 377-82.

Yamaguchi, M., et al. "Quantification of the Mycelial Mass of the White-Rot Fungus *Pleurotus Pulmonarius* by Real-Time PCR." *Bulletin of the forestry and forest products research institute* 411 (2009): 133-41.

Yang, Ji Wu. "Effect of Uniform Suction on Laminar Film Condensation on a Porous Vertical Wall." Journal of Heat Transfer-Transactions of the ASME 92.2 (1970): 252-256.

CHAPTER 2

MODELING AND SIMULATION OF THE DRYING OF CABIN SOLID WASTE IN LONG-TERM SPACE MISSIONS

INTRODUCTION

This study is part of a research project on the use of an energy-efficient closed air-loop heat-pump dryer system (DRYER) for astronaut cabin waste (Hunter et al., 2006). Wet trash, including food residues, moist hygiene wipes and wet paper towels, poses two problems on long term space missions: first, the generation of odors and potential health hazards by microbial growth; second, the diversion of water from the available recovery loops. The DRYER system is designed to stop microbial activity by both pasteurization and desiccation, and to recover humidity from the closed air loop in a gravity-independent Porous Media Condensing Heat Exchanger. Finally, the DRYER system may be adapted for use in the drying of crew laundry, water recovery from water-reprocessing brines, and ultimately, food and biomass drying in a biogenerative life support system.

Optimization of the entire closed-loop system consisting of dryer, condenser, and heat-recovery modules requires a computational model. The schematic for the system is shown in Figure 2.1a. We present here the formulation and validation for the packed-bed trash drying component of that model. The experimental studies needed to obtain model parameters and data for validation were conducted in an open air-loop prototype constructed for research on the heat and mass transport aspects of trash drying (Figure 2.1b). The prototype was designed in collaboration with and fabricated by Orbital Technologies Corporation. (ORBITEC).

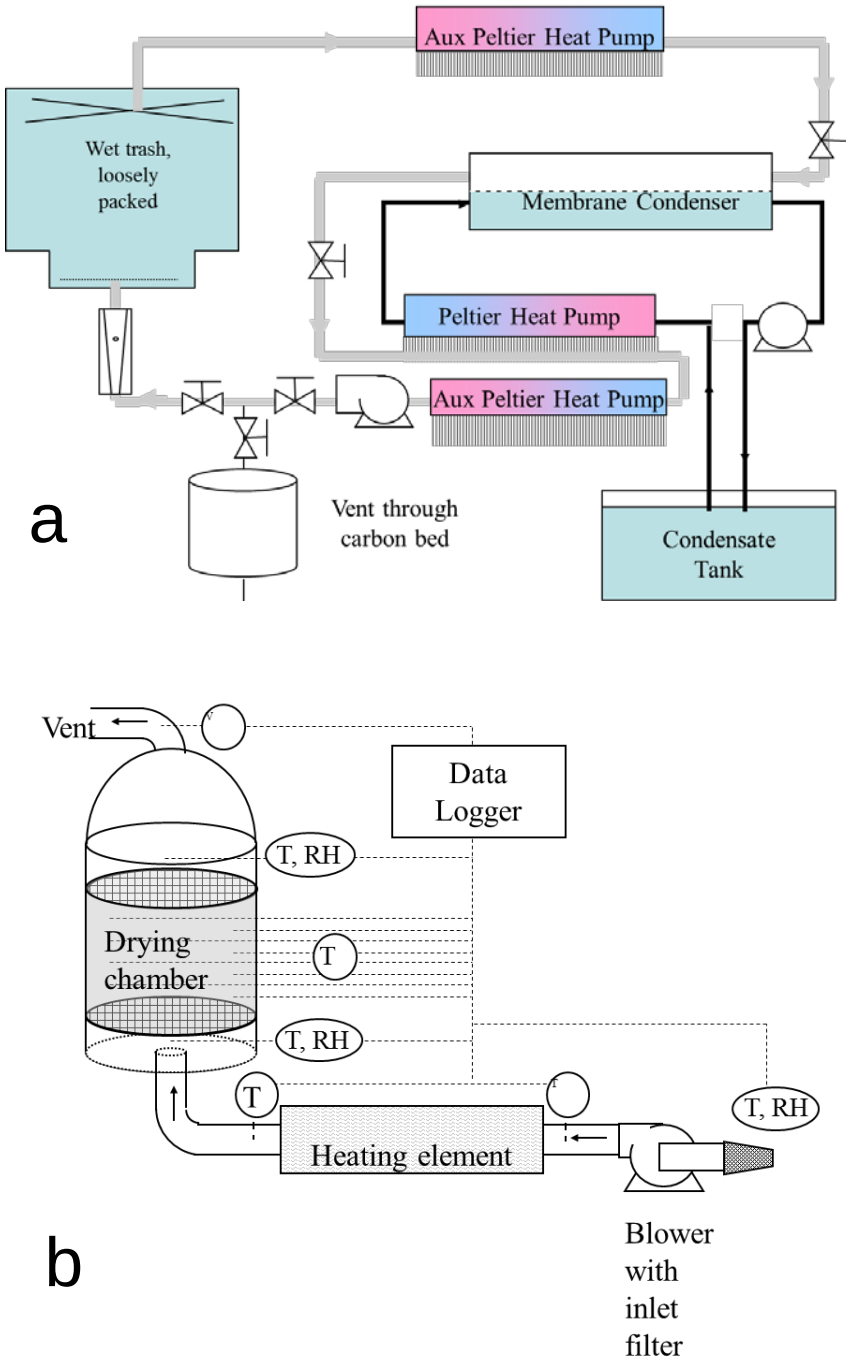

Figure 2.1 (a) Schematic of projected overall closed-loop dryer system. (b) Experimental set-up used for trash drying in the study.

Though a key purpose of trash drying is to prevent spoilage, microbial activity in the trash was not considered in this work for two reasons. First, the DRYER is intended to recover water from trash before substantial decomposition has occurred. Second, due to the low quantity of easily biodegradable matter, and the brief drying period, never exceeding 12 hours, only an insignificant amount of metabolic water could be produced during drying. Microbial activity in dried, stored trash remains an important issue in design of solid waste handling for space flight and is being addressed in a separate study.

MODEL DEVELOPMENT

Problem description

The cylindrical dryer is represented by an axi-symmetric geometry (Figure 2.2). The trash bed is modeled as porous media with large pores (Hoang et al., 2003; Datta, 2007). It is assumed that a pseudo-homogeneous continuum model can be used for the system (Castillo-Araiza et al., 2007). The control volume contains both solid and gas phases with each one having a different temperature (two-temperature model). The solid phase consists of wet and dry pieces of trash while the gas is made up of air and water vapor. The left and right sides of the dryer are assumed to be perfectly insulated (heat and mass flux are both equal to zero). This condition would make the temperatures and moisture contents of the solid and gas phases a function only of the distance from the bottom at any time (1-D model, variation along the z-axis only).

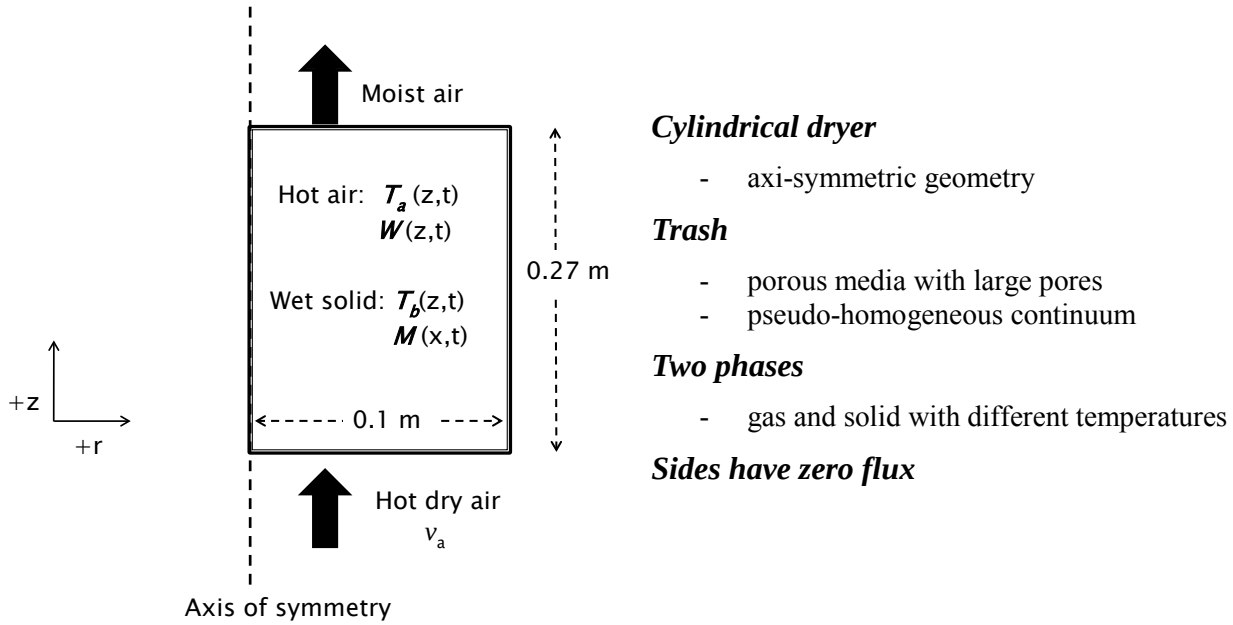

Figure 2.2 Schematic of the axi-symmetric computational domain used in the model. The dryer is represented by a pseudo-homogeneous continuum model with two phases: gas and solid. The variables of interest are the temperature and moisture content in each phase.

Assumptions

Several simplifying assumptions were used in the formulation of the model. The porosity and dry solid composition of the bed are assumed to be both spatially uniform and constant with time (negligible shrinkage and settling). The physical and transport properties of the trash and humid air do not significantly change across the operating temperature range (25 to 60°C). The air velocity throughout the bed of trash is assumed to be constant. This plug flow assumption is justified by the following: (1) expansion of the gas due to decrease in pressure could be neglected since the observed pressure drop was small across the trash bed (<10 mmHg), (2) the increase in mass flow from addition of water vapor to the gas stream was always less than 3.5% (0 to 80% humidity at 30°C), and (3) the maximum air temperature change, from the entering air

temperature of 60°C to the cold bed temperature of 25°C, corresponds only to a 10% increase in air volume. Diffusion of water in the bed is assumed to be negligible.

The trash is composed of wet and dry pieces and during drying, the temperatures of these two are expected to be different. Evaporation of water in the wipes would keep their temperature near the wet-bulb temperature (≈ 25°C) while the plastic pieces would tend to approach the temperature of the hot air passing them. In most cases the plastic will be hotter than the wet wipes and since they are in physical contact with each other, this should result in conduction heat transfer between them. The model assumes that this is not significant. This assumption is likely valid since the trash is not tightly packed (porosity = 0.91) and this greatly reduces the area for heat transfer by conduction.

A schematic representation of the model is given in Figure 2.3.

Governing equations

The equations for the model were derived from enthalpy and moisture mass balances on a differential volume within the dryer containing both the solid and gas phases (Brooker et al., 1992). The resulting four differential equations are given below. These are used to solve for the four unknowns: humidity ratio of the air ($\boldsymbol{W}$), moisture content in the wet components of the bed, dry basis ($\boldsymbol{M}$), air temperature ($\boldsymbol{T_a}$), and bed temperature ($\boldsymbol{T_b}$).

The balances for the solid bed are simplified by assuming that it is composed only of wipes (subscript $\boldsymbol{d}$) and plastic(subscript $\boldsymbol{p}$), where the plastic represented all dry materials including gloves and office paper, and the wipes represented all significantly wet materials, such as wet wipes and uneaten foods. Beverages in closed or nearly-closed vessels were not considered in the model. The same assumption was used in formulating a simplified ersatz trash for experimental determination of heat and mass transfer coefficients.

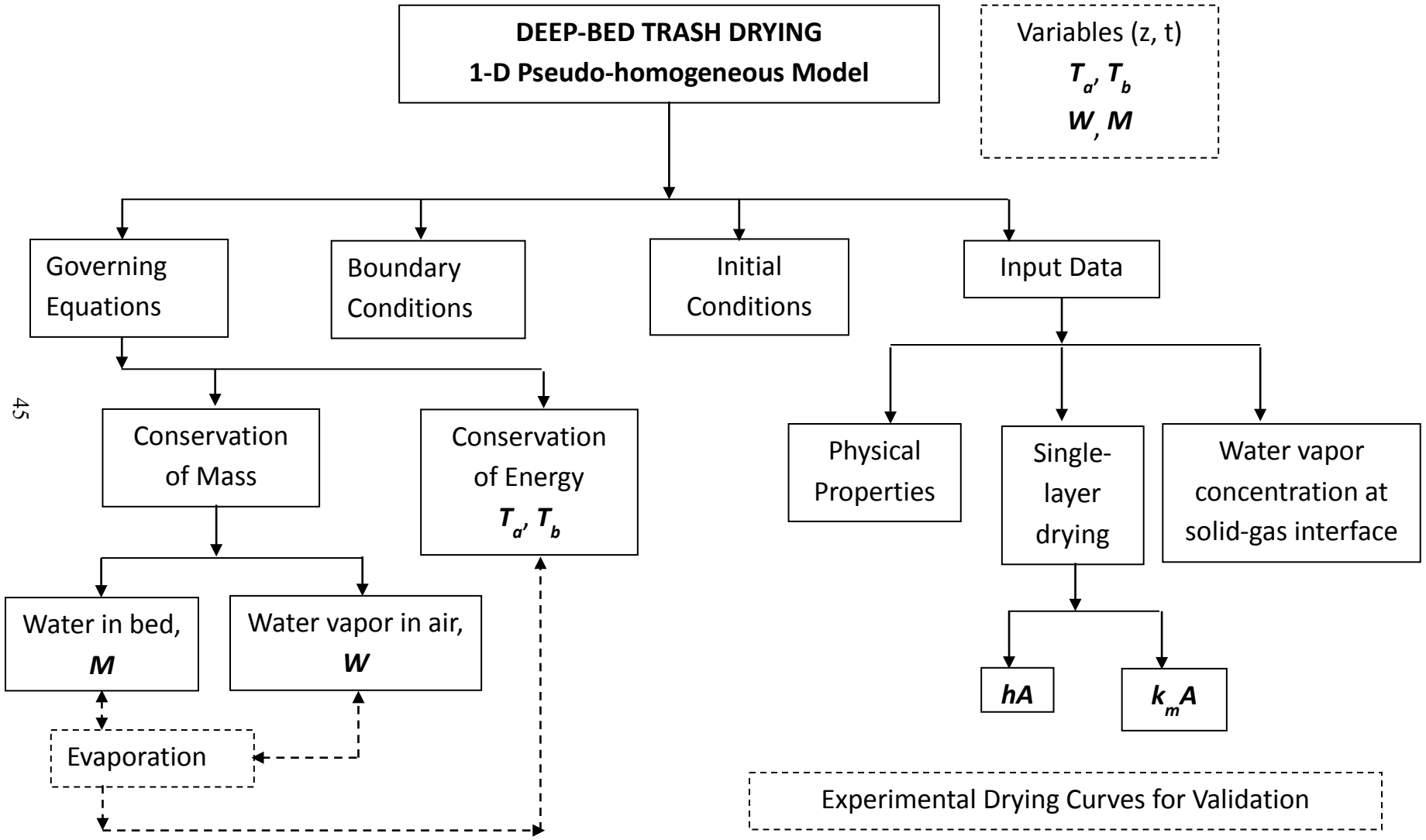

Figure 2.3 Summary of the model showing its components and their relationships. The subscripts are ***a*** for the gas phase and ***b*** for the solid phase.

It should be noted that the use of a single solid phase in the pseudohomogeneous model leads to loss of information about individual pieces of trash. This presents a problem for representing the temperature of the bed since as discussed earlier, the wet and dry components have different temperatures during drying. The model uses a "mean" temperature ($\boldsymbol{T_b}$) for the bed whose value would be between the temperatures of the wet and dry materials. The exact relationship is given by the following equation, for a basis of a unit mass of bone-dry trash solids:

$$\Delta H_{sensible} = \left[c_d X_d + c_p X_p + c_w M X_d\right] T_b = \left[c_d X_d + c_w M X_d\right] T_d + c_p X_p T_p \qquad (1)$$

where $\Delta H_{sensible}$ is the increase in sensible heat of the bed since the start of drying (when everything is at the same initial temperature), $\boldsymbol{c}$ is the specific heat capacity, $\boldsymbol{X}$ is the mass fraction (dry basis), and $\boldsymbol{T}$ is the temperature. The subscripts $\boldsymbol{d}$, $\boldsymbol{p}$, and $\boldsymbol{w}$ are for the bone-dry wipes, plastic and water, respectively. Since $\boldsymbol{M}$ decreases during drying, the relationship changes with time.

As defined by the model, $\boldsymbol{T_b}$ does not correspond to the temperature of the solids at any point in the system except at the end of drying when all the water has been removed and the initially-wet materials are approaching thermal equilibrium with the hot air. However, accurate spatial knowledge of temperature during a process is usually critical only when there are strongly exothermic reactions that may produce hot spots within the equipment. The high temperatures could lead to runaway reaction rates that would be a safety concern. In the trash drying studied here, there is no heat generation within the system and the temperature would always be between the initial and inlet air temperatures. The lack of information about the actual temperatures in the trash when using the model is therefore acceptable.

Solid-phase equations

Bed Enthalpy Balance

$$\rho_s(1-\varepsilon)\left[c_d X_d + c_p X_p + c_w M X_d\right]\frac{\partial T_b}{\partial t} = \underbrace{-m'\left[\Delta H_{vap} + c_v(T_a - T_b)\right]}_{\text{Heat effects associated with evaporation}} \underbrace{+ ha'(T_a - T_b)}_{\text{convective exchange between air and bed}} \quad (2)$$

The average density of the dry solids ($\boldsymbol{\rho_s}$) is computed using the following equation:

$$\rho_s = \frac{1}{\left(\frac{X_d}{\rho_d} + \frac{X_p}{\rho_p}\right)} \quad (3)$$

where $\boldsymbol{\rho_d}$ and $\boldsymbol{\rho_p}$ are the densities of the dry wipes and plastic, respectively.

Water mass balance in bed

$$\rho_s(1-\varepsilon)X_d\frac{\partial M}{\partial t} = -m' \quad (4)$$

Where ***m'*** is the volumetric evaporation rate in the dryer, kg water s^{-1} m^{-3}, assumed to be equal to the convective mass transfer between the bed and air:

$$m' = k_m a'\left(W_{surface} - W\right) \quad (5)$$

$\boldsymbol{W_{surface}}$ is the moisture content of air in contact with the surface of the wet solids.

Gas-phase equations

Ga-phase enthalpy balance for unit area of bed

$$[\rho_a c_a + \rho_a c_v W]\varepsilon\frac{\partial T_a}{\partial t} = \underbrace{\varepsilon\frac{\partial}{\partial z}\left[k_a\frac{\partial T_1}{\partial z}\right]}_{\text{conduction in air}} \underbrace{- [\rho_a v_a c_a + \rho_a v_a c_v W]\frac{\partial T_a}{\partial z}}_{\text{convective transport in air}} \underbrace{- ha'(T_a - T_b)}_{\text{convective exchange between air and bed}} \quad (6)$$

All evaporation takes place only in the solid phase so there is no latent heat term for the enthalpy balance in the gas phase.

Water vapor balance in gas

$$\varepsilon\rho_a \frac{\partial W}{\partial t} = \underbrace{\varepsilon\rho_a \frac{\partial}{\partial z}\left[D_v \frac{\partial W}{\partial z}\right]}_{\text{diffusion in air}} + \underbrace{m'}_{\text{evaporation}} - \underbrace{\rho_a v_a \frac{\partial W}{\partial z}}_{\text{convective transport in air}} \quad (7)$$

Boundary and initial conditions

The boundaries for the system are shown in Figure 2.2. For the solid-phase equations, all of these have conditions of flux = 0. The gas-phase equations also have zero flux conditions for the top, left and right boundaries. The bottom boundary is the air inlet temperature ($\boldsymbol{T_a} \approx 60°C$) and entering humidity ratio for Equations (5) and (6), respectively.

For the initial conditions, the solid phase has $\boldsymbol{M}$ (z, 0) = 2.75 g water (g bone-dry initially-wet solids)$^{-1}$ and $\boldsymbol{T_b}$ (z, 0) = 25°C. The gas phase is set to $\boldsymbol{T_a}$ (z, 0) = 25°C and $\boldsymbol{W}$(z,0) equal to the actual humidity ratio of the inlet air during the run (0.0015 to 0.003 kg water kg^{-1} dry air).

Numerical solution

Equations (2), (4), (6) and (7) were solved simultaneously using a commercially available finite element software, COMSOL Multiphysics (COMSOL Inc., Burlington, MA). The axi-symmetric computational domain is 0.27 m x 0.1 m and has a mesh with 350 x 4 quadrilateral elements. The model simulation gave temperature and moisture content values of the solid and gas phases within the dryer at a given time.

Input Parameters

The input parameters used in the simulations are given in the Table 2.1.

Table 2.1 Input parameters for the model

Parameter	**Symbol**	**Value**	**Units**	**Source**
Density				
Air	ρ_a	Ideal gas	kg m^{-3}	
Dry wipes (cotton)	ρ_d	1500	kg m^{-3}	Perry's Handbook of Chemical Engineering (2007)
Plastic (HDPE)	ρ_p	960	kg m^{-3}	Handbook of Chemistry and Physics
Specific heat capacity				
Air	c_a	1.0	kJ kg^{-1} K^{-1}	Brooker et al. (1992)
Dry wipes (cotton)	c_d	1.3	kJ kg^{-1} K^{-1}	Perry's Handbook of Chemical Engineering (2007)
Plastic (HDPE)	c_p	2.2	kJ kg^{-1} K^{-1}	www.matbase.com
Water vapor	c_v	1.88	kJ kg^{-1} K^{-1}	Brooker et al. (1992)
Water	c_w	4.186	kJ kg^{-1} K^{-1}	Perry's Handbook of Chemical Engineering (2007)
Diffusivity of water vapor in air	D_v	2.81 x 10^{-5}	m^2 s^{-1}	Perry's Handbook of Chemical Engineering (2007)
Thermal conductivity of air	k_a	28.5	kJ m^{-1} s^{-1} K^{-1}	Perry's Handbook of Chemical Engineering (2007)
Bed height	z	0.27	m	This study
Porosity	ε	0.91	m^3 voids m^{-3}	This study

EXPERIMENTAL METHODS

Deep bed trash drying runs

Drying experiments using ersatz trash were performed on the system shown in Figure 2.1B. The cylindrical drying chamber with a height of 30.5 cm and diameter of 20 cm was covered with 10 cm of thermal insulation to minimize heat loss to the surroundings. For each run, the dryer was uniformly loaded with 690 g of ersatz trash to give an uncompressed bed height of about 27 cm. The formulation of the ersatz trash has been described in detail by Hunter and coworkers (2006). The trash is composed by mass of 42.3% plastic pieces (high density polyethylene, 10 mil thickness), 26.6% baby wet wipes (moisture content adjusted to 73%, wet basis) (Huggies All-Natural, Kimberly-Clark, Neenah, WI, USA), 12.4% office paper, 10% dog food (to simulate food scraps, dry dog food plus water to give 73% moisture content, wet basis)(Science Diet, Hill's Pet Nutrition, Inc., Topeka, KS, USA), 5.3% duct tape, 2.1% Kim wipes (Kimberly-Clark, Neenah, WI, USA), and 1.1% non-latex laboratory gloves. The components and proportions of the ersatz trash were based on J. Levri's estimates in the 2002 edition of the Baseline Values and Assumptions Document (Hanford and Ewert, 2002). The calculated total moisture content of the ersatz trash is 0.375 g water g^{-1} bone-dry solids but nearly all of this water is present in the wet wipes and dog food. Considering only the wet materials, their initial moisture content is 2.75 g water g^{-1} bone-dry initially-wet solids. Figure 2.4 shows the dryer loaded with ersatz trash before an experimental run.

Ambient air heated to 60°C enters at the bottom, goes through the material, and then exits from the top. Three air superficial velocities were used in the runs: 1.2, 2.2, and 3.1 cm s^{-1} (380, 690, and 970 ml s^{-1}, respectively). Humidity probes (Hygrotron model, Hygrometrix, Alpine, CA, USA) and thermocouple probes (type J) were placed at the inlet and outlet of the

dryer to measure the percent relative humidity (% RH) and temperature, respectively, of the air entering and leaving the system. These were automatically recorded by an Agilent 34970A datalogger (Agilent Technologies, Santa Clara, CA, USA) every 20 seconds and the data used to calculate the rate of water loss from the bed (Evaporation rate). The evaporation rate was used to determine the total moisture content of the entire trash during drying and these data were used to construct the total moisture content vs. time plots (drying curves) for the batch being dried. The experimental drying curves are shown in Figure 2.8. Each set of conditions tested were performed at least twice with good agreement observed between the results.

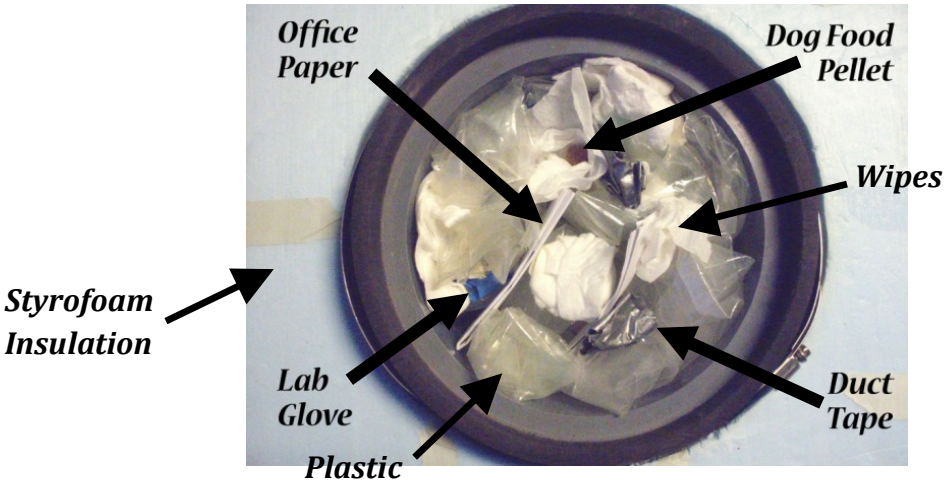

Figure 2.4 Top view of the dryer loaded with ersatz trash.

Determination of heat and mass transfer coefficients with transfer area

The model requires values for the heat and mass transfer coefficients for trash drying. Correlations for ***h*** and ***k*** can be found in the literature but they are for agricultural crops and regularly-shaped catalyst pellets which would not be suitable for the ersatz trash (Krokida et al., 2002). Moreover, the folding and crumpling of planar trash pieces in the vessel makes the parameter ***A***, the effective transfer area between the solids and air, difficult to estimate or even

to measure. A drying study was therefore conducted to determine the product of the transfer coefficients and area (***hA*** and $k_m A$) suitable to our system, using a thin-layer approach as is typical for drying experiments on agricultural materials (Brooker et al, 1992). The $k_m A$ for the drying of the single-layer combinations of wet-wipes and plastic pieces is given by the equation

$$m = k_m A\left(W_{surface} - W\right) \tag{8}$$

where ***m*** is the rate of evaporation, k_m is the mass transfer coefficient, ***A*** is the (unknown) total transfer area for the layer, $W_{surface}$ is the humid ratio of air on the surface of the wet solids, and ***W*** is the bulk humid ratio of air. The $k_m A$ can therefore be calculated if ***m***, $W_{surface}$, and ***W*** are known.

In the single-layer drying runs, the rate of evaporation from the bed was calculated from its loss in mass after regular time intervals (5 minutes). Drying proceeded until the total mass no longer changed between measurements. The constant rate period was identified as the initial linear portion of the drying curve. A humidity probe was used to measure the % RH of the air entering the dryer which is then converted to ***W***. Thermocouple probes were attached to the surface of the wet wipes and just below the single layer to measure the temperatures of the wet wipes and entering air, respectively. The data showed that the air inlet and wet wipes temperatures remained the same during the constant-rate period, further indicating that the system was at steady-state then. It was assumed that at this period, the gas in contact with the surface of the wet wipes would have a water activity of 1 and the $W_{surface}$ would be equal to the gas phase concentration corresponding to the vapor pressure of water at

the temperature of the wet wipes. From the $\boldsymbol{m}$, $\boldsymbol{W_{surface}}$, and $\boldsymbol{W}$ data, the $\boldsymbol{k_m A}$ can be calculated by rearranging Equation (8)

$$k_m A = \frac{m}{(W_{surface} - W)} \tag{9}$$

During the constant-rate drying period for a single layer of trash pieces, it is assumed that all the heat transferred to the bed is used only to evaporate water; no sensible heating takes place. Hence, the rate of heat transfer can be obtained from the evaporation rate:

$$q = m\, H_{vap} \tag{10}$$

The heat is transferred into the layer from the hot air by convection:

$$q = hA\left(T_{surface} - T_a\right) \tag{11}$$

The temperatures are measured during the runs so $\boldsymbol{hA}$ can be calculated:

$$hA = \frac{q}{(T_{surface} - T_a)} \tag{12}$$

Since the trash is about 70% by mass wet wipes and plastic (Hunter et al., 2006) combinations of these components were used as a simpler model of the trash. The plastic pieces were cut into rectangles of the same size as the wet wipes (19.5 by 17.7 cm) and were crumpled into rough spheres. The wet wipes were similarly crumpled. A single layer of crumpled plastic pieces and wet wipes placed in the dryer measured approximately 4.5 cm high. Hence 6 monolayers would form a 27-cm trash bed in the dryer.

There are about 24 wet wipes in a single batch of the ersatz trash used in the dryer runs, which fills the drying chamber to around 27 cm height. Considered in terms of layers, a uniform distribution of wet wipes would consist of 6 layers with 4 wipes in each. The single

layers of trash used in this study consisted of crumpled wet-wipes in multiples of four with sufficient crumpled plastic pieces added to just fill the layer (Table 2.2). The treatments with a higher proportion of wet wipes were intended for simulation of trash with more wet materials.

Table 2.2 Composition of single layers used in the experiment

Trash wet solids load	Number of wet wipes	Number of plastic pieces	Mass fraction, dry basis	
			wipes	plastic
Low	4	9	0.176	0.824
Medium	8	6	0.390	0.610
High	12	3	0.658	0.342

Drying of single layers was studied using air flow rates with superficial velocities of 1.2, 2.2, and 3.1 cm s^{-1}. At least two single-layer runs were done for each treatment level with excellent agreement among the replicates.

RESULTS AND DISCUSSION

Experimental Studies

Heat and mass transfer coefficients with transfer area

Figure 2.5 shows the linear relationship of $\boldsymbol{hA}$ to the inlet air flowrate at 60°C. Each graph for the different wet material loads in the simplified trash (4 wet wipes/9 plastic, 8 wet wipes/6 plastic, 12 wet wipes/3 plastic) represents a constant transfer area, and as expected, the $\boldsymbol{h}$ becomes larger as the air flowrate increases (Geankoplis, 2003). The $\boldsymbol{hA}$ also increases with more wet wipes present since the mass transfer area increases with the number of wet wipes. The resulting values for $\boldsymbol{k_mA}$ are shown in Figure 2.6. The effects of air flowrate and number of wet wipes on $\boldsymbol{k_mA}$ are similar to those observed for $\boldsymbol{hA}$.

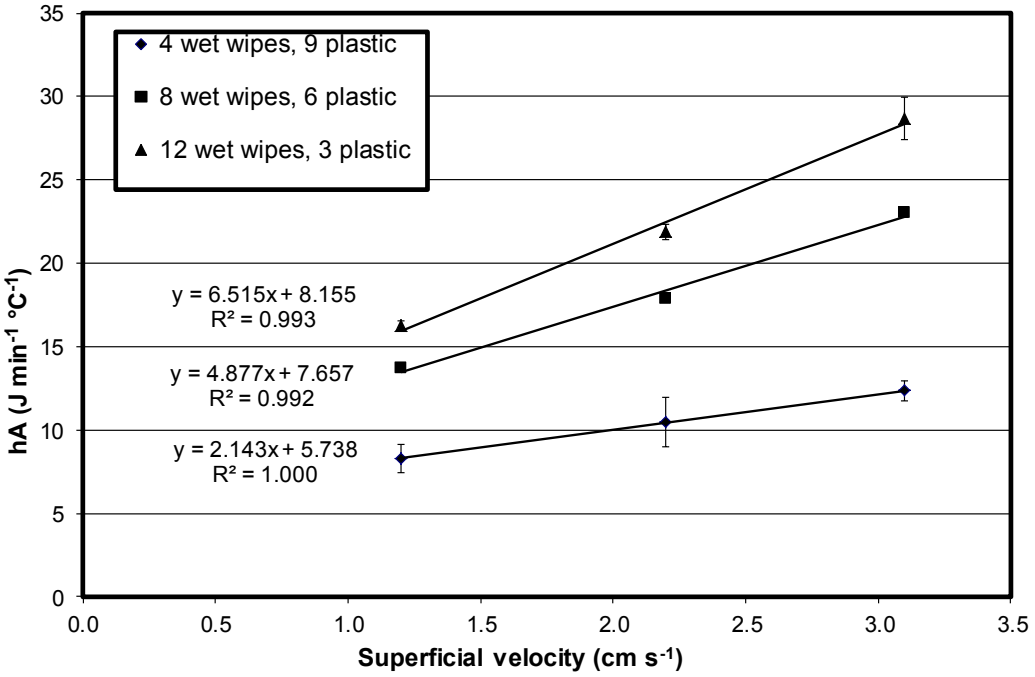

Figure 2.5 The effect of air inlet flowrate on the heat transfer coefficient-area parameter (hA) for different wet-wipes plastic combination (60^{o}C air temperature)

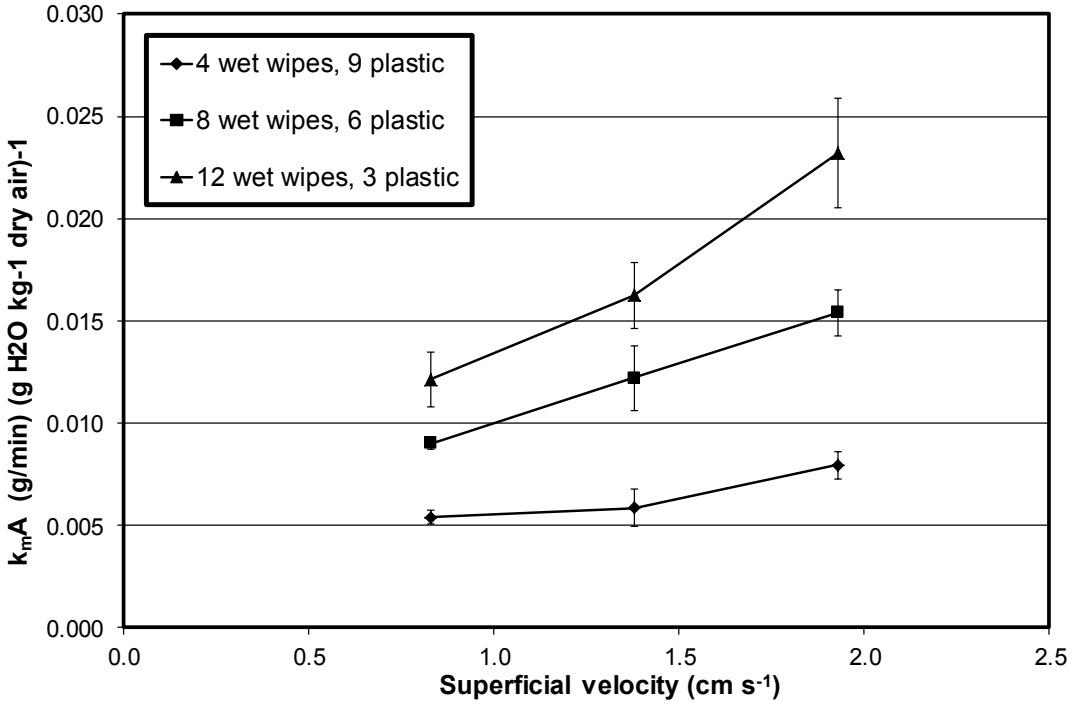

Figure 2.6 The effect of air inlet flowrate on the mass transfer coefficient-area parameter (k_mA) for different wet-wipes plastic combination (60^{o}C air temperature)

McCabe and coworkers (2005) state that the best way for determining the heat and mass transfer coefficients for drying is through experimental measurements. This should be especially true for our system since the trash pieces have irregular shapes and are made up of different materials. The correlations in the literature for predicting the transfer coefficients are therefore expected to provide poorer estimates for trash drying than direct experimentation so single-layer experiments were performed. However, in order to compare trends, the transfer coefficients are calculated from a literature correlation and compared with the experimental results. A correlation that may be applicable to the trash is that recommended for packed beds by Bird et al. (2002). The correlation is derived from a critical analysis of forced convection from gases and liquids flowing through shallow packed beds. It takes into account shape factors and the void volume of the bed. It is applicable to low Reynolds numbers and Prandtl numbers greater than 0.6 (Prandtl number for the system ≈ 0.71). The correlation gives the Chilton-Colburn heat transfer ($\boldsymbol{j_H}$) factor as a function of particle Reynolds number (***Re***):

$$j_H = 2.19\, Re^{-2/3} + 0.78\, Re^{-.381} \tag{13}$$

The $\boldsymbol{j_H}$ and ***Re*** are defined as follows:

$$j_H = \frac{h}{c_a\, \rho\, v_s} \left(\frac{c_a\, \mu}{k}\right)^{2/3} \tag{14}$$

$$Re = \frac{d_p \rho v_s}{(1-\varepsilon)\mu\psi} \tag{15}$$

where ψ is a shape factor, equal to 1 for spheres and 0.92 for cylinders.

The correlations solve for ***h*** but the experimental results give ***hA***. In order to compare the predicted values with the experimental ones, the effective surface area per unit volume of the single layer (***a'***) is required. This quantity is obviously not known for the trash, which is the reason why ***hA*** was the parameter determined in the single-layer experiments. However,

since a' is needed, it is estimated by assuming that the wipes and plastic pieces can be represented by smooth, rigid spheres with uniform diameter. This presents another problem since the diameters of the "spherical" trash pieces would also have to be known. The single layer is about 0.045 m high, so this value should be a good approximation for the diameter. For a packed bed of spheres with diameter d_p and porosity ε, the a' is given by (Bird et al., 2002):

$$a' = \frac{6(1-\varepsilon)}{d_p} \tag{16}$$

The actual porosity of the trash based on density is 0.91 but this includes the void space inside the crumpled plastic pieces. For a random packing of spheres, the porosity is within 0.36-0.40 (Scott, G. D. and Kilgour, D. M., 1969). The upper limit of 0.40 is used and with d_p =0.045 m, a' = 80 m^{-1}. The total volume of the single-layer is obtained from the dryer radius (0.10 m) and single-layer height:

$$V_{single\ layer} = \pi*(0.10\ m)^2*(0.045\ m) = 0.014\ m^3$$

The estimated transfer area for the single-layer is therefore:

$$A_{single\ layer} = a'*V_{single\ layer} = (80\ m^{-1})*(0.014\ m^3) = 0.113\ m^2$$

This transfer area is for all the pieces in the single layer but during the constant-rate drying period, only the wet wipes undergo mass and heat transfer so the transfer area for these wet pieces alone must be further estimated. This can be done by assuming that the following relationship is valid:

$$\frac{A_{wet\ wipes}}{A_{single\ layer}} = \frac{number\ of\ wet\ wipe\ pieces}{total\ number\ of\ pieces} \tag{16}$$

Estimated values of $A_{wet\ wipes}$ for the different combinations used in the single-layer drying experiments are given in Table 2.3

Table 2.3 The calculated transfer area for the wet wipe pieces during the constant-rate drying period for the different combinations of wipes and plastic used in the single-layer drying experiments.

Number of wet wipes	Number of plastic pieces	Total number of pieces	Wet wipe pieces divided by total number of pieces	$A_{wet\ wipes}$* (m^2)
4	9	13	0.308	0.035
8	6	14	0.571	0.065
12	3	15	0.800	0.090

$A_{wet\ wipes} = A_{single\ layer}$(wet wipe pieces/total number)*

The Reynolds numbers are obtained for the superficial velocities used (1.2, 2.2, and 3.1 cm s^{-1}) from Equation (15) and the corresponding j_H values are solved for using Equation (13). The calculated values for ***h*** are given in Table 2.4. The ***hA*** will vary with the number of wet wipe pieces; their values are given and then compared with experimental values for layers with 4, 8, and 12 wet wipe pieces in Table 2.5.

Table 2.4 The values of ***h*** obtained from the correlation, Eqn. (13)

Superficial velocity cm s^{-1}	Reynolds number	j_H	***h*** (kJ m^{-2} s^{-1} °C^{-1})
1.2	48	0.345	0.00561
2.2	87	0.253	0.00753
3.1	123	0.213	0.00894

Table 2.5 The values of ***hA*** from the correlation and estimated transfer areas for different air velocities and combinations of wet wipes and plastic pieces. These are compared with the experimental ***hA*** values from the single-layer runs.

4 wet wipes/ 9 plastic				
Superficial velocity cm s^{-1}	**hA (kJ s^{-1} °C^{-1})**	**hA (J min^{-1} °C^{-1})**	**Experimental hA (J min^{-1} °C^{-1})**	**% difference***
1.2	0.000195	11.71511	8.30	-41.1
2.2	0.000262	15.74212	10.47	-50.4
3.1	0.000311	18.66754	12.37	-50.9
8 wet wipes/ 6 plastic				
Superficial velocity cm s^{-1}	**hA (kJ s^{-1} °C^{-1})**	**hA (J min^{-1} °C^{-1})**	**Experimental hA (J min^{-1} °C^{-1})**	**% difference***
1.2	0.000363	21.75	13.73	-58.5
2.2	0.000487	29.23	17.92	-63.1
3.1	0.000578	34.67	23.02	-50.6
12 wet wipes/ 3 plastic				
Superficial velocity cm s^{-1}	**hA (kJ s^{-1} °C^{-1})**	**hA (J min^{-1} °C^{-1})**	**Experimental hA (J min^{-1} °C^{-1})**	**% difference***
1.2	0.000508	30.46	16.26	-87.3
2.2	0.000682	40.93	21.88	-87.1
3.1	0.000809	48.54	28.67	-69.3

**% difference = 100%*(hA from correlation – experimental hA)/experimental hA*

The dependence of the experimental ***hA*** values on velocity matches well the trend exhibited by the ***hA*** values obtained from the correlation for all wet wipe/plastic combinations. However, ***hA*** correlation values are at least twice as big as that of the experimental ones with the difference getting larger as the number of wet wipe pieces in the single layer increases from 4 to 12. A possible explanation for the higher values of ***hA*** from the correlation is the reduction in the transfer area of the wet wipes due to contact with

neighboring pieces. Unlike rigid spheres, where the contact area between pieces is very small, the wet wipes were observed to be deformed by its neighbors such that there are larger areas of contact. In the single layer, the wet wipes could be touching either plastic pieces or other wipes. The reduction in total transfer area by deformation for the single layer would be worse for wipes-to-wipes contact than that for wipes-to-plastic since the former affects two wipes simultaneously. It was seen that as the number of wet-wipe pieces in the layer increases, there is more wipes-to-wipes contact. This observation would make the difference between the estimated transfer area used in solving for $\boldsymbol{hA}$ with the correlation and the actual area in the experimental system become larger with more wet-wipe pieces. This is turn would produce the observed rise in % difference as the number of wet wipes is increased from 4 to 12 pieces in the single layer.

Construction of curve relating the gas interfacial water vapor concentration with moisture content of wet solid

The water vapor concentration of the gas in contact with the surface of the wet solid ($\boldsymbol{W_{surface}}$) is needed to solve for the evaporation rate $\boldsymbol{m'}$ using Eqn (5). The curve relating this to the moisture content of wet solid was determined using previously obtained single-layer drying curves of combinations of wet wipes and plastic (Table 2.2). The procedure for this is discussed next.

For the single-layer drying runs, the total observed evaporation rate for a given amount of trash sample, $\boldsymbol{m}$, can be expressed as a convective mass transfer term as given in Equation (8). From measurements of $\boldsymbol{m}$ for the complete drying of single-layer trash, the relationship between $\boldsymbol{W_{surface}}$ and the moisture content $\boldsymbol{M}$ of the wet wipes was developed.

The values of k_mA were previously determined from single-layer experiments during the constant-rate drying period, as described above. During the falling-rate period, it is assumed that the value of k_mA remains essentially the same but $W_{surface}$ decreases with time as the drying rate and moisture content of the solids falls. From equation (4) and measurements of m as a function of time during drying, we can determine the value of $W_{surface}$ as a function of m:

$$W_{surface} = W + \frac{m}{k_m A} \tag{17}$$

Since M can be calculated at any time during drying, this plus the m vs. time curve yields m vs. M data, which was combined with the above equation to generate a plot of $W_{surface}$ vs M: the curve relating the gas interfacial water vapor concentration with moisture content of wet solid.

All the $W_{surface}$ vs M plots from the single-layer drying experiments are combined in Figure 2.7, where they are graphed in terms of water activity, a_w, defined as the ratio of actual partial pressure of water vapor to the equilibrium vapor pressure at the same temperature. The portions where the water-activity is unity correspond to the constant-rate period. Polynomial fitting (EXCEL, Microsoft Corp., Redmond, WA, USA) was used to obtain an equation that can be used in the model to solve for the evaporation rate for any solids moisture content.

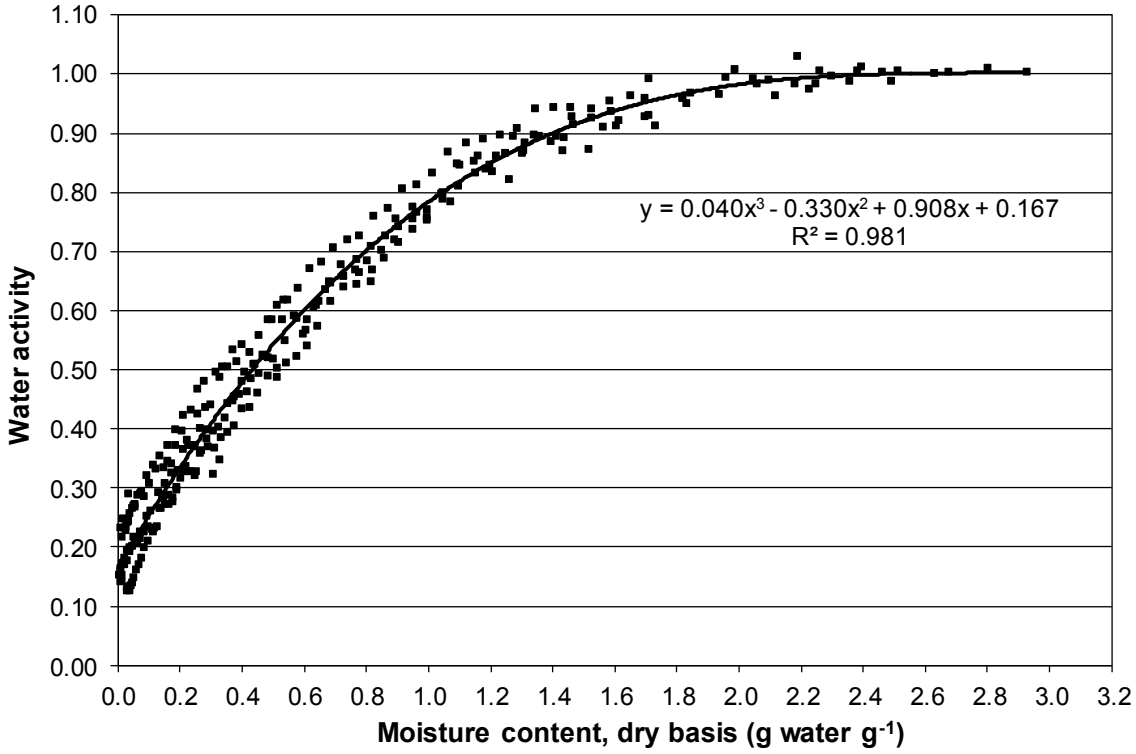

Figure 2.7. The curve relating the gas interfacial water vapor concentration (expressed as water activity) with moisture content of wet wipes based on single-layer experiments.

Model validation by comparing predicted drying curves for deep bed trash drying with experimental results

As discussed earlier, it was hypothesized that the ersatz trash load can be represented in the model by six layers of 4 wet wipes and 9 plastic pieces, one on top of the other. Simulations of the combined six layers were done with COMSOL using the same conditions used in the trash drying experiments. The actual and computational drying curves for the entire batch of trash are shown in Figure 2.8 for the three air superficial velocities used (1.2. 2.2 and 3.1 cm s^{-1}). The moisture content in the plots is all the water in the trash divided by the total bone-dry weights of the trash components that were initially wet (dog food and wet wipes). The plots exhibit the typical pattern observed when biological products are dried in a

deep bed; there is an initial constant-rate drying period (linear portion of the graph) followed by a falling-rate phase (Brooker et al., 1992). The experimental results show that the trash dries faster as the air flow rate through it is increased. This is to be expected since $\boldsymbol{hA}$ and $\boldsymbol{k_m A}$ for the system both increase with higher air velocities.

The model simulations for air velocities of 2.2 and 3.1 cm s^{-1} shown in Figure 2.8 closely approximate the data from the start until the moisture content falls to around 0.50 g water per g^{-1} of bone-dry initially-wet solids. After this point, the model tends to underestimate the moisture content and the percent error becomes greater than 10% upon further drying. This discrepancy may be explained by the difference in properties between the single-layer experimental system (wet wipes-and-plastic only) used to determine the transfer coefficients and the ersatz trash in the deep bed drying runs. In particular, the dog food in the trash contains a significant amount of moisture and its drying behavior would most probably be different from that of the wet wipes. This may be enough to produce the divergence of the simulation from the actual data. Model discrepancies late in the run, however, have little impact on the practical validity of the model. At a moisture content of 0.5 g water g^{-1} bone-dry initially-wet solids, around 81% of the water in the trash has already been removed. Further drying becomes progressively slower and ultimately more costly in terms of power and cooling. Moreover, the residual water at this point is already insufficient to support microbial growth. Figure 2.4 indicates that a moisture content of 0.5 g water g^{-1} bone-dry initially-wet solids corresponds to a water activity between 0.4 and 0.6, low enough for indefinite storage stability; while bacteria and molds can survive for long periods at low water activity, even the most xerophilic molds fail to grow below a water activity of 0.6 to 0.65. (Hocking and Pitt, 1987)

In contrast with the higher flowrates tested, the simulation for 1.2 cm s^{-1} shown in Figure 2.8c gives significantly lower moisture contents the entire drying run, indicating that it overestimates the drying rate. A possible explanation for this would be channeling, where the air finds preferential paths as it goes through the bed. There will then be minimal drying in the sections that are not contacted by the air and the overall drying rate would become lower. This phenomenon usually happens at slow air flows since the low pressure gradient across the dryer makes it harder for the air to pass through the more densely packed areas of the bed where the gas paths are narrower. The model would therefore give a higher drying rate than the actual and this will result in simulation values for bed moisture content that are lower than the experimental ones. Further study is recommended to determine the actual mechanism for this observed discrepancy between the model predictions and experimental data at 1.2 cm s^{-1}.

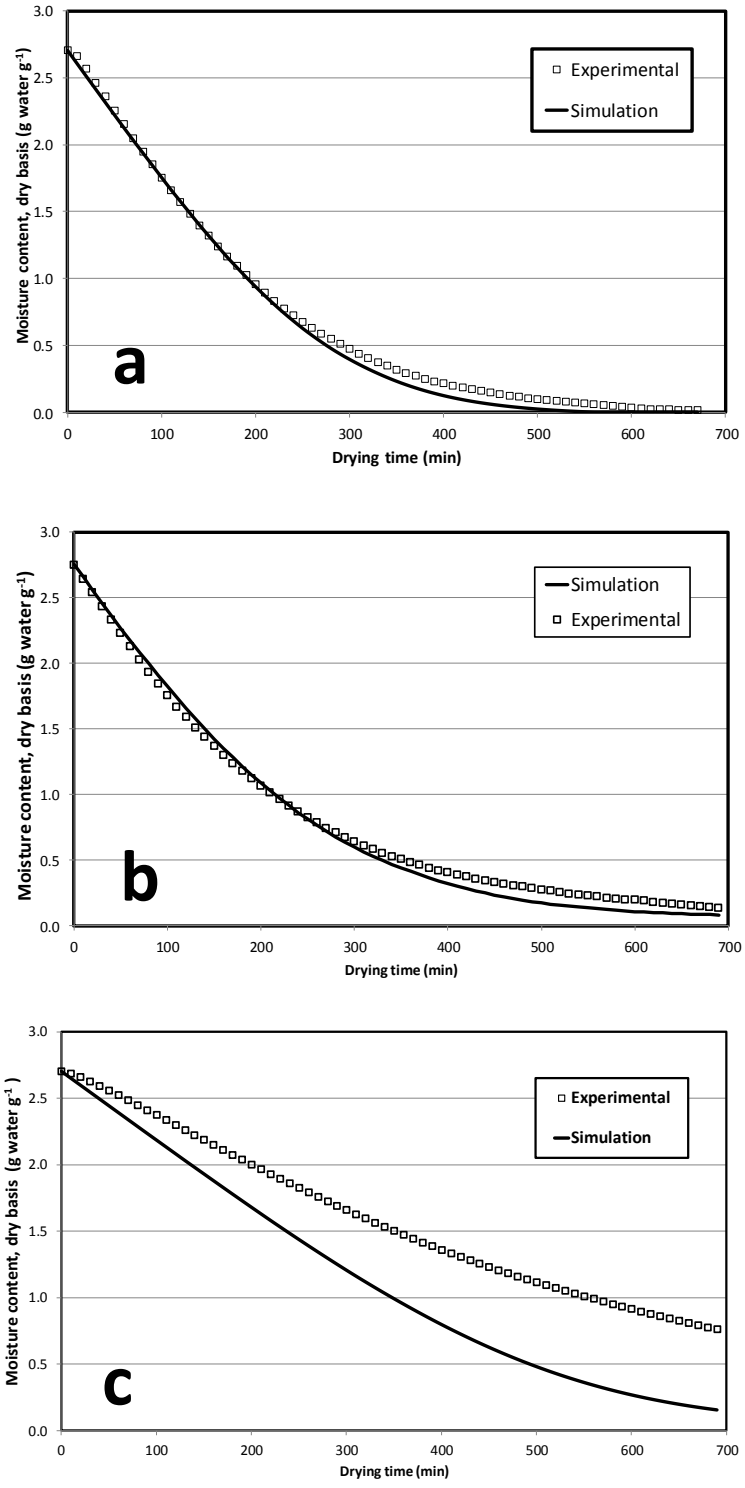

Figure 2.8 Comparison of experimental and simulated deep bed drying curves for all the initially-wet pieces in the ersatz trash at air superficial velocities of: (a) 3.1 cm s^{-1}, (b) 2.2 cm s^{-1}, and (c) 1.2 cm s^{-1}

Moisture contents along the bed height during drying from model

The plots in Figure 2.8 only give the moisture content of the wet materials in the entire batch of trash being dried; they do not show its spatial variation throughout the bed height. This information would be useful if the goal is to ensure that all wet materials in the trash have moisture contents below a minimum value that will prevent microbial proliferation during storage. This data would be tedious to obtain experimentally, involving the sampling of trash from several bed heights at different times during the drying run. However, the model can generate plots of moisture content along the bed height at any time. These are shown in Figure 2.9 for the simulation of trash drying using an air velocity of 2.2 cm s^{-1} and model with 4 wet wipes/9 plastic pieces. Since the hot air contacts the lower layers first, it is expected that the moisture content at a given time would increase going from bottom to top, and this is confirmed by the graphs. The model can therefore be used to determine when to stop drying based on the maximum allowable moisture content of the wet materials in the dried product. For example, if the desired final moisture content is 0.5 g water g^{-1} initially wet material, Figure 2.9 shows that drying can be stopped after 8 hours since all values are below this threshold then.

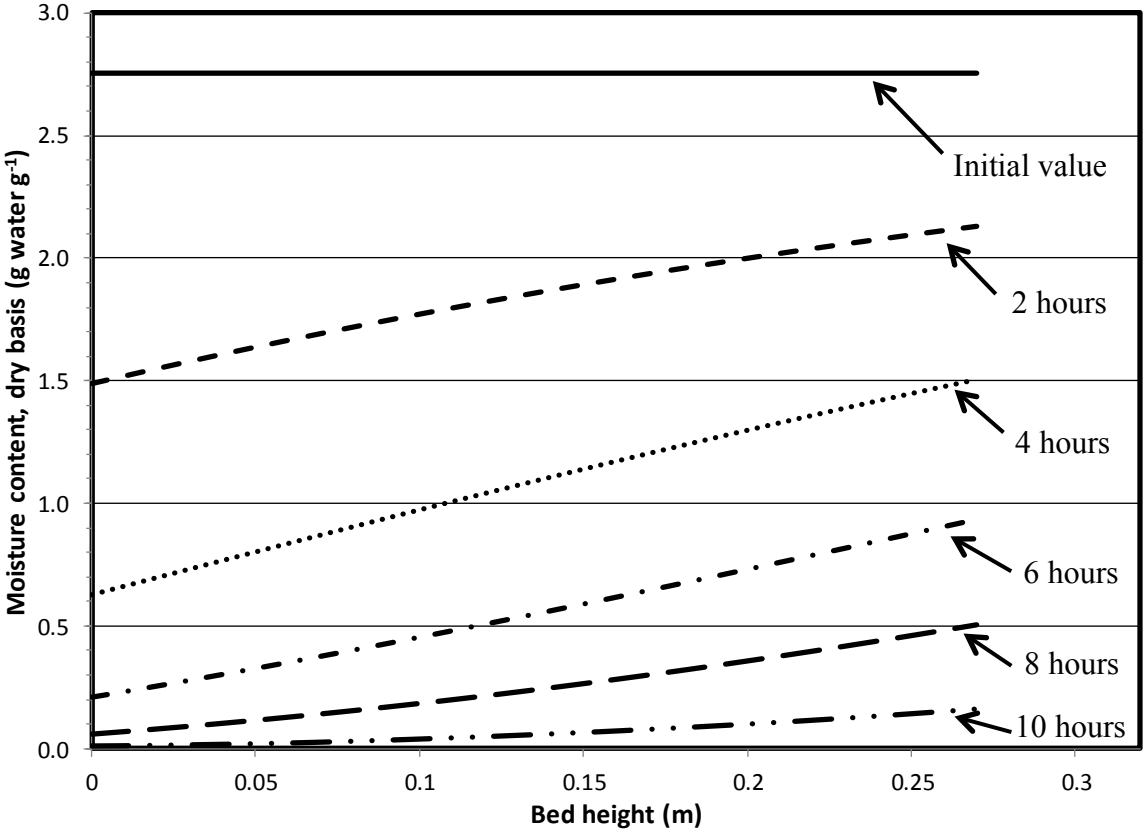

Figure 2.9 Changes in the moisture content of the initially wet materials along the trash bed height at different times during drying. The top of the bed is at 0.27 m. The simulation used an air velocity of 2.2 cm s^{-1} and model with 4 wet wipes/9 plastic pieces.

Simulated evaporation-time profiles

The proposed closed-loop dryer will have a condenser to recover the water removed from the trash. It would therefore be necessary to know the rate at which vapor is produced from the bed to properly design the condenser. The evaporation rate during drying can be obtained from the model. The simulations were done only for air velocities of 2.2 cm s^{-1} and 3.1 cm s^{-1} for which the model predictions better matched the experimental data. The runs used air with 15 % RH which enters the bottom of the dryer at 60°C. The effect of increasing the load of wet materials in the trash on the evaporation rate was also investigated by using

the experimental transfer coefficients for the cases with 8 wet wipes/6 plastic pieces and 12 wet wipes/3 plastic pieces. The simulation results for velocities of 2.2 and 3.1 cm s^{-1} are shown in Figures 2.10a and 2.10b, respectively.

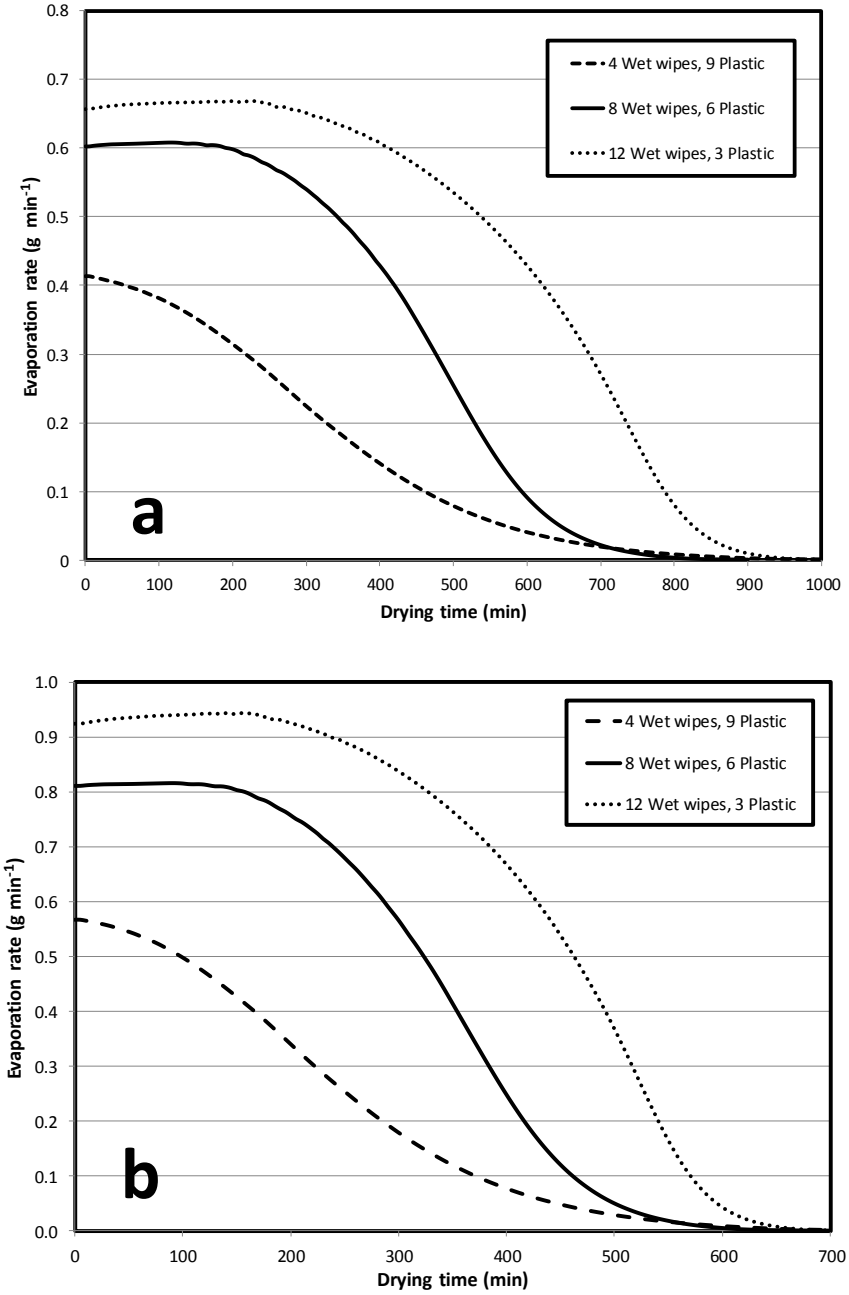

Figure 2.10 Evaporation rates during drying calculated by the model for trash with varying proportions of wet to dry material at different air superficial velocities: (a) 2.2 cm s^{-1} and (b) 3.1 cm s^{-1}.

For both flowrates, the maximum evaporation rate occurs at the start of drying. This is expected since at this stage the moisture content of the bed is largest and consequently the driving force for mass transfer is highest. The maximum evaporation rates also increase as the air moves faster through the bed. The curves for 8 wet wipes/6 plastic and 12 wet wipes/3 plastic show an initial constant evaporation rate period. At 2.2 cm s^{-1}, the 8 wet wipes/6 plastic has an evaporation rate of 0.61 g min^{-1} for about 150 minutes while that for 12 wet wipes/3 plastic is 0.67 g min^{-1} for 250 minutes. Increasing the air velocity to 3.1 cm s^{-1} gives a constant evaporation rate of 0.81 g min^{-1} for 8 wet wipes/6 plastic that lasts for 120 minutes. For the 12 wet wipes/3 plastic, this increases to 0.94 g min^{-1} for 160 minutes.

The plots for 4 wet wipes/9 plastic at the two flowrates do not show a constant evaporation rate period. It only has a period at the beginning where the evaporation rate decreases at a slower rate compared to succeeding portions of the curve. This is probably because of the small amount of wet material in the bed; the lower layers dry up quickly and enters the falling-rate period before significant evaporation has started at the upper sections.

The dependence of the evaporation rate time-profile with the air flowrate has a strong bearing on the design and operation of the condenser to be used for the dryer system. At high flowrates, drying is faster but the condenser has to be able to accommodate large air volumes and to condense vapor at a high rate. Low flowrates require less condenser capacity but extend the drying time. A complete computational model for the entire closed-loop drying system would therefore be needed to optimize its design and operation. The model for the drying of trash presented here is a necessary part of this.

The formulated model produces valid results for ersatz trash in the range of water recoveries of interest for an in-flight or planetary surface system for trash drying. It is worth pointing out that since all air flow through the system occurs by forced convection, and since moisture in the trash bed moves only by evaporation and (to a small extent) capillary wicking, never by saturated flow, the drying process and its model are both completely gravity-independent. This drying model is the first component in a larger model of the entire system, intended for prediction of drying performance and energy cost per unit of recovered water under a range of operating conditions including air temperature, air flow rate, and initial moisture content of the trash. Off-nominal conditions, such as the presence of pools of liquid water in the crevices of the plastic, water enclosed in impermeable beverage bags, or large masses of wet food materials or laboratory residues, would be expected to "break" the model. Performance optimization and estimation of power costs will also depend on other system conditions such as the heat and mass transfer coefficients of the condensers, condenser temperature, surface area, and the performance of the refrigeration system in the enthalpy recovery loop.

CONCLUSIONS

A porous media model has been developed for the forced-convection drying of a fixed bed of ersatz astronaut trash. The model represents the dryer as a pseudo-homogeneous continuum with two phases: gas and solid, with each phase having a distinct temperature and moisture content. Transient differential equations containing these variables are solved numerically using a commercial finite volume element solver (COMSOL). Heat and mass transfer coefficients appropriate for trash drying, together with data for water vapor concentration at the gas-solid interface were obtained experimentally and used as inputs to the model. The experimental procedure and calculations for these parameters were described. The transport coefficients were determined using different ratios of wet and dry trash components since it is expected that the trash will have variable initial water content.

Model predictions deviated less than 10% with drying curves from experiments using superficial air velocities of 2.2 and 3.1 cm s^{-1} except when the moisture content fell below 0.50 g water per g^{-1} of bone-dry initially-wet solids. At the lowest air superficial velocity used (1.2 cm s^{-1}), the model significantly underestimated the rate of water loss during the entire drying run.

The model was used to predict the moisture content distribution along the dryer height and rates of water loss by the trash at 2.2 and 3.1 cm s^{-1}. The experimentally determined heat and mass transfer coefficients for trash with more wet trash pieces also allowed prediction of spatial moisture content profiles and rates of water loss for these conditions.

The formulated drying model will be a major component of the overall model for the closed-loop drying process.

NOMENCLATURE

Symbol	Description	Units
c_a	Heat capacity of air	kJ kg^{-1} K^{-1}
c_d	Heat capacity of dry wipes (cotton)	kJ kg^{-1} K^{-1}
c_p	Heat capacity of plastic	kJ kg^{-1} K^{-1}
c_v	Heat capacity of water vapor	kJ kg^{-1} K^{-1}
c_w	Heat capacity of liquid water	kJ kg^{-1} K^{-1}
d_p	Particle diameter	m
D_v	Diffusivity of water vapor in air	m^2 s^{-2}
h	Heat transfer coefficient	kJ s^{-1} m^{-2} K^{-1}
ha'	Volumetric heat transfer coefficient	kJ s^{-1} m^{-3} K^{-1}
hA	Heat transfer coefficient*area	J min^{-1} K^{-1}
ΔH_{vap}	Heat of vaporization of water	kJ kg^{-1}
j_H	Chilton-Colburn factor for heat transfer	dimensionless
k_a	Thermal conductivity of air	kJ s^{-1} m^{-1} K^{-1}
$k_m a$,	Volumetric mass transfer coefficient	kg s^{-1} m^{-3} (kg water kg^{-1} dry air)
kmA	Mass transfer coefficient*area	g min^{-1} (kg water kg^{-1} dry air)
M	Bed moisture content, dry basis	m^3 voids m^{-3}system
m'	Volumetric evaporation rate	kg s^{-1} m^{-3}
m	Total evaporation rate	kg s^{-1}
Re	Reynolds number	dimensionless
t	Time	s
T_a	Air temperature	K
T_b	Mean bed temperature	K
v_a	superficial air velocity	m s^{-1}
W	Humidity ratio	kg water kg^{-1} dry air
$W_{surface}$	Humidity ratio of air at solid surface	kg water kg^{-1} dry air
z	Bed height	m
ρ_a	Density of air	kg m^{-3}
ρ_s	Density of dry solids	kg m^{-3}
ε	Porosity	m^3 voids m^{-3}system
μ	viscosity	kg s^{-1} m^{-1}
ψ	shape factor	dimensionless

REFERENCES

Bird, R. B., Stewart, W. E. and E. N. Lightfoot. *Transport Phenomena*. 2nd ed. New York: John Wiley & Sons, Inc., 2002.

Brooker, Donald B., Fred W. Bakker-Arkema, and Carl W. Hall. *Drying and Storage of Grains and Oilseeds.* 1st ed. New York: Van Nostrand Reinhold, 1992.

Castillo-Araiza, C. O., H. Jimenez-Islas, and F. Lopez-Isunza. "Heat-Transfer Studies in Packed-Bed Catalytic Reactors of Low tube/particle Diameter Ratio." *Industrial & Engineering Chemistry Research* 46.23 (2007): 7426-35.

CRC Handbook of Chemistry and Physics : A Ready-Reference Book of Chemical and Physical Data. Ed. Haynes, William M., Lide, David R. 92nd ed. ed. Boca Raton, FL: CRC Press, 2011.

Datta, A. K. "Porous Media Approaches to Studying Simultaneous Heat and Mass Transfer in Food Processes. I: Problem Formulations." *Journal of Food Engineering* 80.1 (2007): 80-95.

Geankoplis, Christie J. *Transport Processes and Separation Process Principles.* 4th ed. Upper Saddle River, NJ: Prentice Hall, 2003.

Hanford, A. J. and M. K. Ewert. Advanced Life Support Baseline Values and Assumptions Document JSC 47804 (NASA-Johnson Space Center, Houston, TX, May 8, 2002)

Hoang, M. L., et al. "A Continuum Model for Airflow, Heat and Mass Transfer in Bulk of Chicory Roots." *Transactions of the ASAE* 46.6 (2003): 1603-11.

Hocking, A. D. and J. I. Pitt, "Media and Methods for Detection and Enumeration of Microorganisms with Consideration of Water Activity Requirements". In *Water Activity: Theory and Applications to Food*, ed. L. B. Rockland and L. R. Beuchat. Marcel Dekker, NY, 1987.

Hunter, J. B., Arquiza. J.M.R.A., Morrow, R., and W. Butrymowicz. "Energy-Efficient Closed Loop Heat Pump Dryer for Solid Waste Stabilization on Long Duration Space Missions." 36th International Conference on Environmental Systems. Norfolk, VA, 17-20 July 2006. SAE Paper 2006-01-2088.

Krokida, M. K., Z. B. Maroulis, and D. Marinos-Kouris. "Heat and Mass Transfer Coefficients in Drying: Compilation of Literature Data." *Drying Technology* 20.1 (2002): 1-18.

McCabe, W. L., Smith, J. C., and P. Harriott. *Unit Operations of Chemical Engineering.* 7th ed. Boston: McGraw-Hill, 2005.

Perry's Chemical Engineers' Handbook [Electronic Resource]. Ed. Perry, Robert H., 1924-1978. Green, Don W. 8th ed. ed. New York: McGraw-Hill, 2008.

Scott, G. D. and D. M. Kilgour. "Density of Random Close Packing of Spheres." *Journal of Physics D-Applied Physics* 2.6 (1969): 863-866

Acknowledgement

We thank NASA for funding this work under STTR Phase I award OTC GS0144-FR-05-1 and Phase II award GS0180-TR-06-01.

CHAPTER 3

MODELING OF A CLOSED-LOOP, FORCED-CONVECTION, HEAT-PUMP DRYING SYSTEM FOR SPACE OPERATIONS

INTRODUCTION

Astronauts living in space generate wet cabin wastes such as food and drink containers with unconsumed portions, moist hygiene wipes, and wet paper towels. It has been estimated that a four-person crew would discard an average of 1 kg day $^{-1}$ of water in their trash (Fisher et al., 2009). For long duration missions where resupply is not possible, such as the planned rendezvous with an asteroid or future Mars landing, recovery of this water would reduce payload mass and associated lift costs. Wet trash is also susceptible to microbial growth and as the experience of Mir, STS and ISS amply demonstrates, spoilage may lead to the generation of odors, allergens, and potential health hazards (Makimura et al., 2001; Vesper et al., 2008).

Drying of the wet trash by forced convection with hot air is a viable and simple way of stopping microbial activity by combined pasteurization and desiccation. The water vapor produced can also be recovered by a condenser. A prototype of a closed air-loop, heat-pump dryer and condenser system (DRYER) for astronaut cabin waste has been designed, fabricated, and tested (Hunter et al., 2006; Arquiza et al., 2008). The DRYER consists of a blower, air heater, wet material container, a gravity-independent Porous Media Condensing Heat Exchanger(PMCHX), thermoelectric heat pump cooler, and waste heat recovery module. The schematic for the DRYER and the prototype tested are shown in Figures 3.1 and 3.2, respectively. The system may be adapted for use in the drying of crew laundry, water recovery

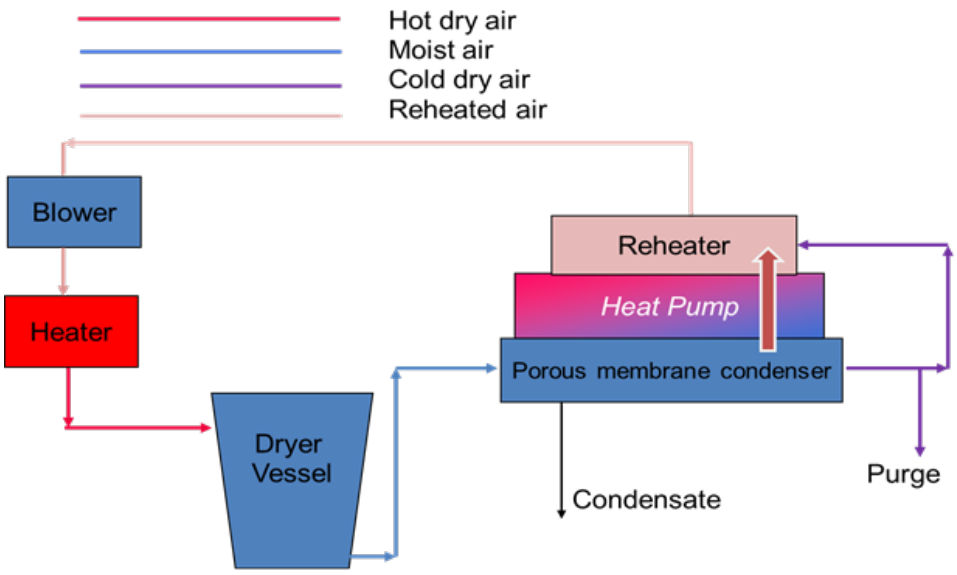

Figure 3.1 DRYER system schematic

Figure 3.2 DRYER system prototype

from water-reprocessing brines, and ultimately, food and biomass drying in a biogenerative life support system.

In this paper we present a computational model of the DRYER that is used to simulate its performance and analyze the energy cost per unit of recovered water under different conditions.

MODEL DEVELOPMENT

Model for drying efficiency: the bypass fraction

Air passing through the DRYER vessel picks up moisture from the wet solids in an adiabatic drying process. The extent of moisture transfer is governed by the internal mass transfer coefficient for diffusion of moisture inside the objects being dried, external mass transfer at their surfaces, and equilibrium moisture content of the materials. The mass transfer resistances are cumbersome to model as the internal resistances depend on the moisture content of the materials being dried, and external resistances on air velocity past the materials (Arquiza et al, 2008). As the materials dry, the governing mass transfer resistance switches from external to internal (McCabe et al., 2004). In order to simplify this complex process we have represented partial adiabatic drying in the vessel empirically, as a combination of equilibrium adiabatic drying and air bypass as shown in Figure 3.3. The bypass fraction denotes the fraction of the air stream considered to "bypass" the drying vessel; the remaining air is considered to reach the adiabatic saturation temperature and 100% relative humidity. The bypass fraction is therefore a measure of the drying efficiency with 1 indicating that no drying has occurred and 0 that maximum drying capacity of air has been reached.

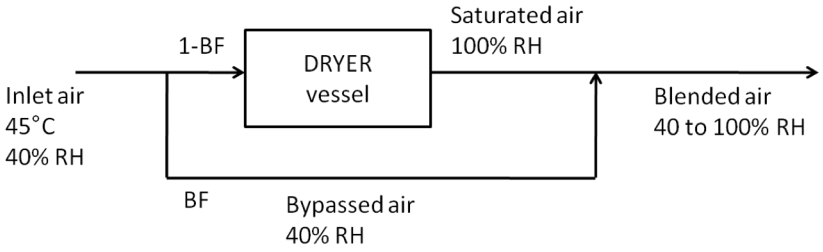

Figure 3.3 Schematic diagram for the bypass fraction (BF). The moist air leaving the vessel is represented as a combination of equilibrium adiabatic drying and bypass. Inlet air temperature and % RH shown is a typical value.

The Porous Media Condensing Heat Exchanger

System description

In terrestrial condensers, gravity separates the gas phase from the liquid condensate due to the difference in their densities. For condensers designed to operate in outer space, the absence of gravity requires the use of other mechanisms for gas-liquid separation. The DRYER system has a Porous-Media Condensing Heat Exchanger that uses capillary force to remove the condensate from the gas phase. The system consists of four components: (1) Moist air flow channel, (2) porous media, (3) condensate collector/water seal, and (4) thermoelectric cooler (Figure 3.4). The humid air passes through the channel and comes in contact with the cold saturated porous plate. The low temperature and corresponding low water vapor pressure at the solid surface cause heat and mass transfer, respectively. The hydrophilic porous media is saturated with water by capillary action to form a gas barrier while allowing condensate to pass through. The water produced flows through the porous media into the water seal and then out of the condenser. The water seal and porous media are kept cold by the thermoelectric cooler which rejects heat to the surroundings. Modeling the operation of the PMCHX therefore involves the governing equations for fluid flow, heat transfer, mass transfer and thermoelectric heat pump.

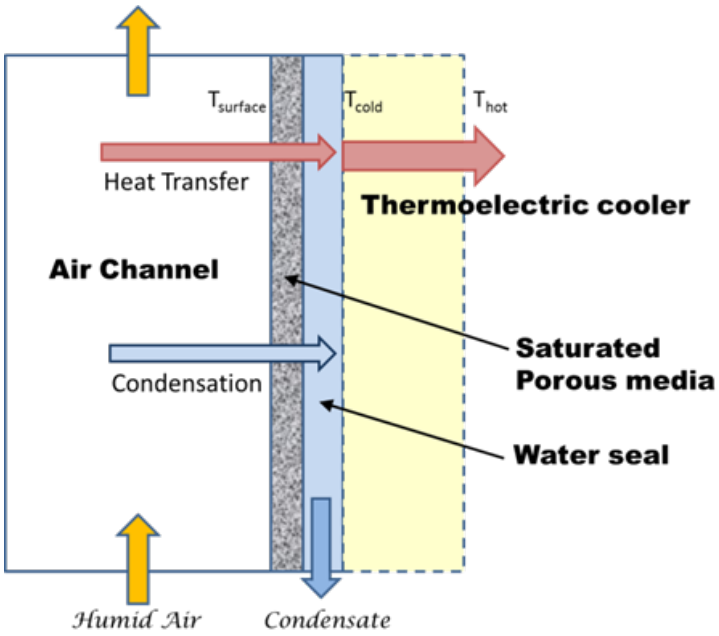

Figure 3.4. Schematic for the Porous Media Condensing Heat Exchanger

The actual condenser is a rectangular channel having 0.032 m x 0.12 m cross-sectional area and 0.11 m length. It is oriented vertically with moist air from the dryer vessel entering at the bottom. Two porous media plates make up the larger walls (0.12 m x 0.11 m) of the condenser (Figure 3.5). The plates are 0.004 m-thick porous aluminum oxide with mean pore size of 15 microns (Refractron Technologies Corp., Newark, NY). During operation, the porous plates are saturated with cold water (primed condition) and their temperatures are maintained by thermoelectric (TE) cooler modules (Melcor model HT8-12-40, Laird Technologies, Newark, NJ). In the experimental runs, the heat rejected by the TE heat pumps were removed from the hot side by an external water loop entering at 25°C. This configuration did not permit recovery of the heat removed (latent and sensible) by the TE coolers.

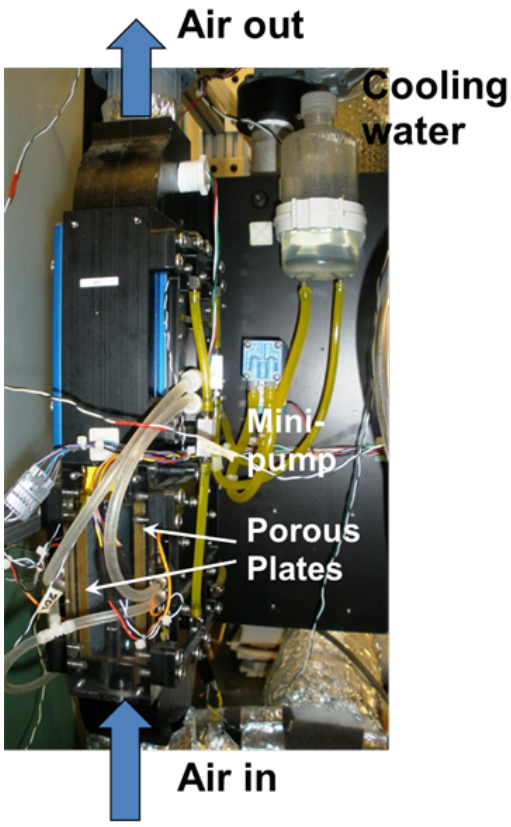

Figure 3.5. Porous membrane condensing heat exchanger.

Problem Description

The condenser is modeled by considering a two-dimensional cross-section along its length. Implicit in this chosen geometry is the assumption that the boundaries at the smaller sides of the condenser do not significantly affect the total heat and mass transfer. Also, since the condenser is symmetric to the plane between the plates, only half of the volume is modeled. The entire computational domain consists of the volume occupied by the flowing moist air (Figure 3.6). The moist air enters from the bottom with a velocity of v_{in}, temperature of T_{in} and humidity ratio $\mathcal{H}_{in}$.

The following assumptions are used in the model:

1. The gas phase is incompressible (because pressure and temperature variations within the condenser are minimal).
2. The inlet velocity is uniform and equal to the average velocity.
3. The flow is laminar (for 9.1 kg h^{-1} air flowrate, Re = 1,726; for 12.9 kg h^{-1}, Re = 2,447).
4. The temperature at the surface of the porous plate is uniform and set at a fixed temperature (T_{plate}).
5. The gas in contact with the plate is in equilibrium with liquid water at T_{plate}.
6. All the condensate produced at the cold surface instantaneously passes through the porous plate so no liquid layer is formed.

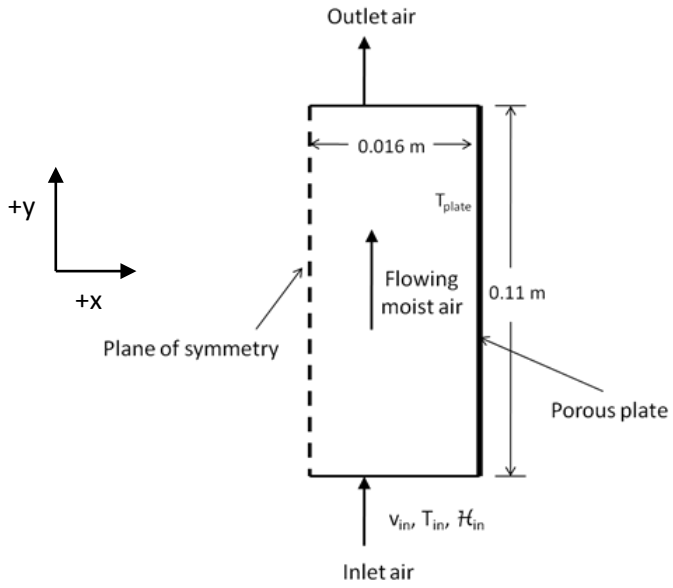

Figure 3.6. Two-dimensional domain for computational model of condenser

Governing equations (Steady-State)

The velocity, temperature, and water vapor mass fraction at every point (x, y) in the computational domain are calculated using the conservation equations for momentum, energy, total mass, and water vapor. These are expressed as differential equations in two-dimensional Cartesian coordinates.

Continuity equation

The assumption of incompressible gas reduces the continuity equation to

$$\frac{\partial u}{\partial x} + \frac{\partial v}{\partial y} = 0 \qquad \text{Eq. (1)}$$

This also simplifies the other conservation equations.

Fluid flow equation

The momentum balance equation for the system is given by the incompressible Navier-Stokes equations

$$\text{x-component: } \rho\left[u\frac{\partial u}{\partial x} + v\frac{\partial u}{\partial y}\right] = -\frac{\partial p}{\partial x} + \mu\frac{\partial^2 u}{\partial y^2} \qquad \text{Eq. (2)}$$

$$\text{y-component: } \rho\left[u\frac{\partial v}{\partial x} + v\frac{\partial v}{\partial y}\right] = -\frac{\partial p}{\partial y} + \mu\frac{\partial^2 v}{\partial x^2} - \rho g \qquad \text{Eq. (3)}$$

The gravitational force is included only in the y-direction since the condenser is oriented vertically. The viscosity is assumed to be not significantly different from that of dry air since its humidity ratio is low.

Energy equation

Both convection and conduction heat transfer are considered in the model.

$$\rho_{ave} C_{p_{ave}}\left[u\frac{\partial T}{\partial x} + v\frac{\partial T}{\partial y}\right] = k_{ave}\left[\frac{\partial^2 T}{\partial x^2} + \frac{\partial^2 T}{\partial y^2}\right] \qquad \text{Eq. (4)}$$

The density and thermal properties are the weighted averages for the moist air and depend on its moisture content.

Water vapor mass balance

The model calculates the condensate production rate based on convective and diffusional transport of vapor from the bulk gas phase to the plate surface. The driving force for this transfer is the reduced water vapor concentration at the interface of the gas and porous plate due to the low temperature maintained there by the TE cooler.

$$u\frac{\partial c_v}{\partial x} + v\frac{\partial c_v}{\partial y} = D_v\left[\frac{\partial^2 c_v}{\partial x^2} + \frac{\partial^2 c_v}{\partial y^2}\right] \qquad \text{Eq. (5)}$$

Boundary conditions

At the condenser inlet (y = 0, 0 < x < 0.016 m), the velocity, temperature, and water vapor concentrations are constant: $u = 0$, $v = v_{in}$; $T = T_{in}$; $c_v = c_{v,in}$

At the symmetry boundary (x = 0, 0 < y < 0.11 m), the momentum, heat, and mass fluxes are zero.

At the surface of the porous media (x = 0.016 m, 0 < y < 0.11 m):

A no-slip boundary condition is imposed, $u = 0$, $v = 0$, the plate temperature is set, $T = T_{plate}$, and the vapor in contact with the plate is assumed to be in equilibrium with liquid water at T_{plate}, so that $c_{v,plate} = c_v^* = \frac{p^*}{RT_{plate}}$, where p^* is the equilibrium vapor pressure of water at T_{plate} and is read from steam tables.

RESULTS AND DISCUSSION

Equations (1) to (5) is solved using the finite element method as implemented by the commercial software COMSOL Multiphysics (Burlington, MA). A representative result is given in Figure 3.7.

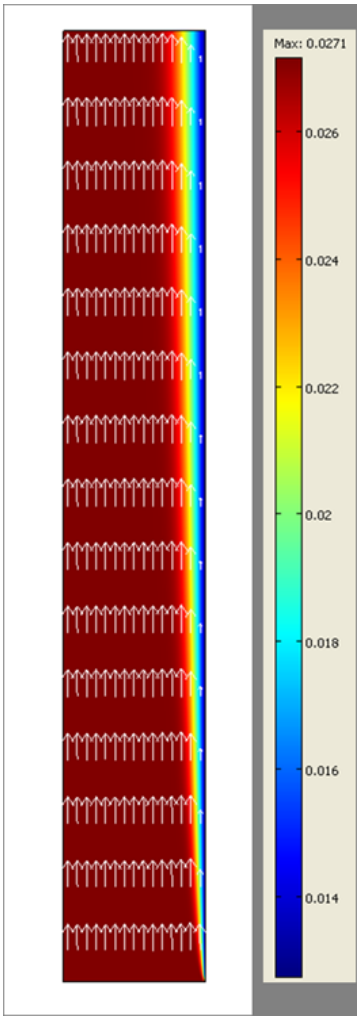

Figure 3.7 COMSOL simulation results. The arrows represent the velocity field while the colors show the mass fraction of water vapor in the moist air. Note the development of a boundary layer along the plate surface on the right. Conditions used are air flowrate of 9.1 kg h^{-1}, inlet humidity ratio of 27.9 g water kg air $^{-1}$ and plate temperature of 18°C.

Model validation

Data were collected from several runs in the DRYER using wet hygiene wipes to produce humid air entering the condenser. The prototype has three identical condensers which may be operated in parallel, but only one was used in the experiments. The air flowrates and condensation rates given here are therefore for a single condenser. The moisture content of the wet wipes was made high enough to give a constant drying rate period of at least two hours. During this time the DRYER operated at steady-state and the rate of condensate production did not vary. Two different air flowrates (50% and 100% fan power, corresponding to 9.1 and 12.9 kg h^{-1}, respectively) were tested and the temperature of the air entering the dryer vessel was adjusted (45°C to 60°C) to produce feed with varying water vapor content. Ideally, the humidity ratios of the air entering the condenser should be the same for each plate temperature setting but the closed-loop configuration of the DRYER produced a coupling effect between the two variables. At lower plate temperatures, the air leaving the dryer tended to have smaller moisture contents (Table 3.1). Comparison of the experimental and simulated condensation rates during the constant-drying rate period shows that the difference between them is always less than 6%, validating the model's reliability. This strongly supports the model's assumption that mass transfer is the main mechanism by which condensate is produced in the PMCHX. The low temperature of the plate is needed only to decrease the water vapor concentration of the gas in contact with its surface. This is in agreement with a previous analysis by Scovazzo and coworkers (1998).

Table 3.1 Comparison of experimental and simulated condensation rates.

Air flowrate (kg h^{-1})	Plate Temperature (°C)	Condenser inlet Humidity Ratio (g water kg air $^{-1}$)	Condensation rate		% difference
			Experimental (g h^{-1})	Simulation (g h^{-1})	
9.1	22	45.6	43.2	42.8	-1.1
9.1	18	27.9	23.5	23.6	0.8
9.1	18	43.5	46.5	47.3	1.7
9.1	14	44.0	51.6	53.1	3.0
9.1	14	42.6	49.6	50.1	1.1
9.1	10	24.0	25.7	26.4	2.5
12.9	22	42.2	42.0	44.3	5.3
12.9	18	27.8	27.4	27.5	0.1
12.9	18	40.8	49.9	50.9	1.9
12.9	14	40.6	53.8	56.5	5.1
12.9	14	30.0	36.6	37.4	2.3
12.9	10	21.9	28.6	27.4	-4.1

Condenser simulation using different inlet humidity ratios

In the DRYER system, the humidity ratio of the air entering the condenser depends on the rate of evaporation in the dryer vessel. The percent relative humidity (% RH) of the air leaving the dryer vessel could therefore range from a little higher than that of its entering value (low evaporation) to 100% (maximum evaporation). To simulate this variable drying effectiveness, the condenser model was run using inlet conditions based on air entering the dryer vessel at 9.1 kg h^{-1}, 45°C and 40% relative humidity. Drying is assumed to be adiabatic and isenthalpic air leaving the dryer vessel with relative humidity of 50%, 60%, 70%, 80%, 90% and 100% were used as input to the condenser model. Simulations were performed using these inlet air properties for four different plate temperatures (10, 14, 18, and 22°C) which can be set by the TE cooler in actual operations. The model was also run using an air flow rate of 12.9 kg h^{-1}. The plots of condensation rate versus plate temperature are shown in Figure 3.8.

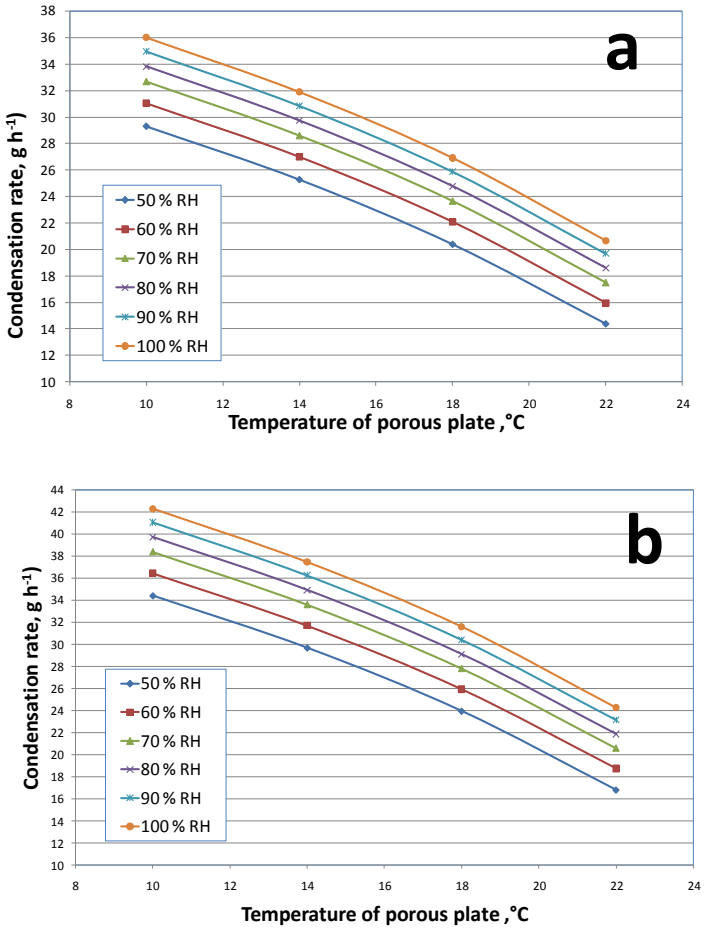

Figure 3.8 Simulation results showing the effect of entering air relative humidity and plate temperature on the condensation rate. Plot (a) is for an air flowrate of 9.1 kg h^{-1} while (b) is for 12.9 kg h^{-1}. Air enters the dryer vessel at 45°C and 40% RH in both cases.

The plots show that the condensation rate increases with higher inlet air % RH for a set plate temperature. This is expected since the driving force for mass transfer is proportional to the water vapor concentration of the moist air. The condensation rate is also seen to increase at the colder plate temperatures, because the water vapor concentration at the gas-plate interface drops as the temperature decreases, increasing the driving force for mass transfer. At the 9.1 kg h^{-1} air flow rate, the highest water recovery rate is 36 g h^{-1} for air entering the condenser at 100% RH and plate temperature of 10°C. Using the same inlet air and plate temperature, an air flowrate of

12.9 kg h^{-1} gives a higher condensate production rate of 42.3 g h^{-1}. Since the DRYER system has three condensers that can be operated in parallel, the maximum water recovery rates are 108 g h^{-1} (2.6 kg day^{-1}) and 126.9 g h^{-1} (3 kg day^{-1}) for air flowrates through each condenser of 9.1 kg h^{-1} and 12.9 kg h^{-1}, respectively. The lowest condensation rate is 14.4 g h^{-1} for 50% RH inlet air and 22°C plate temperature. For three condensers, this gives a total daily water recovery rate of 1 kg day^{-1} which is enough to recover the estimated daily water loss in trash (Fisher et al., 2009).

Steady-state Simulation of Closed-loop System with Different Bypass Fractions

As discussed earlier, the drying efficiency can be modeled by the use of a bypass fraction. For a constant bypass fraction, the compositions of the streams in the closed-loop drying system adjust to steady-state values where the evaporation rate in the dryer vessel equals the condensation rate in the condenser. This steady-state condition cannot be determined analytically but for a given bypass fraction, a pass-by-pass calculation involving the condenser model and water vapor mass balance is used to solve for the evaporation and condensation rate after each loop. The humidity ratios of the moist air streams successively adjust with each cycle until steady-state conditions are reached. DRYER operation was simulated for an air flowrate of 9.1 kg h^{-1}, bypass fractions of zero, 0.2, 0.4, 0.6, and 0.8, and condenser plate temperatures of 10 and 22°C. A representative plot showing the approach of the stream humidity ratios to their steady-state values is shown in Figure 3.9 for a bypass fraction of zero (maximum efficiency) and 10°C plate temperature. At the first pass, the evaporation rate in the dryer vessel is high and the vapor collected by the air exceeds the collection capacity of the condenser so in the next pass, the moist air enters the dryer with a higher humidity ratio. The humidity in the feed to the dryer rises in each succeeding pass and the rate of evaporation decreases until it is balanced by the rate of condensation. Steady-state is established after 20 simulation cycles which is equivalent to

about 5 minutes of DRYER operation. This case shows the condenser-limited operation of the closed-loop drying system which happens when the drying process is at maximum efficiency (bypass fraction of zero). The steady-state condensing rates for different bypass fraction are shown in Figure 3.10. As the bypass fraction increases, the amount of water recovered by the condenser decreases because less moisture is removed from the wet solid. This simulation of the steady-state operation of the closed-loop dryer system can be used to support an energy analysis for the power needed to recover a unit mass of water from specified process variables.

Thermodynamic analysis

The energy required to recover water from the wet material is the sum of the power consumption of the fan, heater, and TE heat pump. The energy required for the fan is not included in the following analysis since it is assumed to be small compared to that for the heater

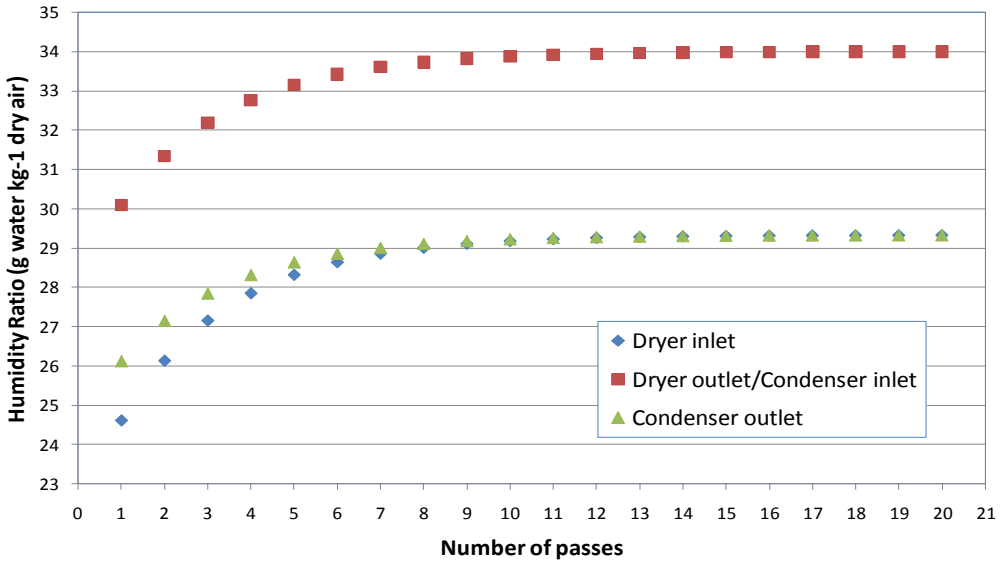

Figure 3.9 Simulation of closed-loop dryer start-up. The humidity ratio of dryer and condenser inlet/outlet streams change as the system approaches steady-state. Air flowrate is 9.1 kg h^{-1}, dryer vessel inlet temperature is 45°C, bypass fraction is zero, and condenser plate temperature is 10°C.

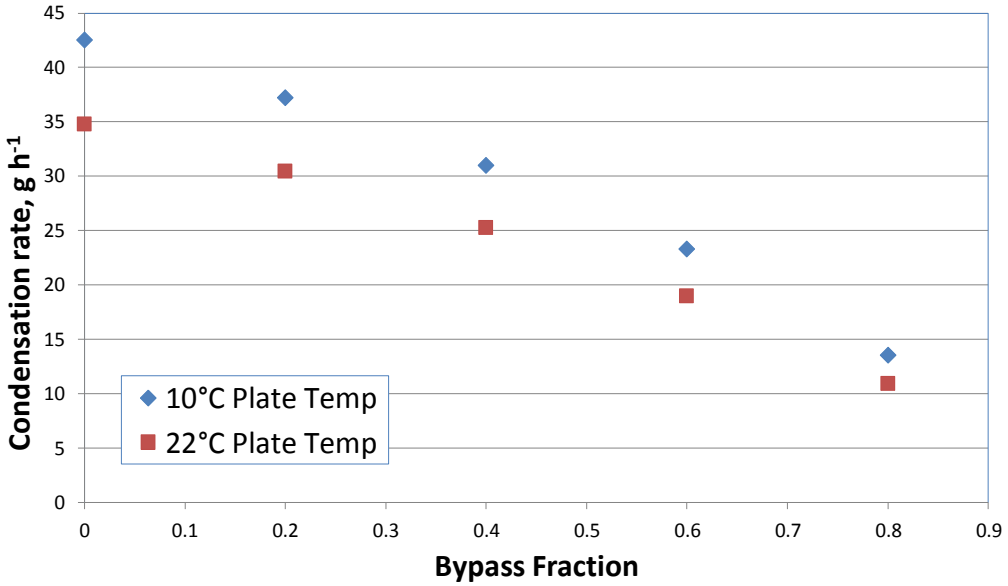

Figure 3.10 The effect of the bypass fraction to the steady-state condensation rates in the closed-loop dryer. Air flowrate is 9.1 kg h^{-1}, dryer vessel inlet temperature is 45°C, and condenser plate temperature is 10°C.

and TE heat pump. The values used in the analysis are for operations involving a single condenser.

TE heat pump power

The simulation calculates both the sensible and latent heat lost by the entering moist air as it passes through the condenser. This gives the total heat removed by the cold side of the TE cooler ($\boldsymbol{Q_c}$). The amount of work ($\boldsymbol{W}$)that the TE needs to pump this heat can then be determined using the following equations (Nolas et al., 2001):

$$Heat\ pumped\ (Q_c) = 2\,N\left[\alpha\, I\, T_{cold} - \left(\frac{(I^2 R)}{2\,G}\right) - K\,G\,(T_{hot} - T_{cold})\right] \quad (6)$$

$$Work\ (W) = I\,V = I\,2\,N\left[\left(\frac{I\,R}{G}\right) + \alpha(T_{hot} - T_{cold})\right] \quad (7)$$

where α is Seebeck coefficient, I is the current, K is thermal conductivity, R is resistivity, G is area/length of TE element, V is the voltage, and N is number of thermocouples. The manufacturer (Laird Technologies, St. Louis, MO), gives the values of G and N as 0.076 cm and 127, respectively. The other parameters depend on temperature and are calculated using equations (8) to (10). The units are shown in parenthesis and T is the average temperature of the hot and cold sides in Kelvin.

$$\propto (V/K) = -9.91\,X\,10^{-10}\,T^2 \;+\; 9.31\,X\,10^{-7}T \;+\; 2.22\,X\,10^{-5} \qquad (8)$$

$$R(ohm-cm) = 6.28\,X\,10^{-9}\,T^2 \;+\; 1.63\,X\,10^{-6}T \;+\; 5.11\,X\,10^{-5} \qquad (9)$$

$$K(W/K-cm) = 4.13\,X\,10^{-7}\,T^2 \;+\; -2.78\,X\,10^{-4}T \;+\; 6.26\,X\,10^{-2} \qquad (10)$$

Heater power

Since the drying is assumed to be adiabatic, the enthalpy of the moist air entering the condenser is the same as that of the 45°C air entering the drying vessel. Therefore, at steady-state and in the absence of heat losses, the amount of heat supplied by the heater would be equal to that removed in the condenser. As mentioned earlier, the condenser duty is obtained from the simulation results so the heater power requirement is also known. Tables 3.2 and 3.3 give the heat removed by the condenser (sensible and latent heat), the power consumption of the TE cooler, its Coefficient of Performance (COP), and the total power used by the TE and heater for plate temperatures of 10°C and 22°C, respectively.

Table 3.2. Steady-state energy analysis of DRYER system during constant-rate drying period for air flowrate of 9.1 kg h^{-1}, dryer vessel air inlet temperature of 45°C, and condenser plate temperature of 10°C.

Bypass Fraction	Condenser air inlet temp. (°C)	Sensible heat removed by condenser (W)	Latent heat removed by condenser (W)	Condenser duty/ Heat to raise temp to 45°C (W)	TE power to maintain plate temp at 10°C (W)	COP of TE	Total energy input (W)
0	33.7	9.72	29.56	39.28	21.46	1.83	60.74
0.2	35.0	10.24	25.98	36.22	19.15	1.89	55.37
0.4	36.6	10.88	21.73	32.61	16.62	1.96	49.23
0.6	38.7	11.69	16.53	28.22	13.85	2.04	42.07
0.8	41.3	12.68	9.81	22.49	10.73	2.10	33.22

Table 3.3 Steady-state energy analysis of DRYER system during constant-rate drying period for air flowrate of 9.1 kg h^{-1}, dryer vessel air inlet temperature of 45°C, and condenser plate temperature of 22°C.

Bypass Fraction	Condenser air inlet temp. (°C)	Sensible heat removed by condenser (W)	Latent heat removed by condenser (W)	Condenser duty/ Heat to raise T to 45°C (W)	TE power to maintain plate temp at 22°C (W)	COP of TE	Total energy input (W)
0	34.1	5.71	23.67	29.38	4.94	5.95	34.32
0.2	35.0	6.15	20.72	26.87	4.21	6.39	31.07
0.4	36.1	6.67	17.20	23.87	3.42	6.99	27.29
0.6	37.4	7.31	12.90	20.21	2.57	7.85	22.78
0.8	39.1	8.14	7.43	15.57	1.69	9.24	17.26

Comparison of the COP values in tables 3.2 and 3.3 illustrates the energy penalty of operating at a low plate temperature since the efficiency of the TE cooler is significantly decreased by a large temperature difference between its hot and cold side ($\boldsymbol{T_h - T_c}$). The temperature of the TE hot side is kept at 25°C during the experiments so a cold side of 10°C gives a $\boldsymbol{T_h - T_c}$ of 15°C while that with 22°C gives a $\boldsymbol{T_h - T_c}$ of 3°C. The condenser duties for

these two plate temperatures are not that much different but the COP for 22°C is at least 3 times more than that for 10°C for the same bypass factor. This result highlights the major disadvantage of a thermoelectric heat pump: its COP becomes very small when the temperature difference between the hot and cold side is high (Nolas et al., 2001).

The energy required to recover a unit mass of water is calculated from the condensation rates in Figure 3.10 and the total energy inputs in Tables 3.2 and 3.3. The values are plotted against the bypass fraction in Figure 3.11 for the 10°C plate temperature and Figure 3.12 for the 22°C plate temperature. The individual heat effects (latent and sensible) involved are also shown in the plots. Since condensation is driven by vapor phase mass transfer, the sensible heat loss in the condenser is not necessary for water recovery and happens only because the plate is colder than the air. This loss becomes more significant as the bypass fraction increases because the greater proportion of bypass in the stream entering the condenser raises its temperature and leads to a larger heat transfer driving force (Tables 3.2 and 3.3). The sensible heat loss is also expected to increase for higher dryer temperatures and since this is undesirable, it is better to use low hot air temperatures (e.g. 45°C).

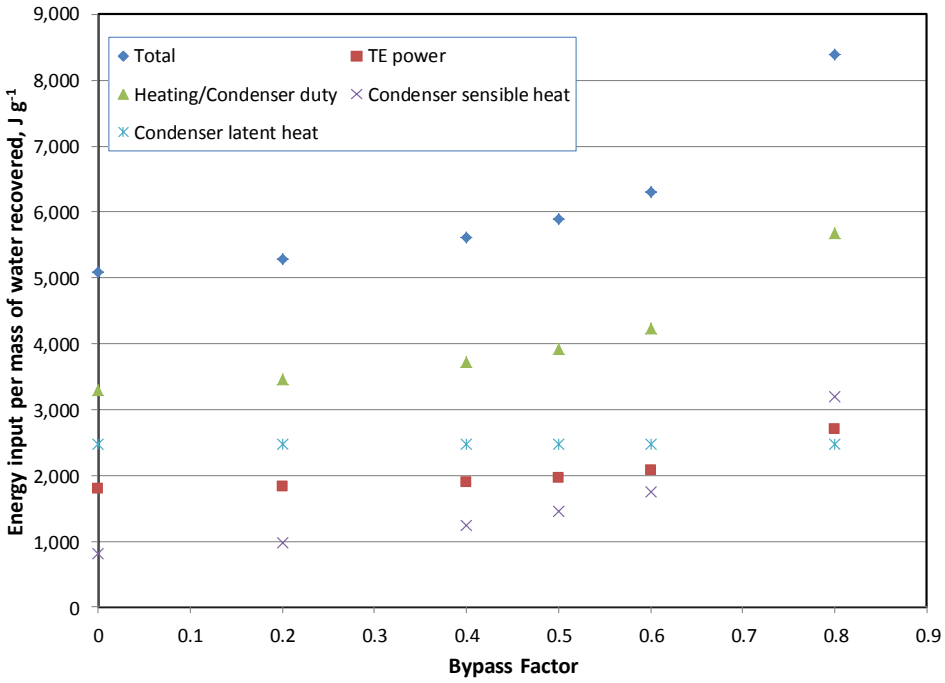

Figure 3.11 Energy Requirement per gram of water recovered for condenser plate temperature of 10°C. Air flowrate is 9.1 kg h^{-1}, dryer vessel inlet temperature is 45°C.

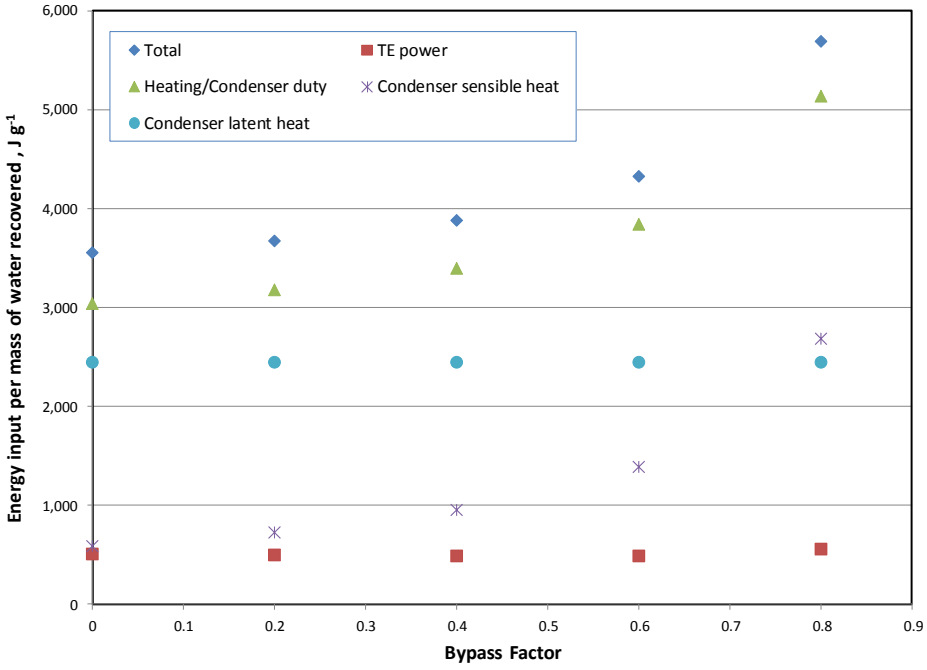

Figure 3.12 Energy Requirement per gram of water recovered for 22°C condenser plate temperature. Air flowrate is 9.1 kg h^{-1} and dryer vessel inlet temperature is 45°C.

Recovery of Heat Removed by Condenser

In our model of the dryer and condenser, the heat removed by the thermoelectric heat pump in the condenser was rejected to a cooling water stream. If this heat could be recovered and used to warm up air entering the dryer vessel, as shown in Figure 3.1, the energy efficiency of the system would increase. This heat recovery scheme was attempted in the fabricated prototype by the use of a circulating water loop that transferred the heat rejected by the hot side of the TE cooler to an extended-surface heat exchanger set within the duct carrying air from the condenser (Figure 3.13). However, testing and further analysis has shown that this set-up does not provide enough heat transfer for the air to completely recover the heat removed by the TE cooler. This limitation is mostly brought about by the small temperature driving force between the hot side of the TE and the air. As a result, the cooling water continuously absorbs the extra heat. Since there is a limited amount of water in the closed cooling loop, it gradually heats up and raises the TE cooler's hot-side temperature. As noted before, large temperature differences between the hot and cold sides of the TE cooler sharply decreases its refrigeration COP. When the $\boldsymbol{T_h - T_c}$ gets high enough, the TE cooler becomes so inefficient that it can no longer remove enough heat from the cold side to maintain the set low temperature. The porous plate gets hot and the rate of condensation is significantly reduced. This problem is not present in refrigeration-heat pump systems using vapor-compression cycles which can give a high COP over a large temperature lift (Sunada et al., 2008). A vapor-compression system is therefore more suitable for recovering the heat removed from the condenser.

The developed dryer bypass and condenser model was used to perform an energy analysis of the dryer set-up using a hypothetical refrigeration system that has a COP of 4 to pump heat from the condenser to reheat the air. The energy needed to extract a unit mass of

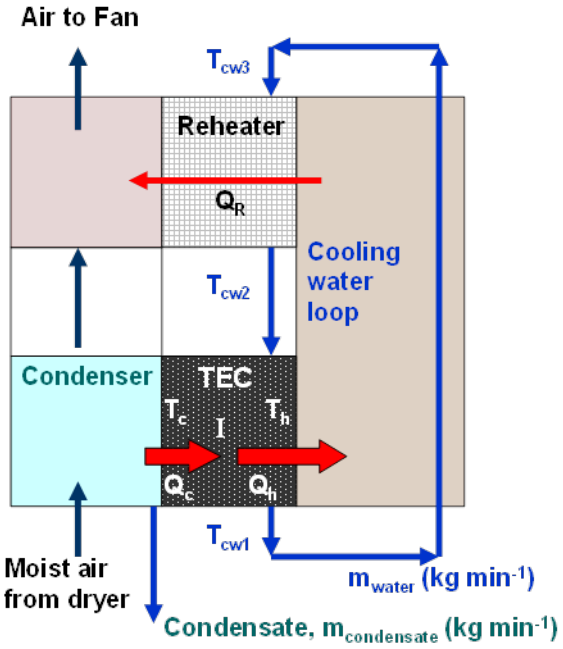

Figure 3.13 Condenser set-up with a closed water loop to transfer the heat rejected by the thermoelectric heat pump to the air leaving the condenser.

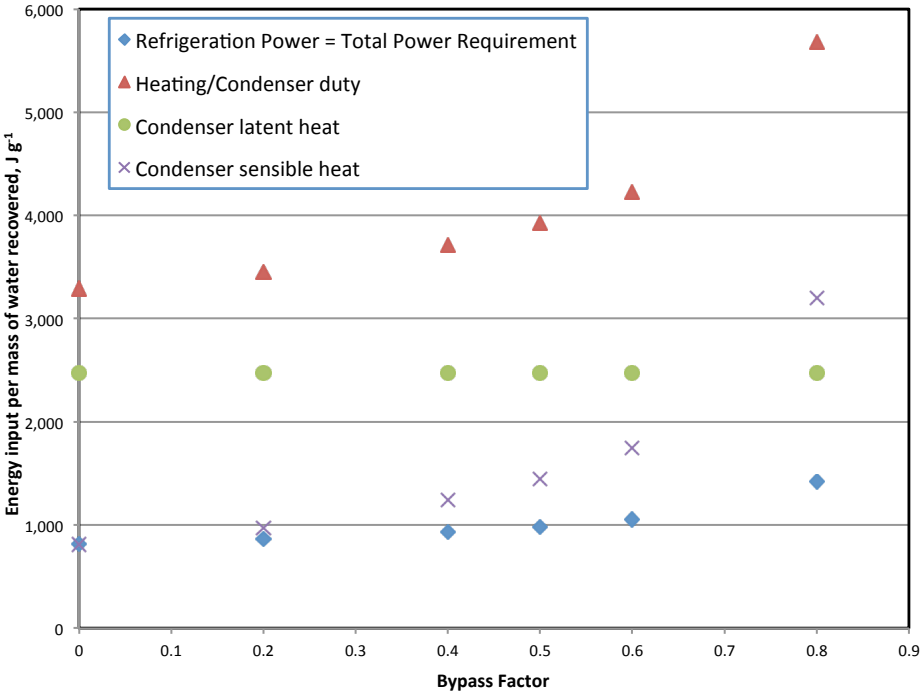

Figure 3.14 Energy Requirement per gram of water recovered using a vapor-compression heat pump with COP of 4. The rejected heat is recycled to increase the dryer vessel inlet air temperature to 45°C. Air flowrate is 9.1 kg h^{-1} and condenser plate temperature is 10°C.

water for an air flowrate of 9.1 kg h-1 and condenser plate temperature of 10°C is shown in Figure 3.14. Since the energy recovered from the condenser is more than enough to reheat the air to the dryer vessel inlet temperature of 45°C, the only energy that must be supplied for the cooling and heating processes is the power for the refrigeration-heat pump system (Total Power Requirement in Figure 3.14). The energy required to recover a unit mass of water from the wet trash goes from 800 to 1400 J g^{-1} as the bypass fraction increases. It should be noted that these are less than the latent heat of water, indicating that some of it is being recovered. These are also significantly less than the 5,000 to 8,500 J g^{-1} required by the TE cooler (Figure 3.11).

CONCLUSIONS

A prototype of a closed-loop, forced-convection, drying system with a condenser cooled by a thermoelectric heat pump was tested for its performance in recovering water from wet trash generated by humans in space habitats. The system consists of a blower, air heater, wet material container, a gravity-independent Porous Media Condensing Heat Exchanger, thermoelectric heat pump, and waste heat recovery module.

A computational model of the condenser was developed and validated using experimental data for various operating temperatures and input humidity at sea-level pressure and unit gravity. The model showed that the condenser removes water from the humid air by mass transfer and not by decreasing the temperature below the dewpoint. However, the air still becomes colder as it goes through the condenser because the porous plate is at a lower temperature. This sensible heat loss becomes significant when the dryer is not operating efficiently (high bypass fraction). Thermodynamic analysis of the DRYER system showed that the thermoelectric heat pump was

not appropriate for heating the air since its COP goes down when there is a large temperature difference between its cold and hot sides. Instead of a thermoelectric heat pump, the incorporation of an efficient refrigeration/heat pump system that uses the heat rejected by the condenser (latent and sensible) to reheat the air has significant potential to decreases the energy required to recover a unit mass of water from the wet trash. It should be noted that any water recovery system that involves evaporation will have to provide the latent heat needed for vaporization. For systems that do not have provision for recovering and reusing this heat, such as those solely using microwave (Wignarajah et al., 2009) or resistive heating, the latent heat represents the minimum energy input needed to recover a unit mass of water. However, the dryer system studied here, which combines closed-loop, forced-convection air drying with heat recovery from a condenser cooled by a refrigerator/heat pump, makes it possible to reduce the energy requirement below the latent heat. This potential for high energy efficiency makes this system an attractive option for use in long-term space missions.

NOMENCLATURE

Symbol	Description	Units
$C_{p,ave}$	Average heat capacity of moist air	kJ kg^{-1} K^{-1}
c_v	Concentration of water vapor	moles m^{-3}
c_v*	Equilibrium concentration of water vapor	moles m^{-3}
$c_{v,\ in}$	Inlet concentration of water vapor	moles m^{-3}
$c_{v,\ plate}$	Concentration of vapor at surface of porous plate	moles m^{-3}
D_v	Diffusivity of water vapor in air	m^2 s^{-2}
g	Acceleration due to gravity	m s^{-2}
$\mathcal{H}_{in}$	Inlet humidity ratio	kg water kg^{-1} dry air
k_{ave}	Thermal conductivity of moist air	kJ s^{-1} m^{-1} K^{-1}
p	Total pressure	Pa
p*	Equilibrium vapor pressure	Pa
R	Universal gas constant	Pa m^3 $mole^{-1}$ K^{-1}
Q_c	Rate of heat transfer into cold side of TE	Watts
Q_h	Rate of heat transfer into hot side of TE	Watts
t	Time	s
T_{in}	Temperature of air entering condenser	K
T_{plate}	Temperature at surface of plate	K
T_c	Temperature of cold side of TE	K
T_h	Temperature at hot side of TE	K
u	x-component of velocity	m s^{-1}
v	y-component of velocity	m s^{-1}
v_{in}	y-component of inlet velocity	m s^{-1}
W	Power used by TE	Watts
ρ_{ave}	Average density of moist air	kg m^{-3}
ρ	Density	kg m^{-3}
μ	viscosity	kg s^{-1} m^{-1}
COP	Coefficient of performance	
TE	Thermoelectric	

REFERENCES

Fisher, J. W., Hogan, J.A., Delzeit, L., Wignarajah, K., Alba, R., Pace, G. Fox, T.A. "Water Recovery from Wastes in Space Habitats - a Comparative Evaluation of SBIR Prototypes" *39th International Conference on Environmental Systems*. Savannah, GA, July 2009. SAE Technical Paper 2009-01-2342.

Makimura, K., et al. "Fungal Flora on Board the Mir-Space Station, Identification by Morphological Features and Ribosomal DNA Sequences." *Microbiology and Immunology* 45.5 (2001): 357-63.

Vesper, S. J., Wong, W., Kuo, C.M. and Pierson, D.L.. "Mold Species in Dust from the International Space Station Identified and Quantified by Mold-Specific Quantitative PCR." *Research in microbiology* 159.6 (2008): 432-5.

Hunter, J. B., et al. "Energy-Efficient Closed Loop Heat Pump Dryer for Solid Waste Stabilization on Long Duration Space Missions." *36th International Conference on Environmental Systems.* Norfolk, VA, July 2006. SAE Technical Paper 2006-01-2008.

Arquiza, J.M.R.A., Hunter, J.B., Morrow, R. and Remiker, R, "Modeling and Simulation of the Drying of Cabin Solid Waste in Long-Term Space Missions." *38th International Conference on Environmental Systems.* San Francisco, CA, June 2008. SAE Technical Paper 2008-01-2194.

McCabe, W., Smith, J., and Harriott, P., *Unit Operations of Chemical Engineering*, 7th ed., New York: McGraw-Hill, 2004.

Nolas, G. S., Sharp, J. and H. J. Goldsmid. *Thermoelectrics : Basic Principles and New Materials Developments*. Berlin: Springer, 2001.

Scovazzo, P., et al. "Hydrophilic Membrane-Based Humidity Control." *Journal of Membrane Science* 149.1 (1998): 69-81.

Sunada, E., Park, C., Miller, J., Ganapathi, G. and G. Birur. "Start-Up Characteristics and Gravity Effects on a Medium/High-Lift Heat Pump using Advanced Hybrid Loop Technology." *38th International Conference on Environmental Systems.* San Francisco, CA, June 2008. SAE Technical Paper 2008-01-1959.

Wignarajah, K., Alba, R., Hogan, J.A., Fisher, J. W., and T.A. Fox. "Investigations into Water Recovery from Solid Wastes using a Microwave Solid Waste Stabilization and Water Recovery System." *39th International Conference on Environmental Systems.*" Savannah, GA, July 2009. SAE Technical Paper 2009-01-2341.

ACKNOWLEDGMENTS

We thank NASA for funding this work under STTR Phase I award OTC GS0144-FR-05-1 and Phase II award GS0180-TR-06-01.

CHAPTER 4

DEVELOPMENT OF A QUANTITATIVE REAL-TIME PCR METHOD FOR MEASURING THE BIOMASS OF FUNGI IN THE FOOD COMPONENTS OF SPACE TRASH

INTRODUCTION

Fungi can colonize a wide variety of solid substrates and their presence can be detrimental or beneficial, depending on the species involved. In situations where the fungi are pathogens, destroy property, or produce allergens and toxins, their growth is a problem and needs to be controlled or eliminated. These include fungal infestation of buildings and houses, mycotoxin contamination of agricultural crops, fungal pathogens on plants, and food spoilage. An accurate method of quantifying the biomass of the fungal species of interest is needed to monitor the effectiveness of the control measures being implemented. On the other hand, fungi with desirable properties have also been actively cultivated. Examples are fungi in fermented foods, fungal biocontrol agents, and solid-state fermentation for the production of useful substances such as enzymes. In these cases, measurement of fungal biomass is necessary to determine if the desired species is growing at the desired rate.

Several methods have been studied in the literature to measure fungal content in solid media and they can be classified as conventional techniques or molecular biology based. The conventional methods are the following (Marin, S. et al., 2005; Raidl et al., 2005; Taniwaki et al., 2006): measurement of colony diameter, evaluation of colony forming units (standard plate counts), direct weighing of biomass, visual measurement of hyphal length under a microscope, and the correlation of biochemical markers such as chitin, glucosamine or ergosterol to biomass.

Among these, it is only the biochemical assays that can estimate fungal biomass growing in three dimensions, that is, with mycelial growth within the matrix of the solid substrate. Ergosterol measurements have been proven to be the most reliable but it cannot distinguish between different fungal species since the amount measured will be from all the fungi in the sample (Taniwaki et al., 2006).

Recent studies have shown that molecular biology methods which detect DNA from individual fungal species can be used to determine their amount in samples. Since the method can be designed to measure only the DNA of a target species, it is possible to quantify the biomass or conidial density of a particular species even in cases where several fungi are growing together. The most promising method for this purpose is real-time polymerase chain reaction (rt-PCR) which involves tracking the rate at which the target DNA sequence is amplified by PCR. In the past years, the use of rt-PCR to quantify fungal load has been demonstrated for building interiors and dust (Haugland et al., 2004), samples from the International Space Stations (Vesper et al., 2008), soils (Luo et al., 2009), animal feedstock (Suanthie et al., 2009), ectomycorrhizae (Raidl et al., 2005), fungal biocontrol agents (Eikenes et al. 2010), white rot fungi for bioremediation (Yamashita et al., 2009), and fungal contamination of agricultural crops (Gil-Serna et al., 2009; Gonzales-Salgado et al., 2009; Milderos et al., 2009). These studies have shown that rt-PCR can be a reliable, sensitive, and specific assay for quantifying fungal DNA or spores. The availability of affordable rt-PCR machines, commercial DNA extraction kits, publicly accessible database of fungal gene sequences, and rt-PCR master mixes have also made it easier to perform rt-PCR. Results can be obtained within one to two hours after DNA extraction (Mackay et al., 2007).

The data for these are taken from two-dimensional fungal growth on petri dishes since the diameter cannot be measured with three-dimensional growth on porous substrates (Marin et al., 2008). The development of an rt-PCR assay will allow the modeling of fungal growth with extensive substrate infiltration and in the presence of other fungal species.

The rt-PCR based method that will be developed to quantify fungi growing in a solid matrix can be used to investigate how drying astronaut cabin trash affects the growth rate of fungi in the food components present. Knowing the effect of water activity on fungal growth will be important in determining the extent of drying needed to prevent microbial proliferation. The setting of a minimum moisture content for the production of stable trash for storage will avoid extra energy consumption by drying beyond this point.

Objectives

1. To develop a real-time PCR assay for fungal DNA that can be used to quantify fungal biomass growing on solid media
2. To develop a model for fungal growth in terms of biomass (In the literature, fungal growth models are expressed in terms of colony diameter)
3. To determine the effect of water activity on the biomass growth rate of a fungi
4. To test the capability of the developed rt-PCR assay to measure the biomass of a target species growing in a mixed cultures with other fungi

MATERIALS AND METHODS

Fungal strains

Freeze-dried *Penicillium chrysogenum* (NRRL 807) and *Aspergillus niger* (NRRL 330) were obtained from the Agricultural Research Service (ARS), United States Department of Agriculture. These were revived and grown on Potato Dextrose Agar (Sigma-Aldrich, Saint Louis MO) by following the included instructions.

Fungal inoculum preparation

Spore suspensions were prepared by harvesting spores from fungi grown for a week on Potato Dextrose Agar (PDA) with the use of an inoculating loop that was then shaken in DI water containing 0.05% Tween 20. The number of colony forming units (CFU) in the spore suspension was determined by standard plate counts on PDA after incubation at 25°C for 72 hours.

Collection of fungal biomass from solid culture

Penicillium chrysogenum spore suspensions were spread-plated on PDA agar covered with cellophane (Bio-Rad Laboratories, Inc., Hercules, CA) and then incubated at 25°C. The cellophane was previously autoclaved while submerged in water inside a glass petri-dish for 15 minutes at 121°C and then aseptically placed on top of the PDA. The fungus was also grown on PDA without a cellophane overlay for comparison. No observable difference was seen between growth on PDA with or without the cellophane.

It was observed that spore formation (blue-green spots against the white mycelia) occurred after 60 hours of growth under these conditions. Therefore, biomass classified as without spores were harvested at 55 hours while those with spores at 72 hours. Gentle scraping with a sterile

polyester swab was enough to completely separate the mycelia from the cellophane-covered surface. The collected biomass was then transferred to a tared aluminum weigh boat and its fresh mass measured. The sample was placed afterwards in a dessicator with Drierite and allowed to dry under vacuum for at least two days.

Solid media preparation and inoculation

Commercially available Matzo meal (The Manischewitz Company, Newark, NJ) was chosen as the solid media in the study. This food was selected because of its particulate nature and simple composition: it is made by crushing dried crackers consisting only of wheat flour and water (no yeast). Matzo pieces passing through a screen with 3 mm square openings were used in the study.

One hundred milligrams of media were wetted with 200 μL of DI water and then placed in tared aluminum boats before autoclaving for 15 min at 121°C (Fig. 2.1). The sterile media were inoculated by evenly distributing 80 μL of a spore suspension whose concentration has been adjusted so that it delivers the desired number of CFU's. For runs involving *P. chrysogenum* only, 100 CFU's were added to the media. For the co-culture studies, the inoculum contained 100 CFU's each of both *P. chrysogenum* and *A. niger*.

After inoculation, the water activity of several samples were measured using an Aqualab water activity meter (Decagon Devices, Inc., Pullman, WA). The values obtained were always higher than that desired so the samples were placed in dessicators with Drierite to decrease their moisture contents. In order to make the drying go faster, several dessicators were used so that each contained only a maximum of 15 samples. This moisture adjustment period was found to vary with the required final water activity: 30 minutes for 0.973, 1 hour for 0.936 and 2 hours for

0.843. Based on the typical germination times for *P. chrysogenum* of at least 10 hours (Judet et al., 2008), the spores should remain dormant during this period.

Controlled water activity studies

The inoculated samples were placed in dessicators in which the desired water activities were maintained using saturated solutions of K_2SO_4, KNO_3, and KCl for 0.973, 0.936, and 0.843, respectively (Labuza and Bell, 2000). These were kept in 25°C incubators for the duration of the experiment.

At set time intervals, three samples were randomly selected, quickly removed from the humidity-controlled dessicators, weighed, and representative samples observed with a digital bright field microscope (KH-7700Hirox-USA, River Edge, NJ). These were then placed under a vacuum in a dessicator with Drierite. The samples were allowed to dry for at least 48 hours before DNA extraction.

DNA extraction

Dried samples were weighed and then finely ground by mortar and pestle. Three independent extractions were done for every sample. The amount used in each extraction was 7 mg for pure fungal mycelia and 10 mg for fungi together with solid substrate. The DNA extraction procedure was adapted from Sambrook and Russell (2006). Samples inside microcentrifuge tubes were suspended in 600 µl of a buffer containing 0.1 M sorbitol, 0.1 M EDTA, 28 mM β-mercaptoethanol, and 800 units of Lyticase enzyme (Sigma Aldrich, St. Louis, MO) and then incubated at 37°C for 2 hours. The solids were collected after the enzyme treatment by centrifugation for 30 s at 10,000 ***x g***. These were then resuspended in another buffer (50 mM Tris Cl, pH 7.5 and 20 mM EDTA) by vortex mixing for a minute. After addition of 50 µl of 10%

SDS, the tubes were incubated at 65°C for 30 minutes. During this period, mixing of the contents was done every ten minutes by rapidly inverting each tube several times. Two hundred microliters of 5 M KCH_3COO were then added and the tubes kept in ice for 1 hour. The cell debris was then separated from the nucleic acids in solution by centrifugation at 10,000 ***x g*** for 10 minutes. The supernatant was transferred to a new tube and 700 µl of isopropanol added to it to precipitate the DNA. The mixture was allowed to sit at room temperature for 5 minutes and then centrifuged at 10,000 ***x g*** for 3 minutes. The supernatant was discarded and the DNA pellet was dried under vacuum for 3 minutes. The DNA was then resuspended in 75 µl of TE buffer and stored at -20°C.

DNA Quantification

The genomic DNA in the extracts was quantified with the fluorescent nucleic acid stain Picogreen. The Quant-iT Picogreen dsDNA Reagent and Kit from Invitrogen (Life Technologies, Carlsbad, CA) was used following the manufacturer's instructions. The standard curve was constructed from the included Lambda DNA standard and fluorescent measurements (excitation, 480 nm; emission, 520 nm) were done on a Perkin Elmer Fluorescent Spectrophotometer Model 650-10S (Perkin Elmer, Inc., Waltham, MA).

Primers and Probe

The primers and Taqman probe used for the rt-PCR of *P. chrysogenum* were those tested by Haugland et al. (2004). These are posted on the EPA Technology for Mold Identification and Enumeration website (http://www.epa.gov/microbes/moldtech.htm#primers). The target DNA fragment is within the internal transcribed spacer region with size 70 bp and Genebank Accession number GQ458038.1. The Forward Primer, designated as PchryF4-1 has the sequence

5'-GCC TGT CCG AGC GTC ATT. The Reverse Primer (PchryR8) is 5'-CCC CCG GGA TCG GAG. The probe is Pen P6 with sequence 5'-CC AAC ACA CAA GCC GTG CTT GAG G. The primers and probes were obtained together in one tube through the PrimeTime qPCR Assays service of Integrated DNA Technologies (Coralville, IA). The primer to probe ratio used was 2:1 with the probe having a fluorescent dye and quencher combination of FAM and ZEN/Iowa Black FQ, respectively. The primers and probe mixture was received in solid form and a 40X solution was prepared by following the included instructions.

Real-time PCR

Real-time PCR was carried out using the CFX96 Real-Time PCR Detection System (Bio-Rad Laboratories, Inc., Hercules, CA) in the Biofuels Research Lab (Cornell University, Ithaca, NY). Reactions were performed in triplicate with total volumes of 20 µl. The reaction mixtures were placed in Low-Profile 0.2 ml PCR Tube Strips that were covered with matching transparent Cap Strips (Bio-Rad Laboratories, Inc., Hercules, CA). Each reaction tube contained 10 µl of 2X iQ Supermix (Bio-Rad Laboratories, Inc., Hercules, CA), 0.5 µl of 40X Primer/Probe solution, 8.5 µl milliQ water and 1 µl of DNA extract. Standard procedures specified by the manual for the CFX96 machine were followed. The rt-PCR protocol used consisted of an initial heating step of 10 minutes at 95°C, followed by 40 cycles of 15 seconds at 95 °C for template denaturation and 1 minute at 60°C for probe/primer annealing and primer extension (Haugland et al., 2004). Cycle threshold (C_t) determinations were automatically calculated by the CFX Manager Software using default parameters. Every rt-PCR run included a standard curve and no template control (milliQ water) samples which were also done in triplicate. Absolute quantification of DNA in the experimental samples was determined by comparing C_t values against the standard curve. A

series of standards were generated from serial dilutions (10 to 10^6) of an extract containing a known amount of genomic *P. chrysogenum* DNA. The 10^6 standard solution contained 15.1 ng DNA μl^{-1}.

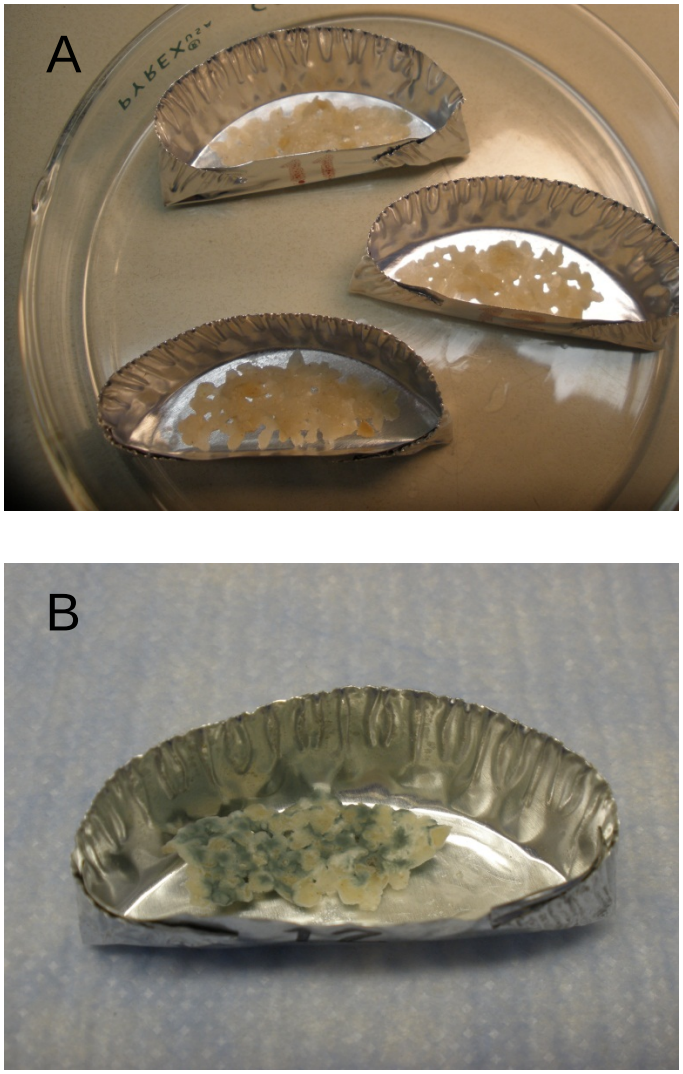

Fig. 4.1 (A) Matzo meal media (cooked wheat flour) already autoclaved and ready for inoculation. (B) *Penicillium chrysogenum* growing on the media.

RESULTS AND DISCUSSION

DNA-to-biomass ratio

DNA was extracted from *Penicillium chrysogenum* mycelia with and without spores. The measured amounts of DNA per mass of dry sample for both cases are given in Table 4.1. The two values were found to be not statistically different ($p > 0.05$). Since it is expected that the spores will significantly increase the DNA content, this result indicates that the method was not able to extract spore DNA. This is a reasonable conclusion since fungal spores have evolved to withstand extreme conditions and more severe steps such as freezing with liquid nitrogen (-80°C) or heating to high temperatures (95°C) are needed to extract their DNA (Rodriguez et al., 2012). The protocol also involved a preliminary enzyme treatment step where the biomass was separated from solution by centrifugation at 10,000 ***x g*** for 30 s. It is highly probable that most of the spores remained in the supernatant and was discarded with it. The obtained DNA-to-biomass ratio can therefore be used to convert the mass of *P. chrysogenum* DNA into mycelial biomass. The average value for all the data (with and without spores) is 0.948 ng DNA μg^{-1} biomass, dry basis. This is close to the values reported by Le Drean et al. (2010) for *Penicillium camemberti* (0.8 ng DNA μg^{-1} biomass) and *Penicillium roqueforti* (1.5 ng DNA μg^{-1} biomass) grown in Potato Dextrose broth.

Table 4.1 Measured DNA content of *P. chrysogenum* grown on Potato Dextrose Agar.

Sample	DNA content (ng DNA μg^{-1} biomass, dry basis) Mean + S.D. (n = number of independent cultures)
Mycelia before spore formation	0.973 ± 0.158 (n = 12)[a]
Mycelia with spores	0.897 ± 0.138 (n = 6)[a]

[a] Values are not statistically significant ($p > 0.05$)

Real-Time PCR standard curve and efficiencies

Standard curves were included in every real-time PCR run. The PCR efficiencies were calculated from the slopes of the standard curves and the values went from 93 to 105 % with all $R^2 \geq 0.985$. These are within the accepted range of 80 to 110 % efficiency and $R^2 \geq 0.98$ (Fredlund et al., 2008). A representative standard curve is given in Fig 4.2.

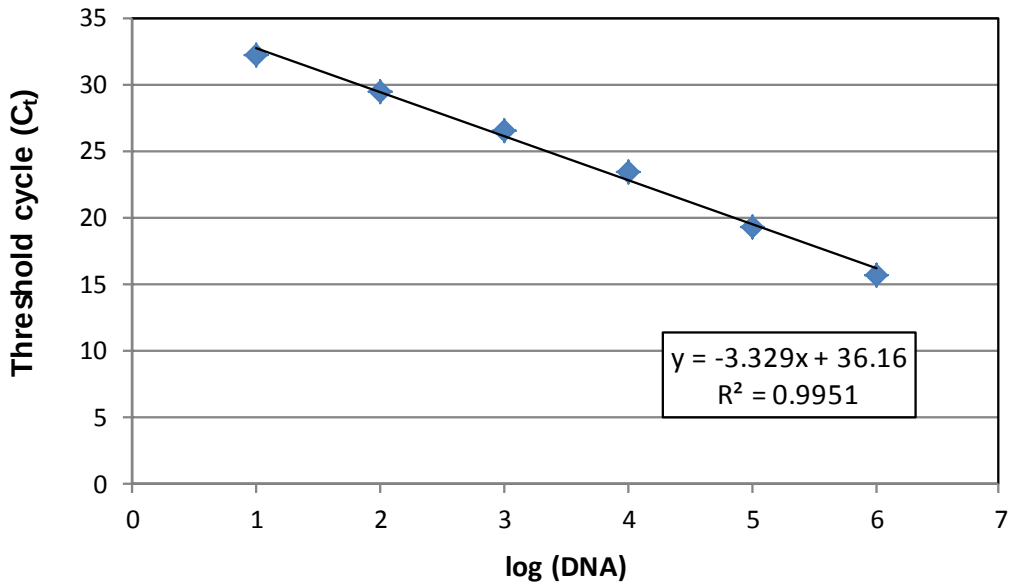

Fig. 4.2 Representative standard curve for the real-time PCR assay of *P. chrysogenum*. The efficiency calculated from the slope is 99.7%. The amount of genomic DNA in the reaction mixture corresponding to log(DNA) = 6 is 15.1 ng.

As discussed in the Methodology section, the standard curve used genomic DNA extracted from pure culture of *P. chrysogenum* on PDA because the cooked flour used in the study also contributes DNA. Since something in the flour may decrease the efficiency of the real-time PCR, the assay was performed on DNA extracted from *P. chrysogenum* growing on the flour. The DNA concentrations used in the reaction were the same as that for the standard curve (10 to 10^6). The Ct vs. log (DNA) plot of the data gives an efficiency of 98 % and R^2 of 0.99, which is within the values obtained for the standard curve. The standard curve can therefore be

reliably used to quantify the DNA in the flour samples because their PCR efficiencies are comparable.

Effect of water activity on growth

The change in biomass with time for *P. chrysogenum* incubated at water activities of 0.843, 0.936, and 0.973 are shown in Figure 4.3. The fastest growth was observed at 0.973 while no growth was seen at 0.843. (There is additional data for 0.843 at 15, 20, and 25 days of incubation which also shows negligible biomass but this was not shown in the figure to avoid compressing the graphs for the other water activities). The plot for 0.973 shows that biomass started to increase only after day 1 and continued to do so until day 3 (9.2 μg biomass mg^{-1}, dry basis). The biomass decreased to 7.6 μg biomass mg^{-1} the next day but increased again on day 5 (8.5 μg biomass mg^{-1}). However, the values for days 3, 4 and 5 are not significantly different ($p > 0.05$) so there was essentially no growth during this period. The curve seems to follow the typical lag, exponential, and stationary phases for fungal growth (Moore et al., 2011). The same pattern was observed for incubation at 0.936. The biomass increased from day 3 to day 5, reaching 1.2 μg biomass mg^{-1}, where it remained constant until day 7. Growth seemed to resume after this as a higher biomass of 1.8 μg biomass mg^{-1} was recorded on day 10. This is probably due to the emergence of a second generation of mycelia produced from spores that were seen on day 5 (Fig 4.3).

The lag phase is the period before the spores germinate after finding a favorable environment for growth. The data would show this as the time period after inoculation during which the biomass remains almost zero. From Figure 4.3 the observed lag phase for 0.936 is 2

days while that for 0.973 is 1 day. This in agreement with the findings of Judet et al. (2008) that the germination time of *P. chrysogenum* spores becomes longer as water activity is lowered.

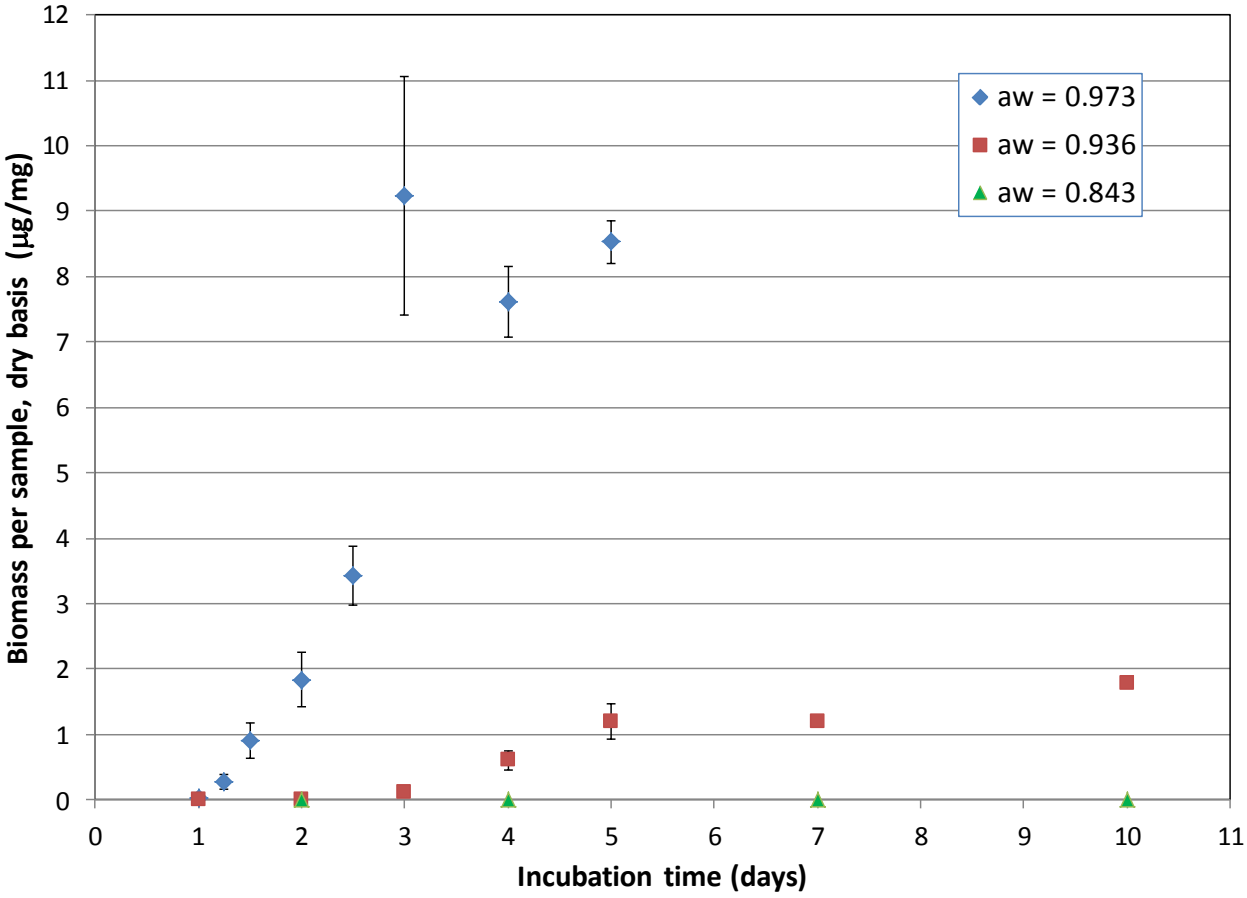

Fig. 4.3 The time evolution of *P. chrysogenum* biomass growing on solid media (cooked flour) maintained at different water activities (n = 3). Additional data for 0.843 at 15, 20, and 25 days that also show negligible biomass are not shown to avoid compressing the other graphs.

If the amounts at the stationary phases are taken as the maximum biomass produced from the initial inoculum, then that for 0.973 is about seven times greater than that for 0.936. The difference is most likely due to a smaller percentage of spores germinating at 0.936 compared to that at 0.973. Judet et al. (2008) reported that *P. chrysogenum* spores had a percentage germination of 95.9-100% at 0.99 water activity but at 0.95, this decreased to 47.7-64.6%.

Microscopic observations also show that mycelia at 0.973 have much more aerial hyphae than that at 0.936 and this should translate to more biomass at the higher water activity level (Fig. 4.5).

The later start of the stationary phase for 0.936 (day 5) compared to that for 0.973 (day 3) can also be explained by the smaller percentage of spores germinating at the lower water activity. Filamentous fungi quickly invade their environment by the apical elongation of sparsely branched hyphae across the media. However, when they get near mycelia from another colony, the hyphae tries to extend away from it and if there is no space to go to, growth slows down (Moore et al, 2011). With fewer spores germinating at 0.936, the colonies formed will be farther apart than those at 0.973 and it would therefore take longer for their advancing hyphae to reach each other. This, combined with slower growth (to be discussed later), would result in a delay in the onset of the stationary phase at the lower water activity.

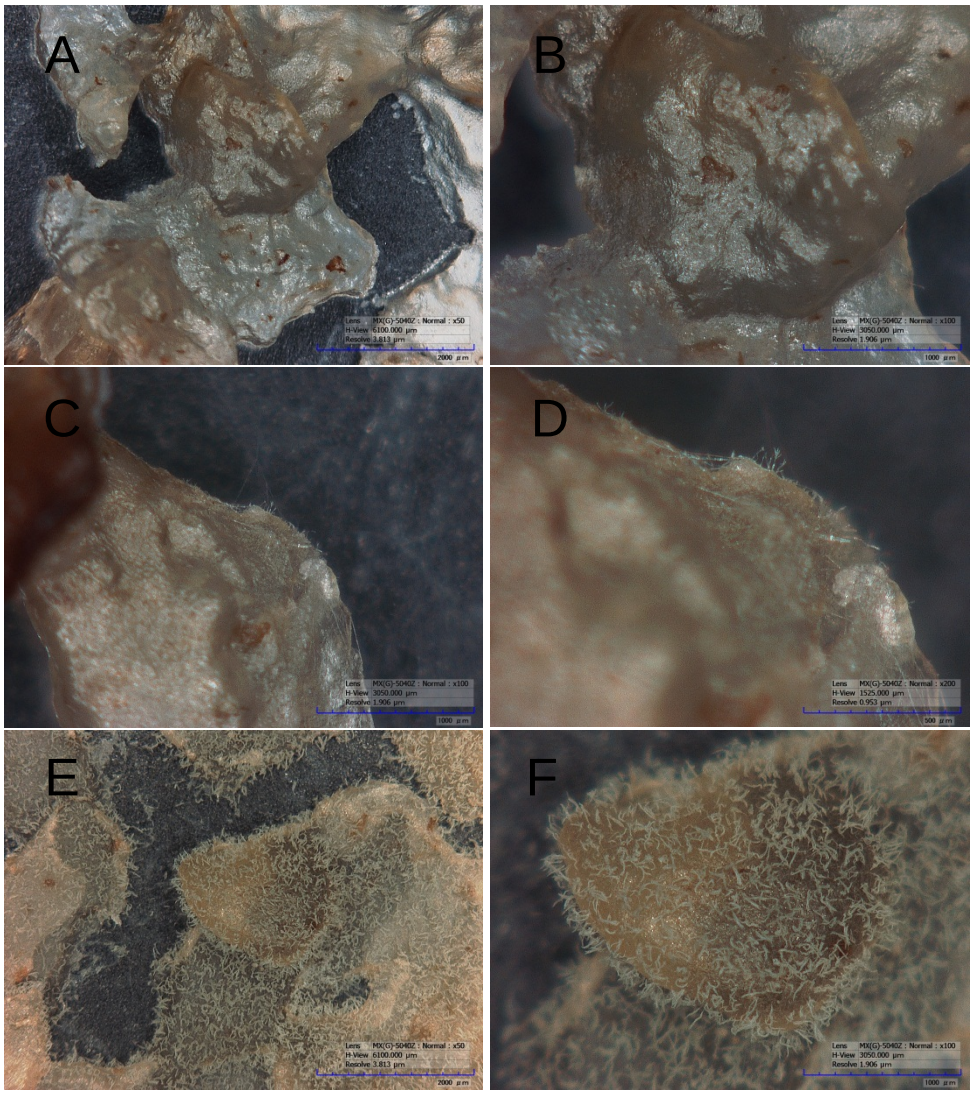

Fig. 4.4. Microscopic observation of Penicillium chrysogenum growing on cooked flour at 0.936 water activity. The magnification power is given in the image labels (50X, 100X, and 200X). (A) and (B), after 2 days of incubation, there is still no visible growth. (C) and (D), after 3 days, a few aerial and sparsely-branched hyphae can be seen. (E) and (F), after 5 days, mycelia with mature spores (blue-green) are now present.

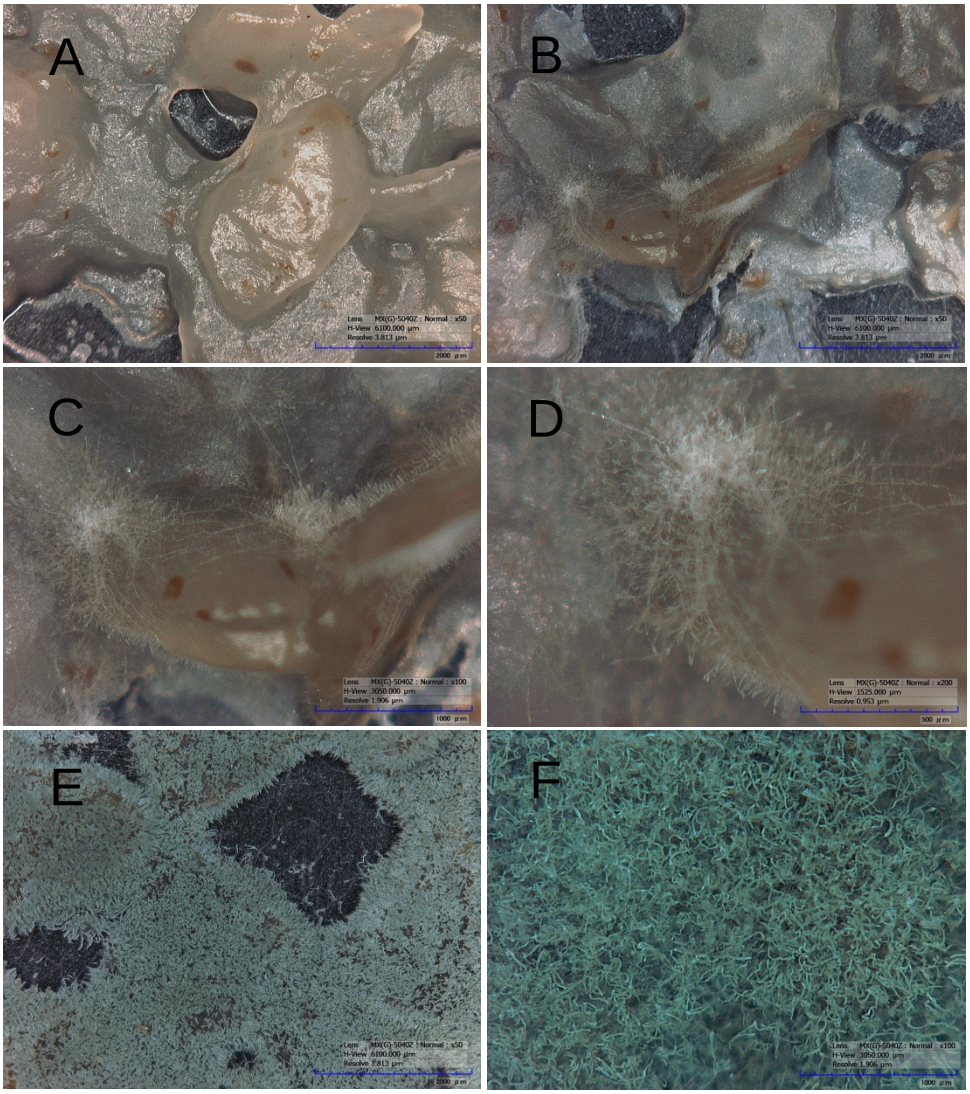

Fig. 4.5. Microscopic observation of *Penicillium chrysogenum* growing on cooked flour at 0.973 water activity. The magnification power is given in the image labels (50X, 100X, and 200X). (A) No visible growth after 1 day. (B), (C) and (D), Images of increasing magnification showing mycelial growth after 2 days. Abundant aerial hyphae and those extending across the media are both present. (E) and (F), after 3 days, the media is completely covered by mycelia with mature spores (blue-green).

Quantitative model of growth

After spore germination, the germ tube elongates to explore its environment. When the conditions are favorable for the fungus, the hyphae rapidly extends away from its original location and forms branches along its sides. The growth rate in terms of the total mycelial length (apically extending hyphae and branches) at this period is exponential (Moore et al., 2011). If the mass of the growing colony is directly proportional to the total mycelial length, then it should be possible to locate this exponential phase in the biomass data obtained in the study.

The exponential phase of growth is modeled by the following differential equation:

$$\frac{dX}{dt} = \mu X \tag{3-1}$$

Where X is the biomass concentration and m is the specific growth rate. Integration leads to

$$\ln X = \mu t + constant \tag{3-2}$$

Application of the initial condition (t = 0, X = X_0) produces

$$\ln X = \mu t + \ln X_0 \tag{3-3}$$

A plot of ln(X) against time is a straight line with slope μ and y-intercept ln(X_0). If the natural logarithm of the obtained biomass data for *P. chrysogenum* is plotted against time, the exponential growth phase will be the linear portion of the graph. The ln(X) vs. time plots for growth at water activities of 0.973 and 0.936 are shown in Fig. 4.6 and Fig. 4.7, respectively.

The graph for 0.973 shows a rapid increase in biomass from 24 to 30 hours, corresponding to the period when the spores germinate. This is followed by a section that appears linear up to 72 hours. These data are placed in a new plot (Fig 4.6B) and a best-fit line passed through them. The line has a slope of 0.0752 h^{-1} and an R^2 of 0.956. The plot for 0.936 shows that the data from 24 to 96 hours approximate a line. The rapid increase seen immediately

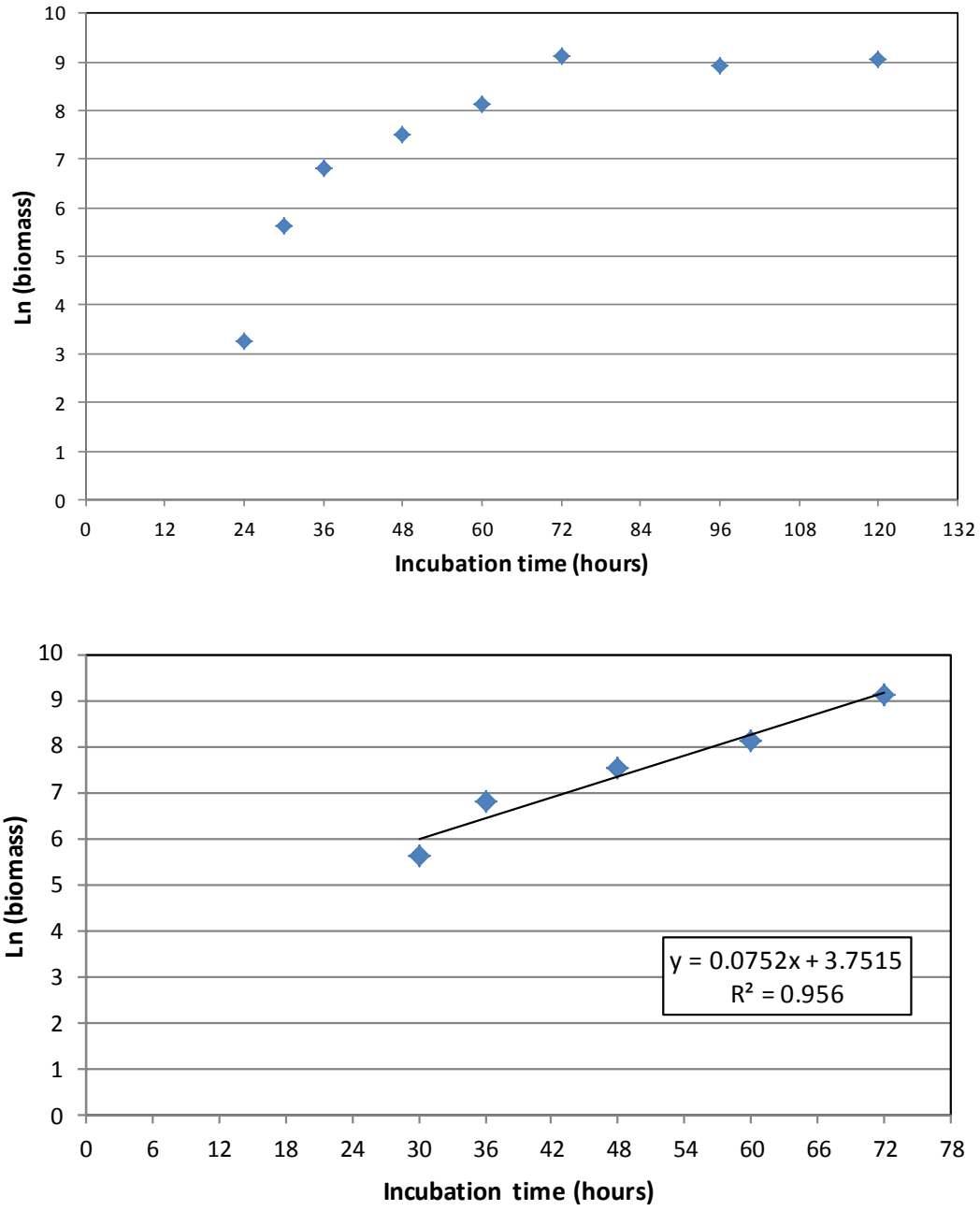

Fig. 4.6 (A) Transformation of the biomass data at 0.973 water activity into ln values to locate the exponential growth phase. **(B)** Regression analysis of the linear portion of the graph to determine the specific growth rate, μ (the slope).

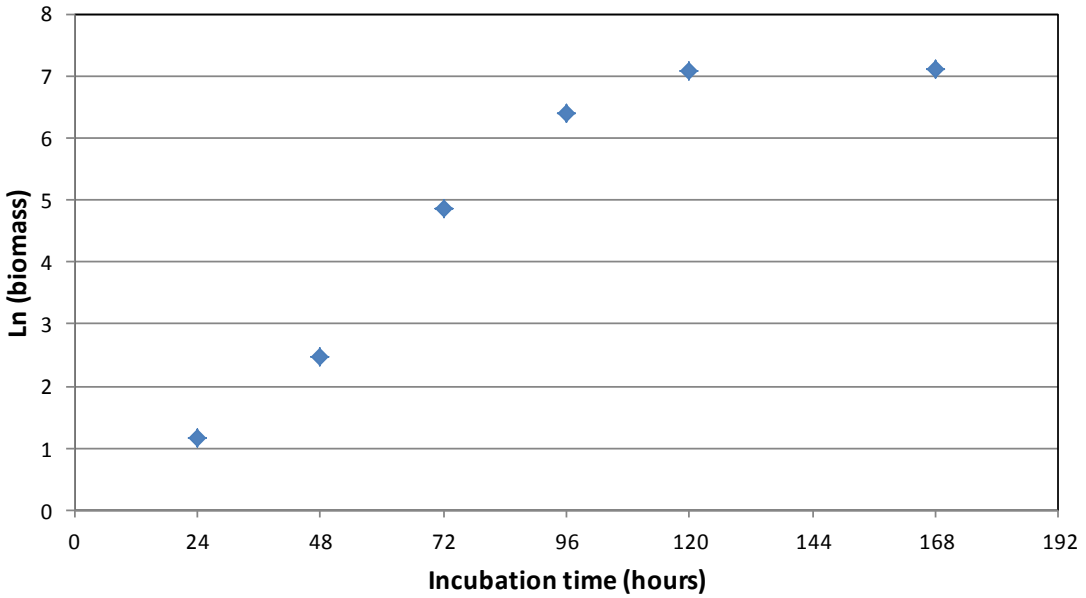

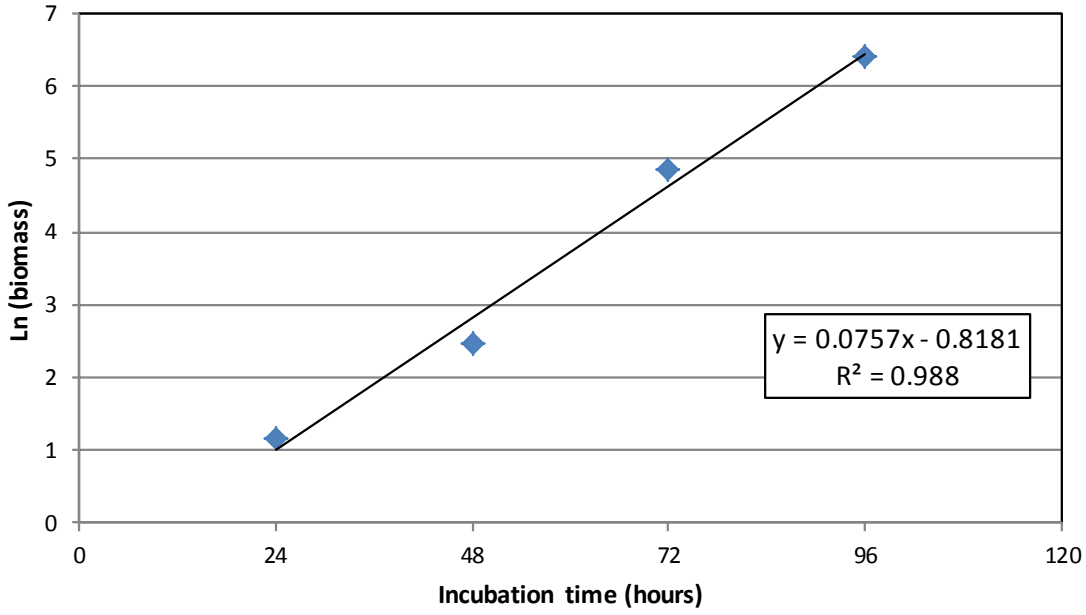

Fig. 4.7 (A) Transformation of the biomass data at 0.936 water activity into ln values to locate the exponential growth phase. **(B)** Regression analysis of the linear portion of the graph to determine the specific growth rate, μ (the slope).

after 24 hours in 0.973 is not observed here. This would seem to indicate that at the higher water activity, the spores produce more biomass upon germination, possibly through aerial hyphae and extensive branching in order to take advantage of its favorable surroundings. Afterwards, the colony proceeds to extend sparsely-branched hyphae away from it and this growth is captured by the linear portion of the plot. Since the graph at 0.936 is linear starting from 24 hours, this could indicate that at this lower water activity, the fungi finds its environment after spore germination to be less than ideal and therefore immediately sends out hyphae to look for better conditions. The points for 24 to 96 hours are graphed separately in Fig 4.7B and then subjected to linear regression analysis. The slope of the line is 0.0757 h^{-1} with an R^2 of 0.988. The slopes of the lines in Fig. 4.6B and Fig. 4.7B are the specific growth rates (μ) for *P. chrysogenum* at water activities of 0.973 and 0.936, respectively. Since they are essentially equal, it would therefore seem that this parameter is not affected by the difference between the two water activities used here. To our knowledge, this is the first time that the specific growth rate of a fungus growing on a solid media at different water activities has been determined using real-time PCR. The measured specific growth rate of 0.0757 h^{-1} is near the value for maximum specific growth rate (μ_{max}) of 0.103 h^{-1} reported by Goudar and Strevett (1998) for growing in liquid batch fermentation with an initial glucose concentration of 40 g L^{-1}. Since the substrate in this study is starch, it is expected that the observed specific growth rate will be less than that for glucose because the fungus still has to breakdown the starch by producing hydrolytic enzymes.

It would seem surprising that the specific growth rates at 0.973 and 0.936 for *P. chrysogenum* are the same given that the biomass produced at the higher water activity is very much larger than that at the other. However, it should be noted that the actual growth rate is μ multiplied by the biomass concentration and since the biomass concentration at the start of the

exponential phase for 0.973 (0.281 µg biomass mg^{-1}) is greater than that at 0.936 (0.011µg biomass mg^{-1}), growth would be faster at the higher water activity. This finding emphasizes the importance of knowing the biomass production immediately after spore germination when predicting fungal growth rates and biomass concentration. The developed rt-PCR method would be appropriate for this since the traditional method of measuring colony diameters would be difficult at this early stage. The total growth rates in terms of µg biomass mg^{-1} sample h^{-1} (dry basis) were computed for the two water activities and their plots are shown in Fig. 4.8.

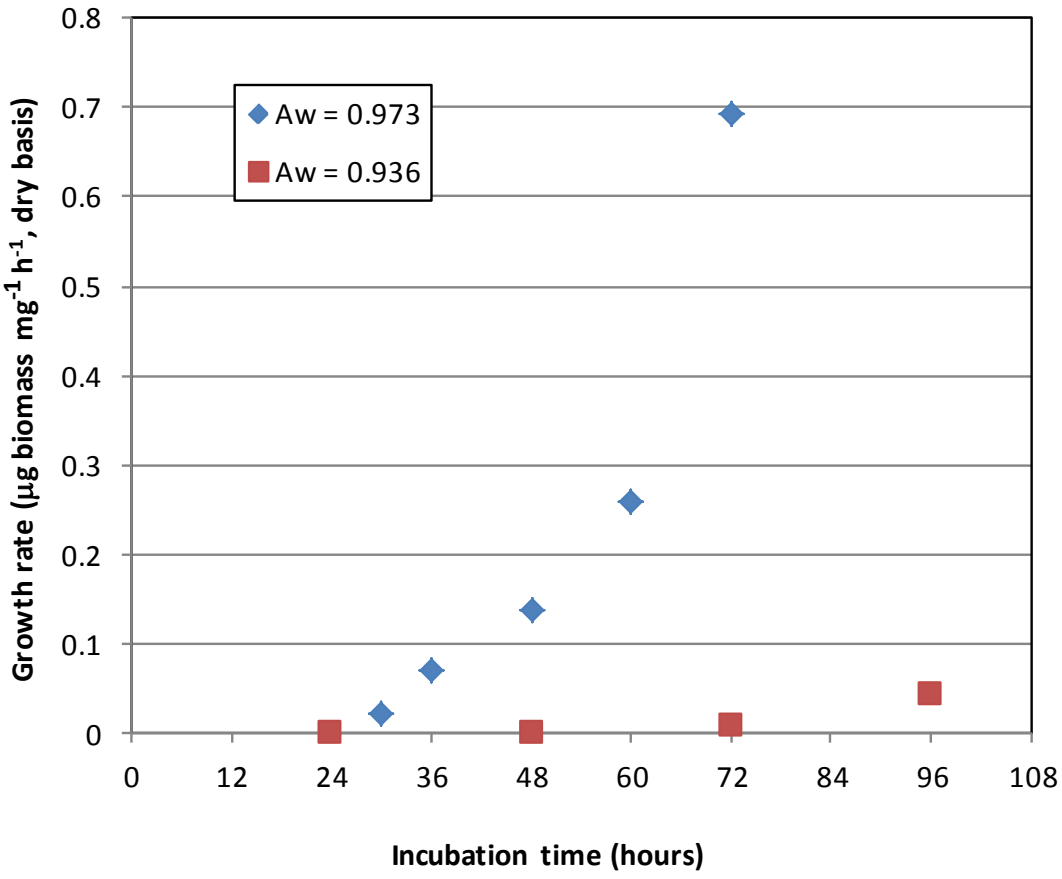

Fig. 4.8 Total growth rates of *P. chrysogenum* at different water activities.

At 0.973, the fungus initially grows at a rate of 0.021 μg biomass mg^{-1} sample h^{-1} (dry basis). This then increases to maximum of 0.694 μg biomass mg^{-1} sample h^{-1} (dry basis) at the end of the exponential phase. For 0.936, the growth rate goes from 0.0002 to 0.043 μg biomass mg^{-1} sample h^{-1} (dry basis).

Measuring P. chrysogenum growth in mixed culture

Effect of Aspergillus niger DNA on the P. chrysogenum rt-PCR standard curve

Quantification of the amount of *P. chrysogenum* DNA in a sample by the developed rt-PCR method depends on the standard curve. If the presence of other species in the media makes the standard curve different from that with *P. chrysogenum* only, then the rt-PCR method will give erroneous results. To test how the rt-PCR method is affected by another DNA, *Aspergillus niger* DNA was added to the solutions used for the standard curve. Each of the solutions used for the standard curve (10 to 10^6) were prepared with increasing mass ratios of *A. niger* DNA to that of *P. chrysogenum* (1:1, 2:1, 3:1, and 5:1). These *A. niger* + *P. chrysogenum* solutions were then subjected to rt-PCR together with the normal *P. chrysogenum* only standards. The resulting standard curves are shown in Fig. 4.9.

It can be seen that the C_t values are unchanged by the presence of *A. niger* DNA for all ratios tested as long as the amount of *P. chrysogenum* DNA is at least the 10^3 dilution (0.0151 ng DNA in reaction mixture). For ratios of 1:1 and 2:1, the unaffected dilutions go down to 10^2 (0.00151 ng DNA). When the dilution is 10 (0.000151 ng DNA), all ratios give Ct values different from that of the standard curve for *P. chrysogenum* DNA only. The changes in Ct values for the very dilute solutions can be due to competition between the desired hybridization reactions of the primers and probe with *P. chrysogenum* DNA and non-specific hybridization

with *A. niger* DNA. This would be more pronounced when there is only a small concentration of *P. chrysogenum* DNA and large amount of *A. niger* DNA relative to it. From this, it can be concluded that the developed method can reliably quantify *P. chrysogenum* DNA even in the presence of five times more *A. niger* DNA as long as the reaction sample used in the rt-PCR has a target DNA of at least 0.0151 ng . This result highlights the importance of testing the effect of other DNA on the standard curve before using an rt-PCR protocol on samples with mixed cultures.

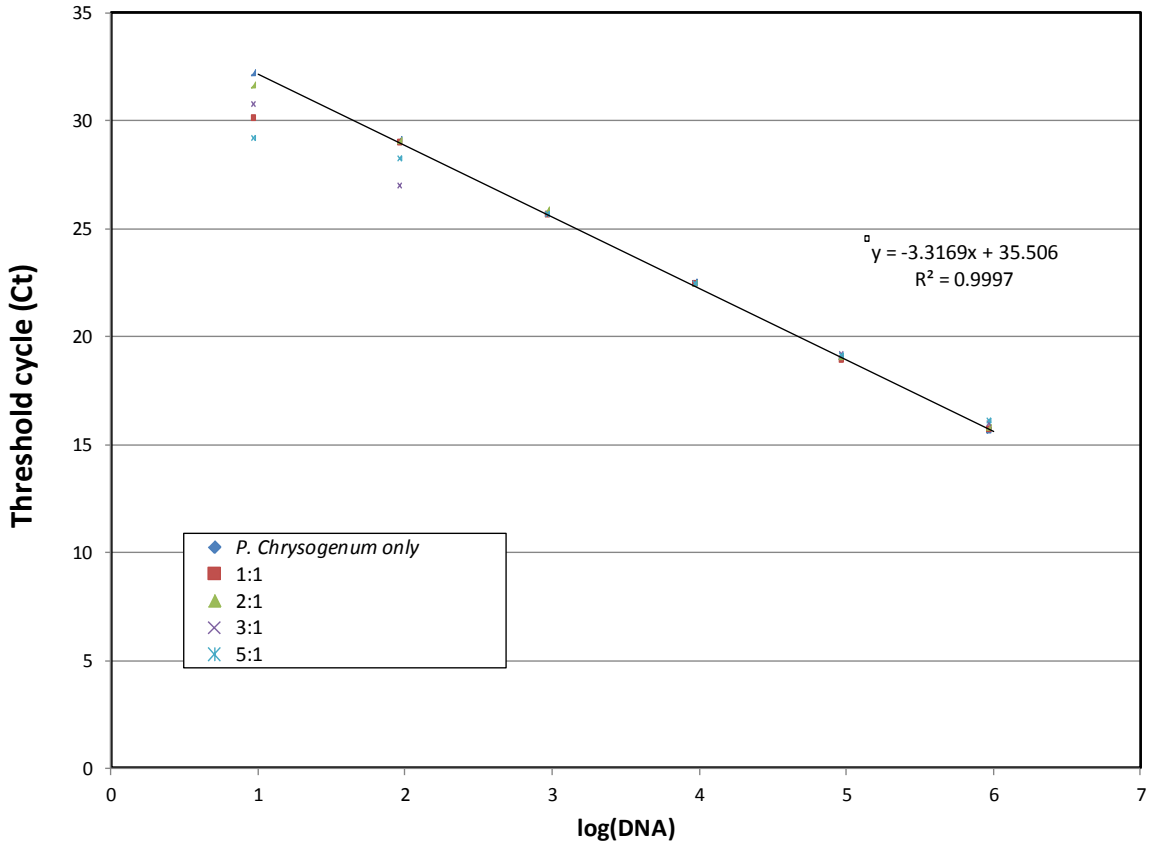

Fig. 4.9 The Effect of increasing ratios of *A. niger* to *P. chrysogenum* DNA on the standard curve of the real-time PCR assay.

P. chrysogenum growth in co-culture with A. niger

The earlier experiments on growth with *P. chrysogenum* show that Ct values that are greater than those corresponding to the 10^3 standard are only observed for incubation periods less than 30 hours at 0.973 water activity. It was therefore decided to use the rt-PCR protocol to measure the biomass of *P. chrysogenum* growing together with *A. niger* after 2 and 3 days. The cultures are shown in Fig.4.10. It can be seen that the *A. niger* seems to dominate the *P. chrysogenum* on the surface. The Ct values obtained for the DNA extracts from the mixed cultures were between that for 10^4 and 10^6 standards. This is within the range of *P. chrysogenum* DNA concentrations where the standard curve remains valid even in the presence of *A. niger* DNA. The biomass values obtained for samples with *P. chrysogenum* only and mixed *A. niger* + *P. chrysogenum* that were grown simultaneously in one desiccator at 0.973 are shown in Fig. 4.10.

4.10. Samples with *Penicillium chrysogenum* growing alone (A) and in co-culture with *Aspergillus niger* (B) on cooked flour at 0.973 water activity. The characteristic color of the conidiophores for both fungi can be seen in (B).

The amount of *P. chrysogenum* biomass in the mixed culture is less than that for just *P. chrysogenum* for both days. It is 28% and 62% lower in co-culture with *A. niger* at day 2 and day 3, respectively. This supports the visual observation in Fig. 4.10. The larger decrease at day 3 may be due to *A. niger* extending its hyphae faster than *P. chrysogenum*, therefore preventing further expansion of the newly-formed colonies. The *A. niger* may also be secreting substances that inhibit the growth of *P. chrysogenum* . Microscopic observations for the mixed culture are shown in Fig. 4.12.

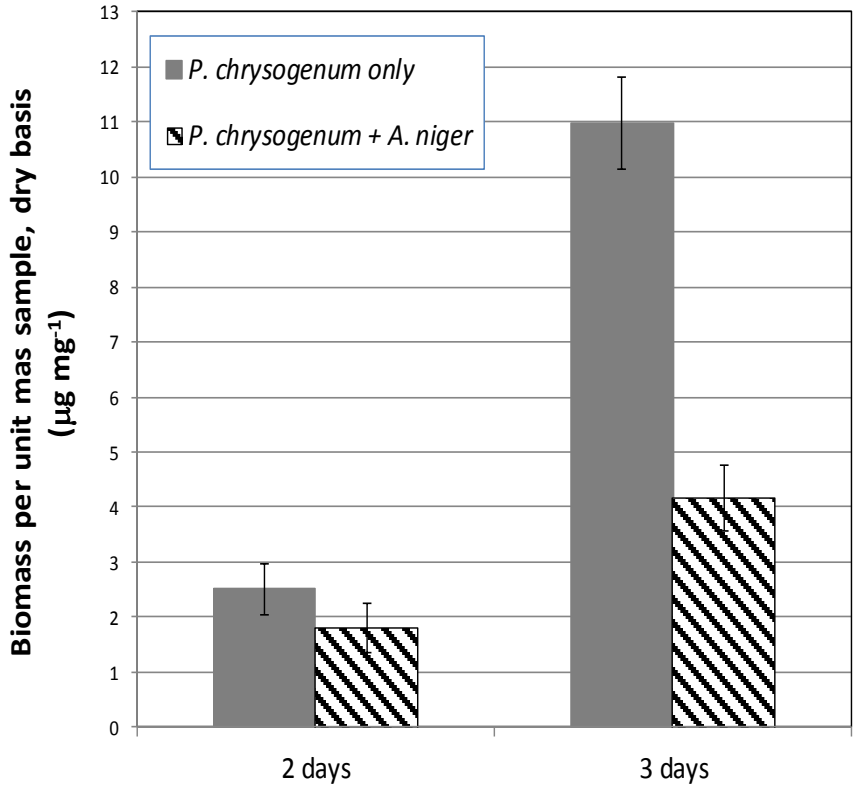

Fig 4.11 Comparison of *P. chrysogenum* biomass produced when grown by itself and in co-culture with *A. niger* (n = 3)

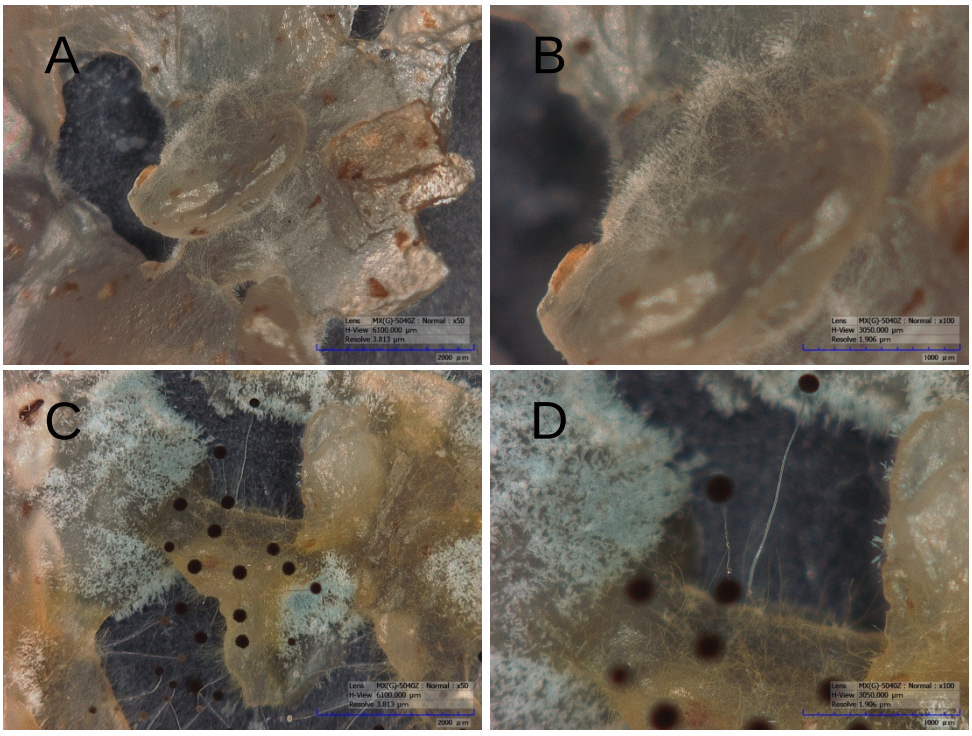

Fig. 4.12. Microscopic observation of a co-culture of *Penicillium chrysogenum* and *Aspergillus niger* growing on cooked flour at 0.973 water activity. The magnification power is given in the image labels (50X and 100X). (A) and (B), mycelial growth after 2 days showing the characteristic aerial hyphae of *P. chrysogenum*. (C) and (D), After 3 days, separate regions of growth have been established by both *P. chrysogenum* and *A. niger*. Conidiophores for both fungi are now present.

CONCLUSIONS

The study demonstrated the use of a real-time PCR assay to measure the biomass of a filamentous fungus infiltrating a solid media. This method was successfully used to plot the time evolution of *Penicillium chrysogenum* biomass as it grew on autoclaved Matzo meal (cooked wheat flour) under different water activities (0.973, 0.936, and 0.843). The protocol had a minimum detection limit of 7.6×10^{-5} ng genomic *P. chrysogenum* DNA per µl of PCR reaction mixture. The total biomass became smaller as water activity decreased until no growth was observed at 0.843. The growth curve on solid media was found to have a lag, exponential and stationary phase. Data from the exponential phases were used to calculate the specific growth rates (µ) for *P. chrysogenum* at water activities of 0.973 and 0.936. The absence of relevant papers in the literature suggests that this is the first time that the specific growth rate of a fungus growing on a solid media at different water activities has been measured using real-time PCR. The specific growth rates were found to be equal, and this may indicate that the parameter is not affected by water activity within the range tested. Since the growth rate in the exponential phase is given by µ multiplied by biomass concentration (µ*X), this result showed that it is the concentration at the start of this period that determines the difference between the fungal growth rates and total biomass concentrations observed for the two water activity levels. It is therefore important to understand the rate at which newly-germinated fungal spores produce biomass before they start growing exponentially. The fungal biomass rt-PCR assay developed here would be a useful tool for this kind of studies.

It was also shown that the rt-PCR assay is specific to a particular fungal species and can consequently be used to measure its biomass even in the presence of other fungi growing on solid media. This would not be possible for biomass estimation methods that use biochemical markers (e.g. ergosterol, chitin) since these would also be extracted from the other fungal species. The rt-PCR assay can therefore be used to determine the specific growth rate of a single fungal species growing in a mixed culture. This would be useful for competitive or synergistic studies of fungi involved in important and useful microbial communities (e.g. compost, activated sludge).

The capability of the rt-PCR assay to measure the biomass of a target species of filamentous fungi growing on a solid media makes it possible to perform kinetic studies that relate substrate consumption, product formation, and metabolic heat generation to the biomass growth rate. This information should prove to be invaluable in the development and validation of mathematical models for simulation of processes involving fungal growth on solid substrates (e.g. solid-state fermentation, microbial consortia for degrading lignocellulose in nature). This would greatly advance our understanding and future utilization of these systems.

REFERENCES

Bellanger, A-P, et al. "Indoor Fungal Contamination of Moisture-Damaged and Allergic Patient Housing Analysed using Real-Time PCR." *Letters in applied microbiology* 49.2 (2009): 260-6.

Eikenes, M., et al. "Comparison of Quantitative Real-Time PCR, Chitin and Ergosterol Assays for Monitoring Colonization of *Trametes Versicolor* in Birch Wood." *Holzforschung* 59.5 (2005): 568-73.

Fredlund, E., et al. "Method Evaluation of Fusarium DNA Extraction from Mycelia and Wheat for Down-Stream Real-Time PCR Quantification and Correlation to Mycotoxin Levels." *Journal of microbiological methods* 73.1 (2008): 33-40.

Gil-Serna, J., et al. "ITS-Based Detection and Quantification of *Aspergillus Ochraceus* and *Aspergillus Westerdijkiae* in Grapes and Green Coffee Beans by Real-Time Quantitative PCR." *International journal of food microbiology* 131.2-3 (2009): 162-7.

Gonzalez-Salgado, A., et al. "Specific Detection of *Aspergillus Carbonarius* by SYBR Green and Taqman Quantitative PCR Assays Based on the Multicopy ITS2 Region of the rRNA Gene." *FEMS microbiology letters* 295.1 (2009): 57-66.

Goudar, C. T., and K. A. Strevett. "Estimating Growth Kinetics of Penicillium Chrysogenum by Nonlinear Regression." *Biochemical engineering journal* 1.3 (1998): 191-9.

Haugland, R. A., et al. "Quantitative PCR Analysis of Selected *Aspergillus*, *Penicillium* and *Paecilomyces* Species." *Systematic and applied microbiology* 27.2 (2004): 198-210.

Judet, Daniela, et al. "Distributions of the Growth Rate of the Germ Tubes and Germination Time of *Penicillium Chrysogenum* Conidia Depend on Water Activity." *Food microbiology* 25.7 (2008): 902-7.

Labuza, Theodore P., and Leonard N. Bell. *Moisture Sorption : Practical Aspects of Isotherm Measurement and Use*. 2nd ed. St. Paul, MN : American Association of Cereal Chemists, 2000.

Le drean, G., et al. "Quantification of *Penicillium Camemberti* and *P. Roqueforti* Mycelium by Real-Time PCR to Assess their Growth Dynamics during Ripening Cheese." *International journal of food microbiology* 138.1-2 (2010): 100-7.

Luo, Y., et al. "Quantification of Conidial Density of *Aspergillus Flavus* and *A. Parasiticus* in Soil from Almond Orchards using Real-Time PCR." *Journal of applied microbiology* 106.5 (2009): 1649-60.

Mackay, I. M., et al. "Quantification of Microorganisms - Not Human, Not Simple, Not Quick." *Real-Time PCR in Microbiology. from Diagnosis to Characterization*. Ed. I. M. Mackay. 1st ed. Norwich , United Kingdom: Caister Academic Press., 2007. 133-182.

Marin, S., et al. "Fitting of Colony Diameter and Ergosterol as Indicators of Food Borne Mold Growth to Known Growth Models in Solid Medium." *International journal of food microbiology* 121.2 (2008): 139-49.

Marin, S., A. J. Ramos, and V. Sanchis. "Comparison of Methods for the Assessment of Growth of Food Spoilage Moulds in Solid Substrates." *International journal of food microbiology* 99.3 (2005): 329-41.

Mideros, S. X., et al. "*Aspergillus Flavus* biomass in Maize Estimated by Quantitative Real-Time Polymerase Chain Reaction is Strongly Correlated with Aflatoxin Concentration." *Plant Disease* 93.11 (2009): 1163-70.

Moore, D., Robson, G. D. and A.P.J. Trinci. *21st Century Guidebook to Fungi; Twenty First Century Guidebook to Fungi*. Ed. Cambridge ; New York : Cambridge University Press, 2011.

Raidl, S., R. Bonfigli, and R. Agerer. "Calibration of Quantitative Real-Time Taqman PCR by Correlation with Hyphal Biomass and its Copies in Mycelia of *Piloderma Croceum*." *Plant biology* 7.6 (2005): 713-7.

Rodríguez, A., et al. "A Comparative Study of DNA Extraction Methods to be used in Real-Time PCR Based Quantification of Ochratoxin A-Producing Molds in Food Products." *Food control* 25.2 (2012): 666-72.

Sambrook, J. and D. Rusell. *The Condensed Protocols from Molecular Cloning : A Laboratory Manual*. Cold Spring Harbor, N.Y. : Cold Spring Harbor Laboratory Press, 2006.

Suanthie, Y., M. A. Cousin, and C. P. Woloshuk. "Multiplex Real-Time PCR for Detection and Quantification of Mycotoxigenic *Aspergillus*, *Penicillium* and *Fusarium*." *Journal of stored products research* 45.2 (2009): 139-45.

Taniwaki, M. H., et al. "Comparison of Hyphal Length, Ergosterol, Mycelium Dry Weight, and Colony Diameter for Quantifying Growth of Fungi from Foods." *Advances in food mycology* 571 (2006): 49-67.

Vesper, S. J., et al. "Mold Species in Dust from the International Space Station Identified and Quantified by Mold-Specific Quantitative PCR." *Research in microbiology* 159.6 (2008): 432-5.

Yamaguchi, M., et al. "Quantification of the Mycelial Mass of the White-Rot Fungus *Pleurotus Pulmonarius* by Real-Time PCR." *Bulletin of the forestry and forest products research institute* 411 (2009): 133-41.

CHAPTER 5

SUMMARY AND RECOMMENDATIONS

A closed-loop, forced convection drying system for water recovery and stabilization of astronaut cabin trash was analyzed in this study. Computational models were developed for the two major processes involved: drying of the fixed bed of trash and recovery of the water vapor produced using a porous membrane condensing heat exchanger (PMCHX). These models were based on a prototype of the system on which experiments were performed. The resulting data were used to validate the model. In this section, a general discussion of the research project will be presented since the details have already been given in the previous chapters.

Deep bed drying of trash

A few factors complicated the formulation of the trash drying model and it became necessary to adopt simplifying assumptions. One was that the trash components do not have defined shapes and as a result their packing in the bed would be highly non-uniform. This led to the modeling of the trash as a porous media with large pores (Datta, 2007). Another was the heterogeneous nature of the trash; it was composed of different materials and their relative amounts could vary considerably. Since it was not possible to experimentally test all the probable combinations, a simplified version of the trash with only wet wipes and plastic in different proportions were used. The components of the trash could also be either wet or dry. Since the dry materials get heated up much faster than the wet ones, the temperature in the bed would be uneven, with the dry components hotter than the wet ones. This would result in conduction between the hot and cold components. The model assumes that this is not significant. This assumption is likely valid since the wet wipes have poor thermal conductivity and the trash is not too tightly packed, reducing the transfer area. These conditions would result in low heat

transfer by conduction. The model considers the trash bed as a pseudo-homogeneous region with only one temperature and so the actual temperatures of the wet and dry materials are not given by it. Even with all this simplifications, the drying curve predicted by the model closely approximated the experimental ones for the two higher flow rates used (2.2 and 3.1 cm s^{-1}). Simulations with the lowest flowrate (1.2 cm s^{-1}) gave moisture contents very much lower than the actual, indicating that drying rate was being overestimated by the model. The decrease could be due to channeling of the air through the bed at this slow flow, but further studies should be done in to explain this observation. The model was used to predict the maximum rate of evaporation and the drying time needed to ensure that the wet materials in the trash have moisture contents below the minimum value for microbial growth. These variables are necessary for the proper design of the drying system and the model should prove useful in estimating them for scale-up of the process.

The trash drying model was derived from the application of the conservation of energy and moisture to the gas and solid phases. The resulting system of differential equations identified the parameters and data needed for simulation. These included the volumetric heat and mass transfer coefficients ($\boldsymbol{hA}$ and $\boldsymbol{k_mA}$), together with the water vapor concentration of the gas in contact with the surface of the wet solids ($\boldsymbol{W_{surf}}$). Since these were not available in the literature, experiments had to be conducted to acquire them. The study presented a systematic procedure which involved the single-layer drying of representative configurations of the trash to produce characteristic drying curves, analogous to thin-layer drying studies in the literature. The transfer coefficients were obtained from the constant rate period. The water vapor concentration of the gas at the solid surface was related to the mean moisture content of the solid using the falling-rate portion of the graph. The model used this information to calculate the evaporation rate,

$\boldsymbol{dM/dt}$, using the convective transport equation: $\boldsymbol{dM/dt = k_m A(W_{surf} - W_{air})}$. It should be pointed out that in the literature, the drying curve is also used to obtain an equation for the evaporation rate during the falling-rate period. However, this is usually of the form $\boldsymbol{dM/dt = k(M - M_{eq})}$ where $\boldsymbol{k}$ is an experimental "drying constant" and $\boldsymbol{M_{eq}}$ is the solid's equilibrium moisture content (Brooker et al., 1992). It would be interesting to study how these expressions can be transformed into the equivalent convective term which is more useful for packed bed modeling since they explicitly include the effect of the hot gas ($\boldsymbol{k_m A}$ and $\boldsymbol{W_{air}}$).

The water vapor concentration of the gas at the solid surface is usually taken from the equilibrium moisture curves (EMC) of the material being dried. The experimental procedure for obtaining the isotherms requires several desiccators containing saturated salt solutions of known water activities and an equilibration period of a few days. The method applied in this study to get the $\boldsymbol{W_{surf}}$ used data from the single layer drying experiments only. Since these have to be performed anyway to determine the evaporation rate expression, no additional work or set-up is needed. The $\boldsymbol{W_{surf}}$ obtained from the drying curve may be more appropriate than that from the EMC because of the difference between the actual drying conditions and that for the EMC. In the EMC, there are no moisture gradients in the solid but during drying this may be large, especially when there is rapid evaporation near the surface. Also in the EMC, the solid is in thermal equilibrium with the gas in contact with it and this is not the case during drying since the gas is always at a higher temperature. A detailed study comparing the results of deep bed drying simulations using the $\boldsymbol{W_{surf}}$ from the drying curves and that from the EMC should show if there is a significant difference between the two.

The porous media condensing heat exchanger with thermoelectric cooling

The porous membrane condensing heat exchanger (PMCHX) was modeled using the conservation equations for momentum, energy, total mass, and water vapor. A unique feature of this condenser is the use of a porous media to separate the produced liquid water from the gas phase. The porous media is kept cold to maintain a low water vapor pressure at its surface. This produces a concentration gradient between the bulk gas and the surface that drives the transfer of water vapor into the wall where it condenses. In essence, the PMCHX is actually a dehumidifier. A major assumption of the model is that all the condensate produced at the cold surface instantaneously goes through the porous plate so no liquid layer is formed. Since the model correctly predicts the condensation rate, this assumption was valid for the conditions used during testing. The validated model was utilized in the simulation of the closed-loop drying system to give values for the energy required to recover a unit mass of water from the wet trash.

The use of the closed-loop dryer system together with an efficient refrigeration/heat pump that can reheat the air using the heat rejected by the condenser significantly decreases the energy required to recover a unit mass of water from the wet trash. Any water recovery system that is based on evaporation needs to provide the latent heat for vaporization and if this heat cannot be reused, such as those solely using microwave or resistive heating, this will be the minimum energy input needed per unit mass of water. However, the dryer system/heat pump combination makes it possible to have an energy requirement less than the latent heat. This potential for high energy efficiency makes this system an attractive option for use in long-term space missions.

It should be interesting to test the model's assumption that all the water vapor getting to the wall gets condensed by introducing flow that hits the cold porous media directly. In the

PMCHX used, the gas flow is parallel to the walls and transport of water vapor to the porous media is due to diffusion. The introduction of appropriate baffles will make part of the gas flow to impinge into the porous surface and this may possibly increase the rate of condensation. However, too strong flow may force the water out of the porous media, break the liquid seal, and lead to the undesired mixing of gas and liquid in the condensate collection lines. Further studies on this should produce a more complete model for the PMCHX.

The use of real-time PCR method to measure fungal biomass

The study demonstrated the use of a real-time PCR assay to measure the biomass of a filamentous fungus infiltrating a solid media. The rt-PCR based method that was developed can be used to investigate how drying astronaut cabin trash affects the growth rate of fungi in the food and organic components present. Knowing the effect of water activity on fungal growth will be important in determining the extent of drying needed to prevent microbial proliferation. The setting of a minimum moisture content for the production of stable trash for storage will avoid extra energy consumption by drying beyond this point.

The rt-PCR protocol was successfully used to plot the time evolution of *Penicillium chrysogenum* biomass as it grew on autoclaved Matzo meal (cooked wheat flour) under different water activities. Since the growth kinetics observed are most likely species- and media-specific, the next step would be to apply the method to several test fungi species growing on different trash components. The part of the trash that is most prone to microbial growth would be uneaten food so it would be crucial to determine fungal growth behavior on the most common types of food in an astronaut's diet. It should also be noted that the rt-PCR assay will work not only with drying but also with other antimicrobial measures. Quantitative modeling of the growth rate

using the rt-PCR protocol will give an accurate evaluation of the effectiveness of these treatments.

It was also shown that the rt-PCR assay is specific to a particular fungal species and can consequently be used to measure its biomass even in the presence of other fungi growing on solid media. This would not be possible for biomass estimation methods that use biochemical markers (e.g. ergosterol, chitin) since these would also be extracted from the other fungal species. The rt-PCR assay can therefore be used to determine the specific growth rate of a single fungal species growing in a mixed culture. Microbial communities containing fungi are involved in important and highly beneficial processes here on earth (e.g. compost, activated sludge for wastewater treatment). The rt-PCR assay developed here can be used to determine the growth behaviors of fungal species present in them. This knowledge may prove indispensable in the future should humans start building colonies away from earth and require the establishment of these microbial processes there.

REFERENCES

Brooker, Donald B., Fred W. Bakker-Arkema, and Carl W. Hall. *Drying and Storage of Grains and Oilseeds.* 1st ed. NY, New York USA: Van Nostrand Reinhold, 1992.

Datta, A. K. "Porous Media Approaches to Studying Simultaneous Heat and Mass Transfer in Food Processes. I: Problem Formulations." *Journal of food engineering* 80.1 (2007): 80-95.